DEPARTMENT OF MECHANICAL AND INDUSTRIAL ENGINEERING TECHNOLOGY

FACULTY OF ENGINEERING AND THE BUILDENVIRONMENT

Investigation of Material Wear on Centrifugal Fan Impellers

A Dissertation submitted towards fulfilment of the degree of

Magister in Technologiae:

Mechanical Engineering

Student: Kgomotso Aphas Mabunda

Student No.: 802003209

Supervisor: Dr. PM Mashinini

October 2019

COPYRIGHT

DECLARATION

I **KGOMOTSO APHAS MABUNDA** hereby declare that this master's Dissertation report is wholly my own work and has not been submitted anywhere else for academic credit, either by myself or another person.

I understand what plagiarism implies and declare that this report embodies my own ideas, words, phrases, arguments, graphics, figures, results and organization except where reference is explicitly made to another work.

I understand further that any unethical academic behaviour, which includes plagiarism, is seen in a serious light by the University of Johannesburg and is punishable by disciplinary action as stipulated by the university rules and regulations.

Name: Kgomotso Aphas Mabunda

Student No: 802003209

Signature:

Date: 22/09/2019

TABLE OF CONTENTS

LIST OF FIGURES

LIST OF TABLES

ACKNOWLEDGEMENTS

This dissertation is based on a common problem that all ventilation fan designing, and manufacturing companies are facing in the industry. I would like to thank TLT ACTOM a Fan Company for allowing and academically supporting me on conducting this research. I also like to extend my gratitude to TLT-Turbo GmbH in Germany employees Dr.-Ing Dieter Holzdeppe and his master's Student Patrick Baumgaertner for support and sharing their laboratory results on wear determination.

I would like to offer my gratitude to my supervisor Dr. PM Mashinini, for the continuous support of my master's study and research, for his patience, motivation, enthusiasm, and immense knowledge. His guidance helped me through the research of this dissertation.

My sincere thanks are also devoted to Ron Pollhammer a Metallurgist with years of experience from Franktech metallurgical Services for assisting me with laboratory analysis because every result described in this dissertation was accomplished with the help and support from him.

Finally, I would like to acknowledge with gratitude the support and love of my family more especially my wife Mpho Mabunda, she always kept me going and motivating me.

ABSTRACT

Material wear formation on centrifugal fan impeller has been a major problem to many process plants in the whole world and this has been regarded as a grey area to many of OEM of extraction fans. TLT ACTOM has designed and manufactured an ID centrifugal fan for Sugar plant situated in Swaziland. The ID fan after a few months of operation the impeller was found to be subjected to wear. Wear initially took place such that the impeller could not last a season which is made of 9 months.

The research was conducted to study the behaviour of wear taking place on the impeller material used in sugar mill plant. Establish the uncertainty of what type of wear is taking place and what cause this wear. The study focused on the formation particle flow pattern and minimization of wear to give a solution to fan manufacturers and end-user of the extraction fans.

A visit to the plant in Swaziland was organized and during that site visit, bagasse and coal ash samples together with water samples were collected from inside of the venturi wet scrubber after the scrubber has been switched off for over a month for maintenance purposes. These samples were sent to a laboratory to analyse chemical compositions. The test aimed to determine particles sizes, a composition of mass in percentage, elements and mass of a chemical or contaminate per unit volume of water. A physical inspection has been performed on the wet scrubber to inspect if there were any trace that can lead to wear resulting from wet scrubber failing to perform what is expected from it. A correlation on how wear might have taken place on the impeller was conducted by using a CFD simulation. CFD simulation was conducted by using SolidWorks CAD software. Before conducting the simulation, calculations were made to determine parameters to be used as boundary conditions in the simulation software. Calculations were based on the actual centrifugal fan duties provided by the consultant company that was responsible for designing the entire plant system.

After the wet scrubber inspection, it has been found that internal components of the scrubber were subjected to erosive wear and this has resulted in the scrubber poor performance for filtration. The research has also revealed that material wear was caused by particles impaction, which is known as bagasse ash, this is a by-product of crushed sugarcane stalk's, leaves, and roots with soil, coal and dry woods. A CFD analysis has been used as a tool to simulate gas flow pattern to work out the impingement angle and velocity of particles which are factors expected to be contributing on wear.

A critical angle of impingement was found to be between 15° and 45° accelerate the wear when a material is ductile. Research has concluded that material selection to be based on particles impingement angle onto the impeller blades and filtration system to be effective. CFD results have proven that impingement angles and particles velocity correlate with wear damages observed on the impeller during inspection on site.

GLOSSARY OF TERMS

AME:	ACTOM Mechanical Equipment.
Bagasse:	A by-product made of roughage fibre residue that has been treated in a sugar mill.
Biomass:	Organic matter used as a fuel.
Boundary Conditions:	Define the inputs values of the simulation model such as pressure.
CFD:	Computation Fluid Dynamics.
ID Fan:	Induced Draught Fan.
Impingement Angle:	Angle at which particle approaches and interact with the surface.
Junctions:	The points at which the actual contact emerges during entrapment of particles.
MCR:	Maximum Continuous Ratings.
Micrograph:	A photograph taken by means of a microscope.
OEM:	Original Equipment Manufacturers.
PM:	Penetration Mechanisms
Reducer:	Transition piece.
Rotational velocity:	A flow of particles with rotational movement of particles along the air stream.
Trajectory:	The path followed by a shell flying or an object moving under the action of given forces.
Tribology:	The study of wear and related processes.
Tribosystem:	Any system of science and engineering of interacting surfaces in relative motion.
Volute:	Inside of fan casing.
Soluble Electrolytic:	Compound that will dissolve into aqueous ions in a solvent and these ions can conduct electricity.

CHAPTER 1: INTRODUCTION

1.1. Background

In sugar mill plant industry, such as Ubombo Sugar Limited a subsidiary of Associated British Foods plc is one of the largest sugar producers in Swaziland. The existence of Ubombo Sugar Mill plays an important role in contributing to Swaziland's economy. In year 2016/17 Ubombo Sugar managed to produce approximately 215,000 tonnes of sugar. As part of the process to produce sugar, fans such as centrifugal fans are used in process plant system as a tool that takes part during the making of sugar. These fans are highly subjected to material wear. Material wear is a phenomenon that takes place between two surfaces in industry or equipment and cannot be avoided. This is a process that results in loss of the material surface of a solid body. Wear has complex understanding investigations that have resulted in isolated studies toward specific mechanisms or processes. Since the discovery of wear over the past years, the research has revealed common types of wear mechanisms to be different [1], types are as follows:

1. Abrasive wear
2. Adhesive wear
3. Fatigue wear
4. Corrosion wear

Wear takes part between two or more substances when they become in contact. Wear can be found in different industrial processes such as metal refinery, power generation, mineral process, and sugar mill plant and many more. This research will mainly focus on formation and control of wear that is found on centrifugal fan impeller used in sugar mill plant.

A centrifugal fan was invented by Alexander Sablukov [2], a Russian military engineer in 1832 and managed to implement its usage in Russian light industry such as the sugar making process. A centrifugal fan consists of a fan casing, impeller, and inlet cone and is driven by an electric motor. Air enters at the centre of the impeller horizontally, turns at a right angle and moves radially outward between the blades.

Inside volute, high velocity is induced by the impeller and converted into static pressure before leaving the casing. There are three common types of blades used inside fan casing on different applications, namely; backward, forward and radial curved blade [3, 4]. A picture of a typical centrifugal fan is shown in Figure 1-1.

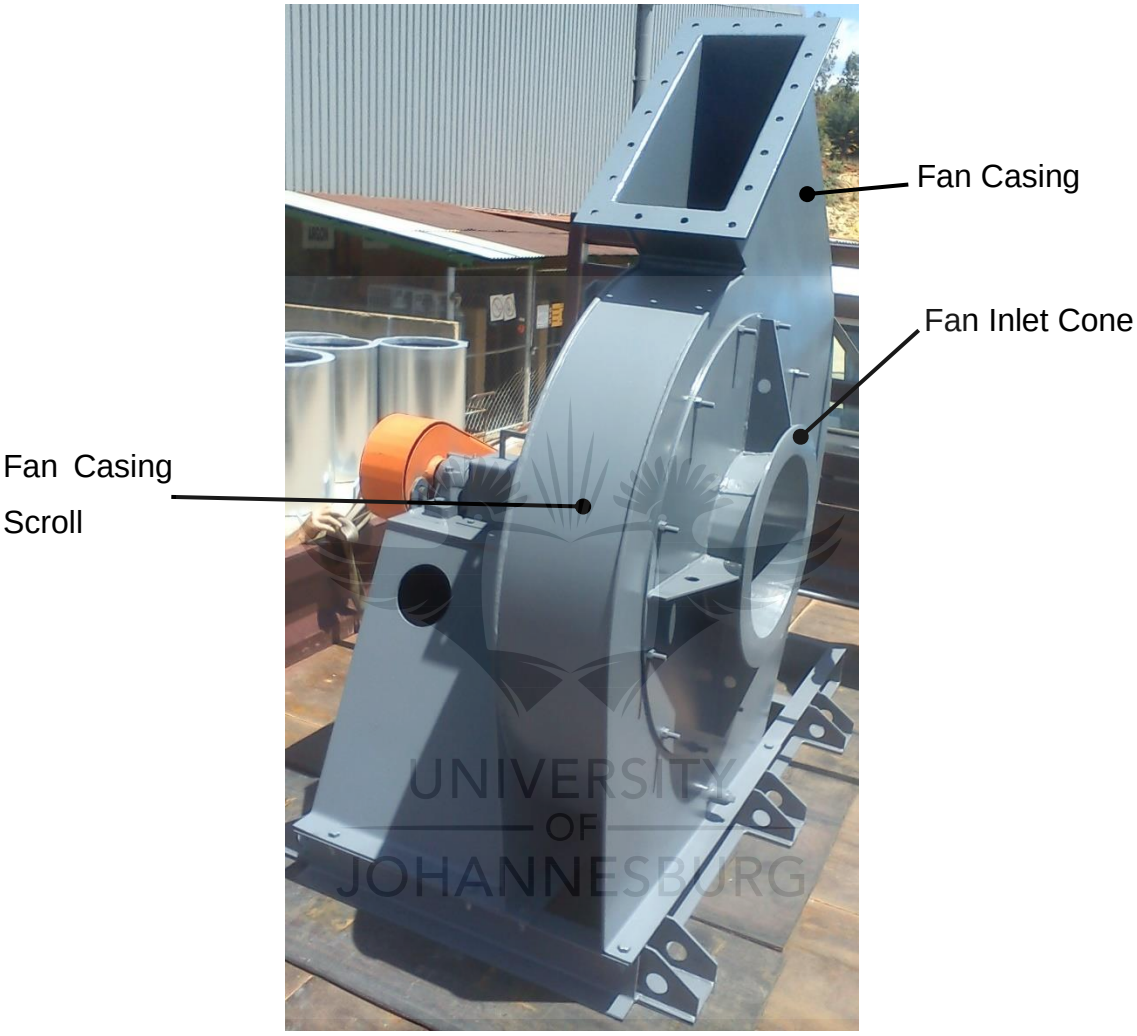

Figure 1 - 1: Picture of typical centrifugal fan.

Centrifugal fans are used in many different applications in industry and in this research study, the focus will be on a centrifugal fan that is installed in the sugar mill industry. The blades type used is forward curved radially tipped blades, design and manufactured by TLT ACTOM. These impeller blades were integrated with wear liners that cover's 25% on the blade surface that is in contact with the substances passing through the fan. These wear liners were welded onto the blades. To protect

blades wearing on the leading edge from an aggressive substance, a hardfacing was overlaid on all blades leading edges.

TLT ACTOM formally known as AME designed and manufactured an ID centrifugal fan for Ubombo Sugar Limited in 2009. The ID fan has been installed and commissioned without any challenges and later during the operational phase, the impeller was found to be subjected to wear. Wear took place such that the impeller could not last a season which is made of 9 months. A site visit has been conducted to Ubombo Sugar Mill in February 2017 to inspect the current situation on the impeller. The impeller was found to be in bad condition. The end-user has managed to source out corrosion protection that can barely prolong the life of the impeller to finish the season. Even though the impeller finishes the season, it cannot be used for the second season. Shown in Figure 1-2 is a schematic layout of scrubber and ID centrifugal fan for Ubombo Sugar Limited.

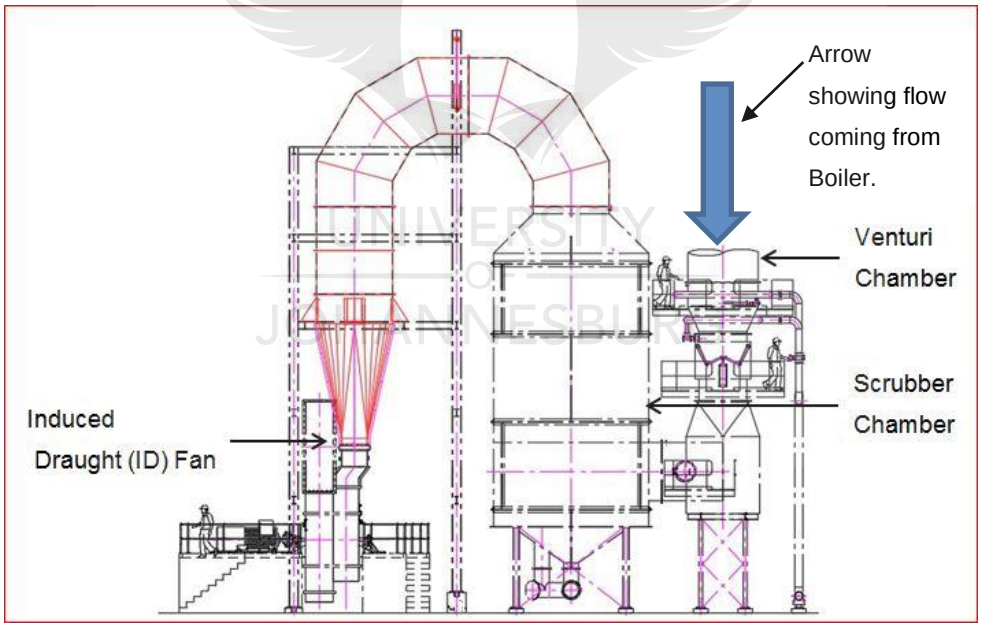

Figure 1 - 2: Schematic diagram of scrubber and centrifugal fan taken from JTB Ubombo drawing.

The induced draught fan draws air from the boiler combustion chamber through a wet scrubber and discharges the gas into the atmosphere through a stack. The boiler combustion chamber is a compartment that bagasse's are fed and burnt to generate necessary heat to create steam. A wet scrubber is a dust particles collection

component that depends on direct and permanent contact of liquid droplets or vapor with the dust particles. The collected dust particles with liquids are then easily discharged. A wet scrubber is generally classified by its construction structure and the methodology that is used to create contact between the liquid and the dust particles. Wet scrubber also plays an important role in collecting explosive and flammable dust, entraps gaseous to reduce pollution and collect vapour. Figure 1-3 shows a scrubber with a venturi which illustrate mechanism and working arrangements of the system.

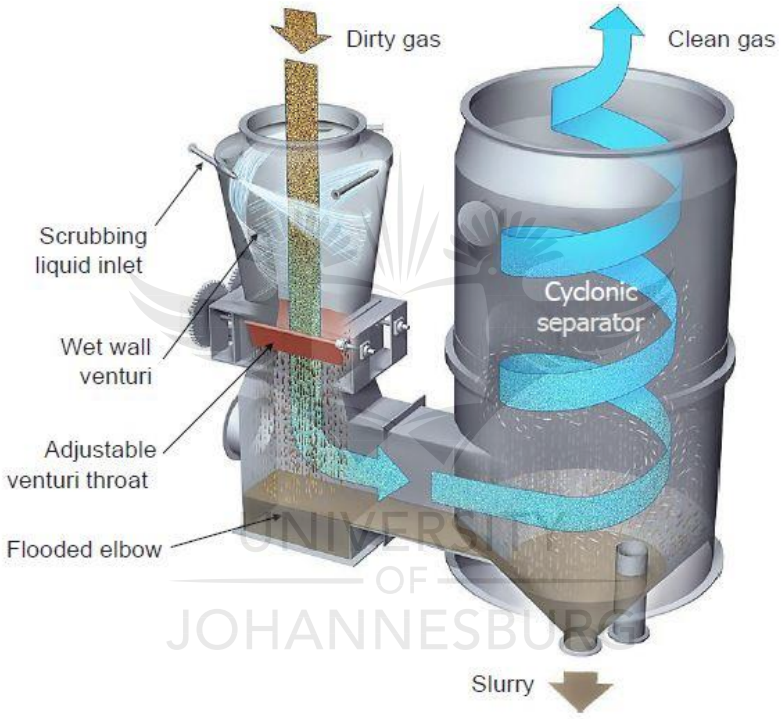

Figure 1 - 3: The mechanically and working arrangements of Venturi scrubber taken from AAP catalogue [5].

In Ubombo sugar mill, the fuel used in the boiler is bagasse, which is made of sugarcane leaves, roots and residuals from sugarcane stalk. Collectively, bagasse is a by-product of roughage fibre residue that has been treated in a sugar mill. The usage of bagasse has been adopted due to the escalating prices of natural gasses, fuel oil, and electricity. Previously bagasse was processed and discarded as solid waste. Bagasse is an abrasive substance that passes through the wet scrubber and is trapped into a liquid droplet and discharged as slurry. For some reasons, droplets

with bagasse ash ending up passing through the ID fan impeller and causes wear. Bagasse ash can be sucked through the fan due to the high velocity at fan inlet. Such reaction might have risen from the fan over performing by sucking more than what is required by the system at fan inlet. Figure 1.4 illustrates a picture of a centrifugal impeller with welded wear liners on the blades leading edges, blades surface, and backplate. Blade leading edge is the beginning of the blade section in the inner side of the impeller, where the intake of air starts and the blade trailing edge is the end of the blade section on the impeller outer diameter, where the air is discharged.

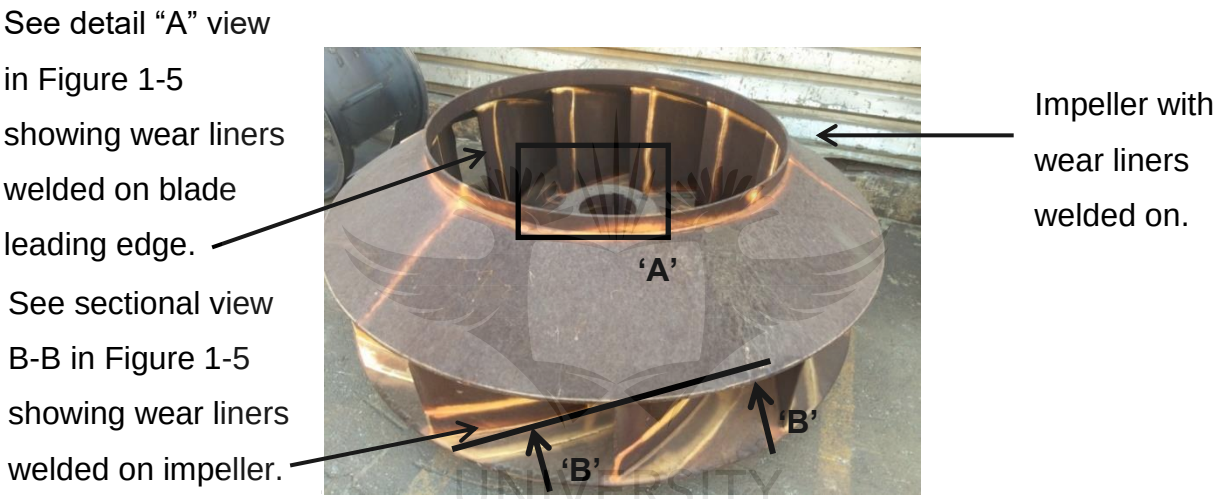

Figure 1 - 4: Centrifugal impeller showing welded wear liners.

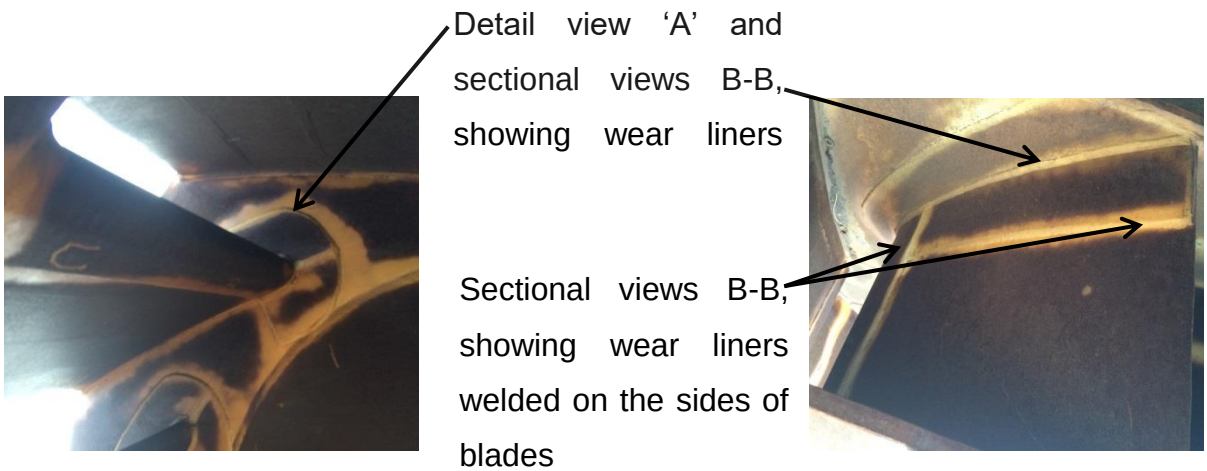

Figure 1 - 5: Centrifugal impeller showing the inside through sectional B-B.

Wear on the impeller led to this current research to identify why bagasse could not be capably filtered efficiently inside the scrubber. Scrubber inefficiency resulted in impeller blades subjected to wear that is taking place on the inside of the curved blades and inner surface of the backplate. The edge of the blades wears off unevenly. Figure 1-6 illustrates wear found on Ubombo ID fan blades and see appendix for more wear found on the impeller.

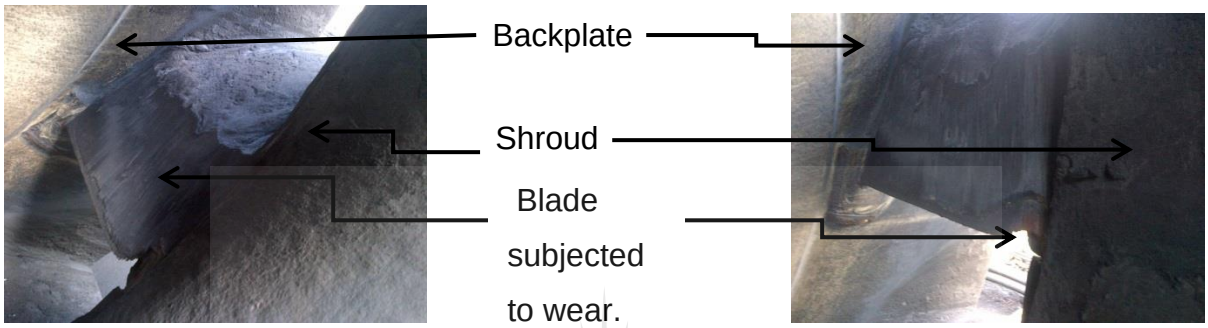

Figure 1 - 6: Wear found on Ubombo ID fan blades.

Based on the consultation with TLT ACTOM [5], formation and factors influencing the cause of wear have been a grey area to the company and their product end-users. The users previously applied many assumptions to deal with this problem in the past and up to this day they have not figured how the loss of material takes place.

1.2. Weld Hardfacing

Along with this wear study, the application of weld hardfacing will also be investigated because of the weld that has been worn-off on the leading edge of the impeller blades during operation of Ubombo Sugar Mill Plant. Weld hardfacing, is a layer that is made of several strengthened welds runs on blade leading edge to prevent abrasive particles to penetrate and cause cavity. After the cavity has been formed, this becomes a soft spot of wear to propagate from the blade leading edge which leaves the rest of the blade vulnerable. This resulted in both the weldment and the parent metal subjected to wear problem. Figure 1-4 and Figure 1-5 illustrate impeller arrangement and wear.

1.3. Significance of research

Industries such as metal refinery, power generation, mineral process and sugar mill plant experience a great challenge on wear of materials. These industries go out and pursue solution from fan Original Equipment Manufacturer (OEM), corrosion protection specialist and steel distribution suppliers to use better steel that can give a permissible wear resistance. The main challenge is that none of these suppliers has given a valid solution, reason being that none of these suppliers has a better understanding of wear theory or experiment that has been conducted specifically for fans. Most of the product on the market has been tested but not specifically for fans. Therefore, such research on wear has great opportunity to present solution that has not yet been discovered in the industry of fans manufacturer and end users.

Due to deficiency of understanding wear theory or experiment work out on fans, this has led to a debate between three parties, TLT ACTOM, Boiler Company and Ubombo Sugar Mill Illovo about what caused wear and who is liable. Debate between three parties was as follows,

- Ubombo Sugar Mill Illovo firstly criticize the corrosion protection used on the impeller. They assumed that corrosion protection used could not resist impingement from water droplet containing penetrant mechanism and suspected that the fan velocity is too high and therefore the fan is sucking more than what is required. Above all criticism, they were happy with the fan performance.
- The Boiler Company, who was the consultant, also suspected that the fan velocity is too high and cause wet scrubber to malfunction. They requested TLT ACTOM to calculate velocity at the fan inlet and prove that the velocity is not too high.
- TLT ACTOM, after calculating velocity and some investigating, the assumption presented to other two parties was malfunctioning of wet scrubber not fan.

After all these discussions between the three parties, could not come to a clear agreement on what causes the wear on the impeller. Ubombo Sugar Mill Illovo remains with wear problem and they have been operating in a same manner since

then and no one provided a solution on what caused and how to control wear problem. Therefore, this research will have an impact between three parties in providing a solution of what initiated wear and how to manage it.

1.4. Motivation for research

The major problem is to solve the behaviour of wear that is taking place at a high rate on impeller blades and backplate. This wear highly interrupts the operations of the plant by causing an unplanned shutdown of the wet scrubber for maintenance. Shutdown results from forced draught fan being subjected to vibration which has been induced from out of balance of impeller due to loss of material eroded during wear. This unplanned event causes the company to encounter a loss in production and an increase in maintenance expenditure. Reduction in production and an increase in maintenance expenditures affect Ubombo Sugar Mill Illovo's business profits. Therefore, study worth to be conducted to understand the theory behind wear formation which enable the implementation of the material wear solutions.

This problem does not only affect the fan end-user but also affects the credibility and marketing campaign of the fan manufacturer. The fan manufacturer is facing a challenge of dealing with a guarantee offered after fan installation. A fan normally comes with a 1-year guarantee and plant maintenance schedule is to have shut down every 9 months, but with the rate at which wear is initiated, the impeller does not last 9 months. Therefore, this leaves fan manufacturer (TLT ACTOM) with a challenge to prove that this has nothing to do with the fan design, except proving that there is a fault in the system that is causing such high rate of wear. This calls for urgent research of prospective findings of the cause and implements the possible solution to manage the wear except not eliminating the fault.

1.5. Aim and objective

The research is conducted to study wear taking place on the centrifugal fan impeller used in the sugar mill industry. The aim is to understand the uncertainty of what type of wear is taking place, how it takes place and what cause this wear. The study will

focus on the formation and minimization of wear to give a solution to OEM and end-user of the product. There are three factors to be considered during this research such as physical sample evaluation through laboratory experiments, poor performance of the wet scrubber that may cause excessive bagasse ash to pass through and land upon the impeller.

1.6. Hypothesis

The wear formation on the impeller may be influenced by the aggressive substances passing through the inefficiency of the wet scrubber as applied in Sugar Mill Plants. The impingement angle and the particles velocity may also have an effect on the impeller wear formation.

1.7. Sub Problems

Consideration to evaluate the wet scrubber mechanical design have to be made as this might have led to poor performance of the wet scrubber to be unable to filter particles as required by the plant system. Another factor is the over-performing of the centrifugal fan such that too much velocity is induced by the fan and resulting in sucking too many particles. However, both stipulated possibilities shall not form part of this study and shall be left for another research topic.

1.7.1. Wet Scrubber

An investigation of wet scrubber operation to be explained in this research and compared to the current wet scrubber operation on-site to determine if there is any evidence regarding the operational methodology that may result in the poor operation of the wet scrubber.

1.8. Brief Methodology

To understand how particles are conveyed inside the fan, a CFD analysis must be performed to determine particles flow path over the impeller. This will be useful information to validate the expectation under the hypothesis. The methodology requires that the appropriate degree of control be used, appropriate measurements and analysis techniques be used, appropriate information and observations be recorded. If any of these elements are not addressed or inadequately addressed in the simulation or testing strategy, correlation with the application is generally reduced [3]. The individual elements of this methodology are treated in the following sections on simulation, Data acquisition, Analysis, and Reporting. A 3D model of the fan shall be modeled to be used to simulate and run several tests to establish the flow patterns inside the system.

1.8.1. Impingement Angle

With the wear that has been observed on the impeller, the expectation is that the angle of impingement would be between 15° and 45° for a ductile material. This will be determined by CFD analysis through studying particles path. Correct data such as fan static pressure and flow rate will be used to initiate simulation to achieve appropriate fluid velocity running inside the ducts through the fan. Impingement angle will be determined and measured as illustrated in Figure 1-7, lines with arrows represent the direction of the air motion passing through the impeller. After the simulation, tangential lines parallel to the flow of motion will be used to determine and measure impingement angle with a datum line taken from the impeller backplate. Letters D to G indicated on schematic layout under Figure 1-7 represent the angle of attacks to be measured on the simulation.

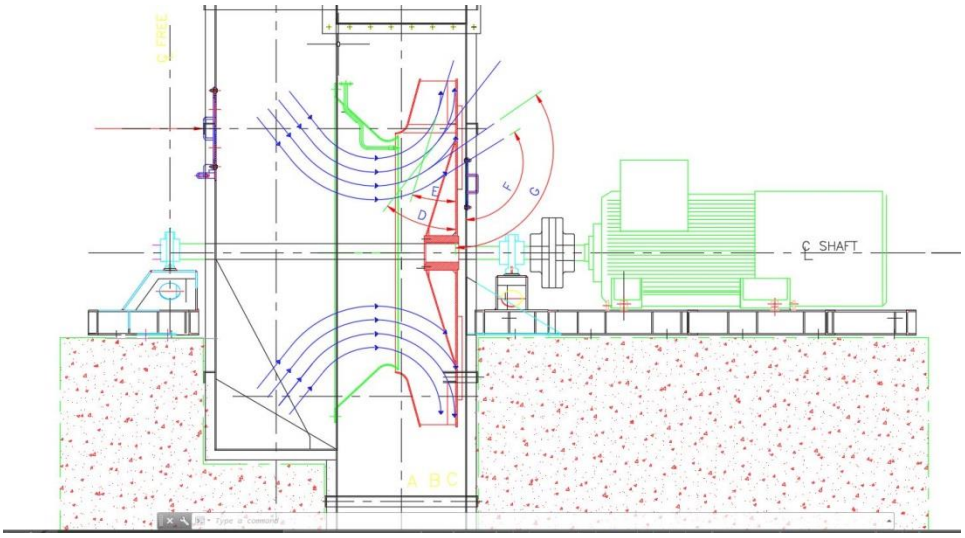

Figure 1 - 7: Fan sectional view illustrating impingement angle of attack to be measured on the simulation.

1.8.2. Velocity of Solid Particles

Bagasse particles found inside Ubombo sugar mill induced draught fan shall be used during the investigation to understand the effects of these particles. Portion of bagasse particles will be taken to the laboratory to analyse size geometry and chemical composition to understand chemical reaction between impeller material and chemical emissions from bagasse particles. Under the micrographs of the particles, the expectation is that the shape of the particle must have sharp edges that able to cut out material surface though rotational movement. Under the same simulation with same data used to initiate simulation to figure out impingement angles, velocity induced through the fan shall be measured in the following manner as illustrated in Figure 1-8. Velocity will be measured along the impeller across the planes indicated on the schematic layout and first velocity measurement will be on plane A-A, second on plane B-B and the last one on plane C-C. These velocities shall be used to justify expectation mentioned under hypothesis.

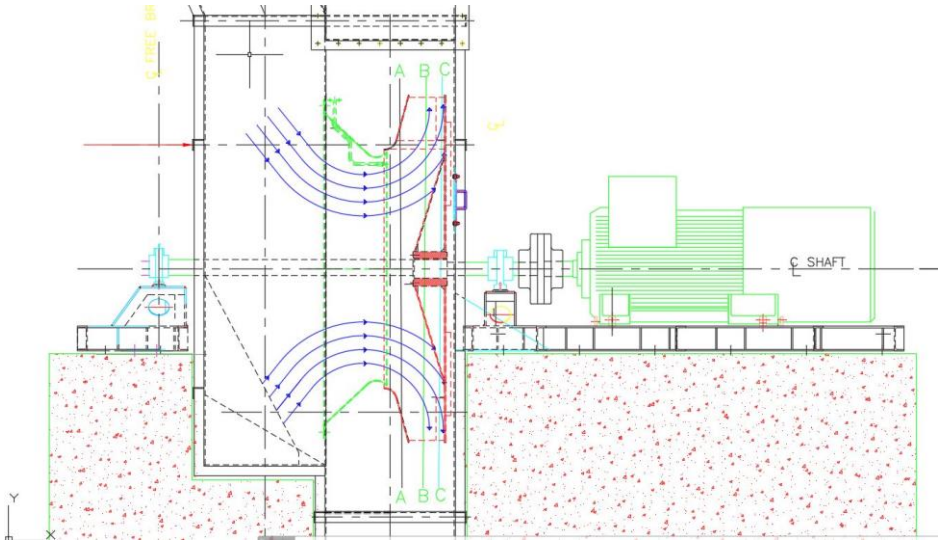

Figure 1 - 8: Fan sectional view illustrating velocity air motion to be measured on the simulation.

1.8.3. Shape of Solid Particle

Solid particle inside the gas approaches the eroded surface with rotational movement at certain velocity and angle, when reached, the surface wear is formed. The solid particles cut the surface with a rotational movement. Therefore, the identification of solid particle's shape is very crucial. The shape of a solid particle will be determined under a microscope. Solid particles shall be evaluated using the microscope to analyse and observe the morphology of particles.

1.9. Dissertation lay-out

Chapter 1: Introduction – This chapter gives a brief history and background of the wear research. The significance of the research has been mentioned including aim and objectives. The methodology on how the research was approach and performed has been indicated briefly in this chapter.

Chapter 2: Literature review – Tests and findings of research on wear formation by other scholars have been discussed in this chapter. This information shall be used to compare the outcome of this current research study.

Chapter 3: Methodology – This chapter explains the methodological approach used and experimental tests conducted to assist in establishing the wear formation onto the impeller.

Chapter 4: Bagasse and Scrubber Analysis – This chapter gives findings of the results and how the comparison was reviewed between the simulation and theoretical wear formation indicated by other researchers This will also cover the analysis of laboratory results.

Chapter 5: Simulation Analysis – This chapter provides the analysing of fluid computation inside the fan to determine what is taking place and what are patterns looks like, to determine how does flow substance contributes to wear found on the impeller.

Chapter 6: Conclusions and Recommendations – A conclusion and recommendations of this thesis will be covered in this chapter. This will be based on understanding the theoretical theory investigated and compared to tests performed in the laboratory.

CHAPTER 2: LITERATURE REVIEW

2.1. Introduction

The research is based on the investigation of the cause of wear formation. This chapter focuses more on giving the theory of mechanisms that affect wear formation and research performed by other researchers. This will assist in understanding wear formation and what type of approach to use for investigating wear formation and solution. In this chapter, a literature review conducted will be reported. A literature review of two types of wear, adhesive, and abrasive wear shall be elaborated in detail.

2.2. Background

In the year 2002, a sugar mill in Swaziland known as Ubombo Sugar Limited placed an order with Boiler Company for the supply and installation of boiler plant. The power plant was designed to provide power and process steam to the factory and to supply excess power to the national grid. The client's intention was to burn biomass fuel for a season and in order to provide sufficient biomass during the off-crop, the bagasse was going to be added with cane tops and trash. The boiler has been designed to burn coal and woods as supplementary fuel if required. Operating steam condition of boiler is 45bar at 450°C through burning mixture of bagasse, woods and coal.

2.3. Brief on plant system

This research is mainly focusing on burning of bagasse, coal and woods through plant system operation and its emissions that cause wear on impeller blades. Plant processes and components functionality are discussed as follows.

2.4. Bagasse

Bagasse is a by-product made of roughage fibre residue that has been treated in a sugar mill. The usage of bagasse has been embraced due to the escalating in prices of natural gasses, fuel oil and electricity because previously bagasse were considered as solid waste disposal. But in recent days, most bagasse is burned as a fuel. Bagasse ash is an abrasive substance that passes through the wet scrubber and impinges into a liquid droplet and discharged as slurry. Formation of bagasse begins with sugarcane harvest. There are three types of methods for harvesting, cutting using hands, Machine cutting and Mechanical raking [4]. Differentiation on the mentioned harvesting methods is based on the condition that the sugarcane stalks reach the mill. The only stalk comprehends sufficient sucrose for processing into sugar. All other parts of the sugarcane, leaves, top growth and roots are converted into bagasse.

When sugarcane reaches the mill, cane undergoes crushing and chopping process through a series of mills to extract the juice. During this process, at least up to 95 percent of obtainable sucrose is extracted. The remaining product is called bagasse and consists of tangled cellulose fibres and crashed particles that are used in the boiler as fuel. Bagasse is a fuel of variable composition, consistency, and heating value, which generally has a heating value between up to 2200 kcal/kg on a wet and as-fired basis. Bagasse generally has a moisture content between 40 and 55 percent in weight. Sulphur and Nitrogen contents from bagasse are generally near or below 0.1% in weight, when entering the boiler, ash contents are generally less than 2% in weight as fired from the boiler.

2.5. Boiler

There are mainly three types of boiler used in sugar mill plant to combust bagasse, Horseshoe, Fuel cells and spreader stoker boilers. In horseshoe and fuel cells boiler, bagasse is gravitationally suckled through chutes and piles up on a refractory hearth. Primary and over fire combustion air flows over ports in the furnace walls and begins

burning on the surface pile. Dumping hearths permits removal of ash while the unit is operation.

Spreader stoker, bagasse fed enters the furnace over a fuel chute and is spread pneumatically or mechanically across the furnace. This is the similar boiler that has been used for Ubombo sugar mill. Biomass is conveyed to the boiler through four 3-drum fibrous fuel feeders driven by VSD drives. Coal is fed through four robust VSD-driven metering screws and discharged into the bagasse feeders. Both, bagasse and coal are carried into the combustion chamber through pneumatic spreaders, which incorporate trajectory control plates to distribute the fuels evenly over the surface of the stoker. The complete combustion of bagasse occurs in two phases, primary and secondary combustion. Primary combustion refers to the physical and chemical change taking place on the fuel bed, this consist of drying, de-volatilization, ignition and burning of the bagasse. Secondary combustion refers to the oxidation of the gases and particulate matter released by primary combustion. Secondary combustion involves high temperature, enough air and commotion in the gas stream. Commotion of mixing remain in the system for sometimes to ensure satisfactory mixing at elevated temperatures. Time, temperature, turbulence and air require a gentle balance for complete combustion [4].

The most important pollutant emitted by bagasse-fired boilers is particulate matter produced by the turbulent movement of combustion with respect to the burning bagasse and subsequent ash. Emissions of sulphur dioxide (SO_2) and nitrogen oxides (NOx) are lower than predictable fossil fuels due to the characteristically low levels of sulphur and nitrogen related with bagasse. Auxiliary fuel (refer to fuel oil or natural gas) may be used during start-up of the boiler or when the moisture content of the bagasse is very high to support combustion, and if fuel is used during these stages, sulphur dioxide and nitrogen oxides emissions will rise. Soil particles characteristics can disturb the magnitude of particulate matter emissions from the boiler. Cane that is inappropriately washed or inaccurately prepared can also affect the bagasse ash content. Aging in combustion conditions can cause increase in emissions of carbon monoxide (CO) and unburned organics that would be measured as volatile organic compounds (VOCs) and entire organic compounds (TOCs) [4].

Emissions found after burning coal are sulphur dioxide (SO_2), nitrogen oxides (NOx), carbon dioxide (CO_2), mercury and particulate matter also known as fly ash. Particulate emissions from bagasse-fired boilers are considered abrasive and can induce erosion within the mechanical collector [4, 6]. A venturi-type wet scrubber with cyclonic droplets separator used as mechanical device to remove particulates from the boiler flue gases during biomass and coal-firing.

2.6. Wet Scrubber

Wet scrubber is a collection mechanism device [6] that depends on direct and permanent contact of a liquid with collection mechanism. Wet scrubbers are generally categorised by the method that is used to persuade contact between the liquid and the collection mechanism. Their function is mainly to collect flammable particles, explosive dusts safely, engage gaseous pollutant and collect vapour where required [4, 6]. There are many different types of wet scrubber, this study will further explain the operational and functionality of venturi-type wet scrubber which has been used in Ubombo Sugar Limited plant.

The design of the venturi wet scrubber consists of a venturi followed by a liquid entrainment separator. As the gas passes through the venturi throat, both the particle velocity and the turbulence increase. The particle-laden gas substance first contacts the liquor stream in the core and throat of the venturi section. The gas substance and liquid stream then pass over annular orifice formed by the core and throat and atomize liquid into droplets which are imparted by particles in the gas stream. Impaction results mainly from high differential velocity between the gas streams by centrifugal action in a cyclone separator. See a picture of venturi wet scrubber on Figure 1 – 3. The mixture of dust and liquid is cleared from the separator bottom drain and the cleaned gas leaves through the top of the separator being sucked by induced draught centrifugal fan [6].

Wet scrubbers have been historically recoded to have penetrant efficiencies of above 90% [4, 6]. Operational problems can transpire with wet scrubbers due to clogged spray nozzles, sludge deposits, dirty recirculation water, improper water

levels, malfunction of mechanical parts and unusually low pressure drops. The spray impingement scrubber is in greater use due to lesser energy requirements and less operating and maintenance. Gaseous emissions may also be absorbed to a significant extent in a wet scrubber. In addition, alkali compounds are sometimes utilized in the scrubber to prevent pH conditions. If compounds such as sodium carbonate or calcium carbonate are used, carbon dioxide emissions will increase [6].

2.6.1. Particle Collection Mechanisms and Efficiency

Penetration Mechanisms (PM) in most wet scrubbers are inertial impaction of the penetrate mechanism onto liquid droplets. This is achieved by generating easily collected large particles by combining liquid droplets with relatively small dust particles. During the process, the dust particles are developed into larger particles by several methods such as impaction, diffusion, direct interception, electrostatic, attraction, condensation, centrifugal force and gravity [6].

Inertial impaction in wet scrubbers occurs as a result of a change in velocity between particles suspended in flowing gas. When the flowing gas approaches liquid droplet, flow gas will change direction and flows around the droplet. The particle in the flowing gas will try to change the direction to flow of the gas path and pass around the droplet. Inertia forces will try to maintain the forward initial motion of the particle towards the object, but the fluid force will try to drag the particle around the droplet along with the gas. This will result in impaction for the particle where inertia dominates and by-pass those particles overwhelmed by fluid drag [6].

Large particles that are greater than 1µm are more easily captured by inertial impaction because these particles have more inertial momentum to resist change in flow of gas and therefore, impact the droplets. Small particles < 1µm are more difficult to collect from inertial impaction because they remain in the flow lines of the gas due to the predominance of the fluid drag force [6].

2.6.2. Collection Efficiency

Efficiency is an important factor that is used to quantify wet scrubber performance. This factor is commonly referred to as collection efficiency. Another way of quantifying scrubber efficiency is to perform an inspection of damage occurred inside the wet scrubber chamber. Damage is more likely caused by wear taking place inside the scrubber. Collection efficiency is usually expressed in terms of penetration which is defined as the fraction of particles in the exhaust system that passes over the scrubber uncollected [7]. It is expressed as:

$$P_t = 1 - \eta \quad (2\text{-}1)$$

Where,

Pt = Penetration of dust particles to droplets.

η =Collection efficiency

2.6.2.1. Diffusion Collection

Collection by diffusion transpires because of both fluid motion and Brownian (Random) motion of particle. This particle movement in the scrubber chamber results in direct particle-liquid contact. Diffusional collection effects are best significant for particles less than 1µm in diameter because they have less impact due to small mass. Interception is restricted by their reduced physical size. This impaction causes them to move first one way and another way unsystematically through the gas. The Brownian diffusion process leads to particle capture in most frequently described by a dimensionless parameter called Peclet number (P_e) [7].

Peclet number is achieved by using the following formula.

$$P_e = \frac{3\pi\eta v d_p d_d}{C_f k_B T} \quad (2\text{-}2)$$

Where,

P$_e$ = Peclet number

d$_p$ = particle diameter

µ = gas viscosity

v = gas stream velocity

d_d = droplet diameter

C_f = Cunningham correction factor

T = temperature of gas stream

k_B = Boltzmann's constant

Equation 2-2 displays that as temperature increase, P_e decreases. As temperature increases, gas molecules move around faster than they do at low temperature. This action leads to increased impaction of the small particles. Increased unsystematic motion and increased collection efficiency by this mechanism. Collection efficiency by the diffusion process is commonly expressed as shown in equation no 2-3 [7]:

$$\eta_{diffusion} = f(\frac{1}{P_e}) \quad (2\text{-}3)$$

Equation (2-3) displays that as the Peclet number decreases, collection efficiency by diffusion increases [7].

2.6.2.2. Droplet Impaction

Wet scrubbing system, particles tends to follow the streamlines of the gas flow. When liquid droplets are introduced into the gas flow system gas flow diverge around the droplet with other penetrant mechanism. However, particle matter cannot always follow these streamlines as they diverge around the droplet. Other particles with heavy mass tend to continue along their path due to inertia force and impact on the droplets. Impaction increases as the velocity of the particles increases relative to the liquid droplet's velocity. In addition, as the size of the liquid droplet decreases impaction also increases. In impaction after the design, the key parameter is known as the impaction parameter (φ) and expressed by the following Equation [7]:

$$\varphi = \frac{C_f p_p v(d_p)^2}{18 d_d \mu} \quad (2\text{-}4)$$

Where,

p_p = Particle density

μ = gas viscosity

v = gas velocity at venturi throat

d_p = particle diameter

d_d = droplet diameter

C_f = Cunningham correction factor

2.6.2.3. Particle Interception

If a small particle is travelling around an obstruction such as droplet in the flow stream, it may encounter that object because of the particle's physical size. This interception of particle on the collector usually takes place on the sides before reaching the top or bottom. Because the centre of a particle follows the path around the droplet, colliding occurs if the distance between the particle and droplet is less than the radius of the particle. Collection of particles by interception results in an increase in overall collection efficiency. This effect is categorised by the separation number which is the ratio of the particle diameter to the droplet diameter [7].

2.7. Induced Draught Fan

The purpose of this fan is to convey dust and emissions of gases from the boiler combustion chamber through the wet scrubber and discharge clean air into the atmosphere through a stack. For every system, a fan is selected with a basic understanding of the system operating parameters as these conditions determine the size and design of the fan required for a specific duty. Certain parameters including pressure, volume flow, temperature, altitude, moisture content, gas density, contaminants such as carryover, erosion, corrosion, sticky particulates and transmission velocities to avoid product dropout or velocity erosion are all crucial to an appropriately sized and designing fan system. Most of ID fan impellers used in the sugar process industry are manufactured with wear liners to protect the impeller from the abrasive substance from the boiler combustion chamber. Ubombo Sugar Limited, the impeller has been manufactured from Weldox 700 and fitted Hardox 500 wear liners to protect the impeller from wear. Table 2 – 1 to Table 2 – 4 illustrate Weldox 700 and Hardox 500 mechanical properties and chemical composition respectively [8, 9].

Table 2 - 1: Weldox 700 Mechanical properties [8].

Thickness mm	Yield Strength MPa (min)	Tensile Strength MPa	Elongation % (min)	Typical Hardness HBW
4 - 43	700	780 - 930	14	260 - 310
(53) - 100	650	780 - 930	14	260 - 310
(100) - 160	650	710 - 900	14	240 - 290

Table 2 - 2: Weldox 700 Chemical Composition [8].

C Max %	Si Max %	Mn Max %	P Max %	S Max %	Cr Max %	Cu Max %	Ni Max %	Mo Max %	B Max %
0.20	0.60	1.60	0.020	0.010	0.70	0.30	2.0	0.70	0.005

Table 2 - 3: Hardox 500 Mechanical properties [9].

Thickness mm	Typical Yield Strength MPa, not guaranteed	Typical Hardness HBW
4 - 32	1250	470 - 530
(32) - 103	1250	450 - 540

Table 2 - 4: Hardox 500 Chemical Composition [9].

C Max %	Si Max %	Mn Max %	P Max %	S Max %	Cr Max %	Ni Max %	Mo Max %	B Max %
0.30	0.70	1.60	0.020	0.010	1.50	1.5	0.60	0.005

2.8. Wear Mechanisms

Wear results from damage that occurs when two surfaces are moving over one another. This involves the removal of micro amounts of materials and results greatly in reduction of the efficiency and lifespan of the device. Wear can induce plastic

deformation, structural changes, and surface cracking. Different wear mechanisms can occur depending on the nature of the surfaces, chemical environment, operational conditions, and main wear processes are summarized in Figure 2-1. Abrasion and erosion are types of wear that are formed by hard particles. In abrasion, the material is worn from the surface by hard swellings on a counter face. While erosion is caused by hard particles striking the surface [10].

Removal of material by solid particles impact is probably the most pervasive of the erosion processes due to the utilization of fine particulates form in energy conversion plants and other combustion product particulates in flue gases in these plants. A major contribution to the material removal process is the repeated loading of the surface during multiple impacts [11], see Figure 2-1.

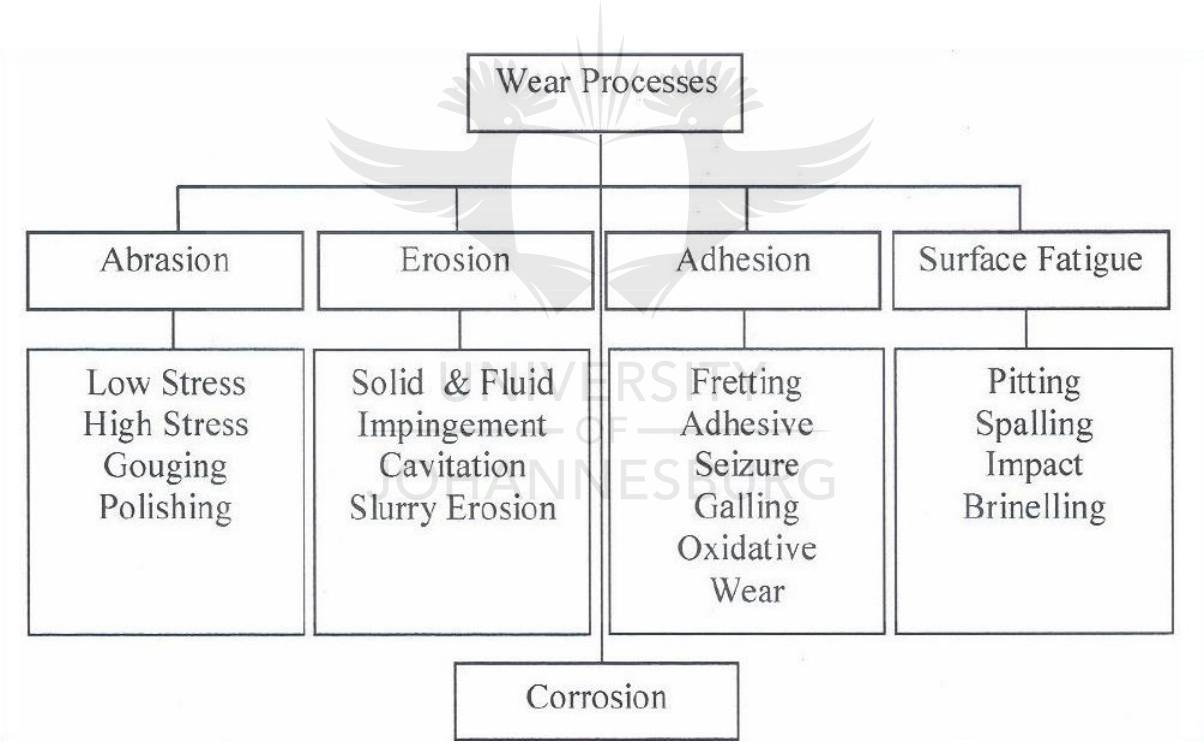

Figure 2 - 1: Types of wear processes [11].

2.9. Adhesive Wear

The basic view is that when two surfaces come into interaction, they adhere to one another at the localized spots. As the two surfaces move relative to one another wear formation transpires by one surface pulling the material out of the other surface at these spots. Adhesive wear mechanism is a single engagement process, similarly, apply to abrasive wear. During interaction material, either deforms breaks off or plucked out at that moment [13]. Pergamon [12], formation of adhesive wear, is produced when two surfaces are pressed against one another. The adhesion of material on one surface is produced by attractive atomic forces that operate in the areas of contact between two surfaces. This is normally resulting in fretting, where an oscillatory motion between the two surfaces is in contact. As the adhesive asperities' contacts are formed between the surfaces, the debris formed is oxides and fatigue cracks can be established [14].

Before adhesive wear formation is concluded, a general concept regarding the nature of the contact between two surfaces must be considered. The critical feature that should be always considered is the contact area. The contact area is usually determined by considerations of the macro-geometry or shape of the bodies in contact. This is usually done by geometrical projection or by models which take into account the deformation, elastic or plastic that materials display. The Hertz contact theory is used to determine the size of the contact region after the adhesive process has been formed. Physical contact takes place at localized spots within the area that is well-defined by the macro-geometry. The area of contact that is determined through the macro-considerations is called the apparent area of contact. Fundamental physical models regarding wear commonly are developed in terms of real area considerations, while engineering formulations and models mostly are related to the apparent area of contact. The points at which the actual contact transpires are referred to as junctions, the roughness characteristics of the surface have an important impact on the number of junctions formed, as well as on the ratio of the real area of contact to the apparent area of contact. The degree to which one surface penetrates the other can also influence by both these features. The size and

number of these junctions and their relationship to the apparent area of contact have been examined by both theoretical and experimental means [13].

To summarise, the most important points to be acknowledged about the contact between two bodies is that actual contact transpires at individual sites within an apparent area of contact and that the real area is usually only a fraction of the apparent area. The features witnessed in most micrographs of wear scars formed under sliding conditions support this view of the contact between two surfaces, as well as the overviews regarding the ratio of real and apparent areas, junction's size and number [13].

2.10. Abrasive Wear

Abrasive wear is categorized as the removal of material from a surface by hard particles sliding between the surfaces. The abrasive particles cause damage on the surfaces and in order to produce such damage, the abrasive particles must be harder than the substrate material to be able to gouge out the surface. Abrasive particles shape is very important because angular particles produce more severe wear than round particles. It is very challenging to evaluate angularity of the abrasive particles but friendlier to evaluate roundness factor using equation 2.5 [15].

$$F = \frac{4\pi A}{P^2} \tag{2.5}$$

Letter "A" is the area and "P" is the perimeter of the projection of the particle. After calculation has been performed and find that "F" is close to 1, this means that the particles shape is almost completely rounder. Abrasive wear can be produced through plastic deformation and brittle fracture and depended of the size of the particles. In many cases these two mechanisms occur at the same time although there are cases where they occur separately. Plastic deformation can be classified as cutting am ploughing modes. The difference between the two modes is that cutting requires high attack angle and ploughing depend on low attack angle. In abrasive wear, there is only ploughing because asperities on the surface have a very slow slope and therefore attack angle is very low. Brittle fracture involves the presence of cracks in the surface and subsurface. The wear mechanisms produced

is of plastic deformation and is mainly grooving. When the abrasive particles are in contact with the surface, scratches are produced creating grooves. Wear mechanism depends on materials properties like grain size, abrasive particle size, hardness fracture toughness and properties of the counter body [16].

In 1957 a researcher Archard has developed an equation by working previous work done by Holm to analyse wear when the deformation of the specimen is in plastic range [15]. The equation gives a relation between the volume of wear, the normal load and the sliding distance. Archard equation is defined by,

$$Q = \frac{K.W}{H} \tag{2.6}$$

Where “Q” is the volume removed from the surface per unit sliding surface, “W” is the normal load applied and “H” is the hardness of the softer material. “K” is the wear coefficient and it is dimensional and less than the unity. Archard equation is not used in brittle material because they have brittle fracture phenomenon, this equation is more suited for ductile materials [15].

Another researcher who found similar meaning of abrasive wear is Bayer [13], state that the contact situation that is generally considered for abrasive wear is different than that considered for adhesive wear. Abrasive wear transpires when material is displaced and/or removed from a solid surface by hard particles or protrusions on a counter face, which are forced against and are sliding sideways that surface. There are two general circumstances for abrasive wear that are identified, and these abrasive wear situations are illustrated in Figure 2-2 [13].

One condition is when hard materials of one surface are pressed against a softer surface. This abrasive wear circumstance is generally referred to as two-body abrasive wear. The second contact condition is one in which hard, loose particles are trapped between the two surfaces and the forces between the two surfaces are conveyed through these particles.

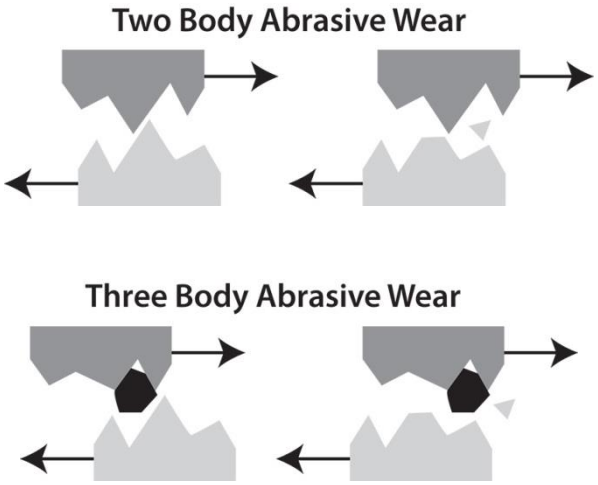

Figure 2 - 2: Illustrating two general situations for abrasive wear [13].

Abrasion is further categorised according to the stress imposed on the abrasive as well as the severity of surface damage. Low-stress abrasion is considered to occur when abrasive remains relatively intact throughout the wear process. High-stress abrasion occurs when the compressive strength of the abrasive particles is exceeded, and the particles are crushed during the wear process. Gouging abrasion describes a special case of high-stress abrasion where large chunks of abrasive material remove large fragments of material from the counter face. A common feature of all abrasive wear process is the indentation of the wearing surface by the abrasive particles, resulting in the formation of continuous grooves. In general, the abrasive wear rate is therefore strongly dependent on the hardness of the wearing material relative to the hardness of the abrasive [13].

The most common mechanisms of abrasive surface damage are ploughing, cutting and fracture. Ploughing is caused by rounded, blunt abrasives and is associated with the displacement of material to the edge of the abrasive groove and little material loss. Cutting results in the removal of material chips like those generated during lathe turning and is associated with sharp, angular abrasives and high abrasion rates. Surface fracture predominantly occurs in brittle materials and becomes more severe with increasing applied load, abrasive particle hardness and angularity, and decreasing fracture toughness of the wearing material [13].

Abrasive wear devices are generally considered to be any mechanisms by which the hard sharpness or particles cause damage in a single action. The damage or wear that they create is of two general types, deformation or particle formation (material removal). These two general types are frequently significant in the treatment and understanding of abrasive wear.

Note, a typically one-to-two order of magnitude decrease in wear rate is found when the hardness of the abraded surface exceeds the hardness of the abrasive. Another difference that is worthwhile to note is that the cutting action mode results in chips or particle formation and in addition to the formation of a groove. The deformation mode or ploughing as it is frequently termed, only results in the formation of a groove. This means that for cutting there is both a geometrical change as well as a material loss aspect to the wear, while for ploughing, only the former. In a wear situation in which abrasive grains are acting in a deformation mode, wear particles will eventually be generated but again, this will occur by means of another mechanism, probably fatigue [13].

It has been confirmed that the angle of attack in Figure 2 – 3, between the leading edge of the particle and the wearing surface regulates whether cutting will take place. Below a critical value, deformation takes place and the critical angle is predominantly determined by the coefficient of friction between the particle and the wearing surface.

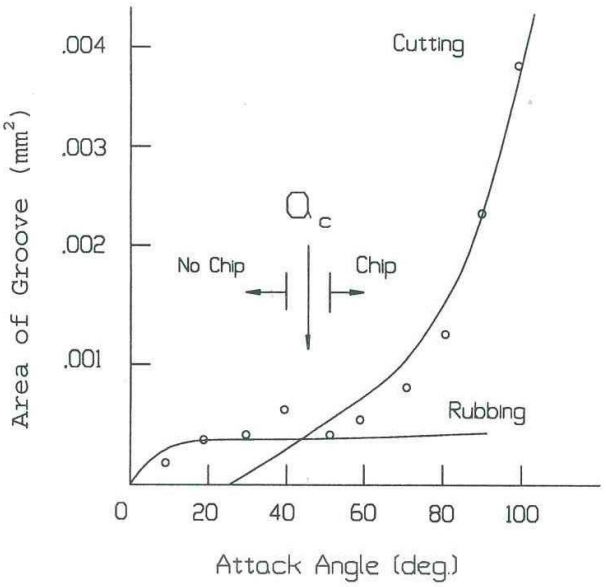

Figure 2 - 3: The effect of attack angle on chip formation in abrasion [13].

To this point, the treatment of the two abrasive modes which are cutting, and deformation assumes that the load between the abrasive grain and the wearing surface results from it being trapped between two surfaces or bodies. This implies a rolling or sliding situation.

2.11. Erosive Wear

Ubombo Sugar Mill impeller is constantly subjected to severe erosive wear. Erosive wear is initiated by impact or kinetic energy acting upon the impeller because erosive wear is referred to repetitive impact of solid particles or liquid droplets on a solid surface. Impact energy results from the impact of particles either solid or liquid against a solid surface. Kinetic energy result from the velocity of the particles, impact angle and size or shape of abrasive particles [17].

Erosive wear [17], is a function of particle velocity, impingement angle (known as impact angle) and type of roughness. Either liquid or solid particles or combination of both comes with velocity and impinge on a solid surface and convey some kinetic energy to the surface, during this stage an angle of impact will be an essential parameter. The main factor that takes part in wear formations is the mass of a particle as well as velocity particle. By increasing the velocity will increase the wear rate and impact angle will affect in either way but, depending on what type of

material being used. See Figure 2 -4, illustrating a damaged surface produced by hard particles that strike the surface.

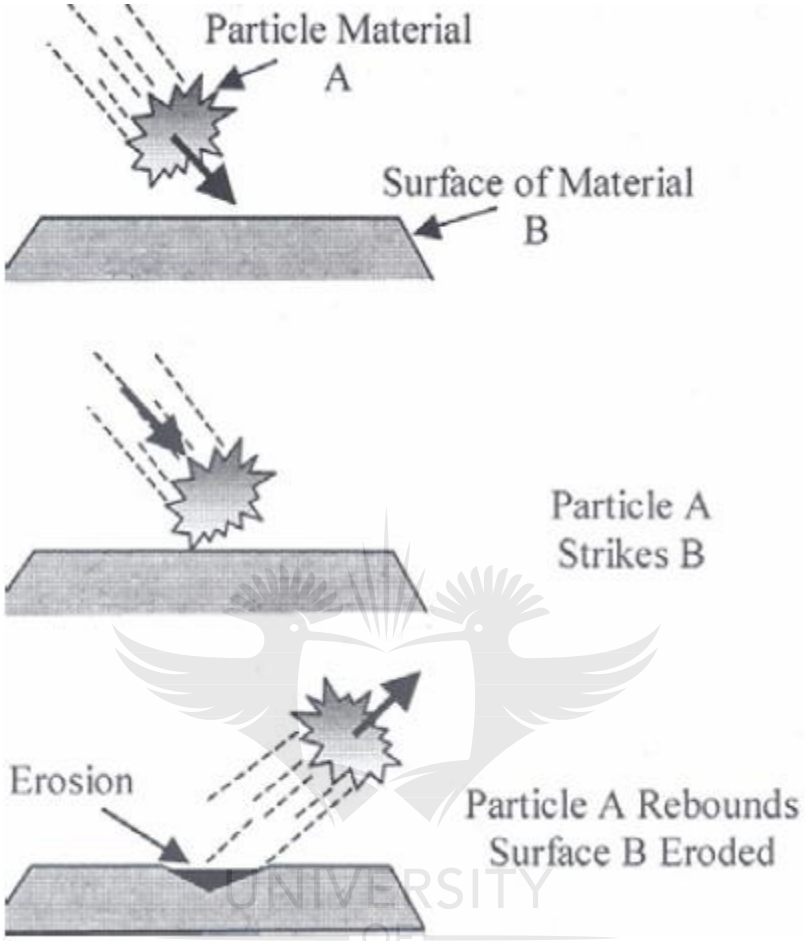

Figure 2 - 4: Wear produced by hard particles strike [18].

Different impact angles will have different characteristics. When particle approaches the eroded surface at a lower angle, the angle between 5° to 15°and collides with the surface, during collision shape of a particle will cause wear by trying to abrade the surface by cutting the surface. During this process shape of a particle does matter because particles work as a cutting tool and therefore wear takes part in a form of abrasion wear. To minimize wear, the hardness of the surface must be higher than the particle.

On the other hand, when the angle of impingement is large and is between 75° to 90°, to resist the wear, softer material will be required because most of the energy is transferred to the component and absorbed all this energy as a compressive load.

Material with more toughness has the capability to absorb energy. A proven theory state that wears by erosion can be calculated by using an equation. The theory behind the equation state that, “Particles either in solid or liquid, will travel at certain velocity onto a solid surface and impart some kinetic energy to that surface, as this movement takes place, angle of impact will be an important parameter [17] to determine the amount of material to be removed.

Particles increasing in particle size will increase wear rate, increase in velocity will increase wear rate and impact angle will affect either way but depending on what kind of material is used, whether a material can absorb the energy or hardness to resist the wear [17].

Referring to Figure 2 - 5a) and 7b), both low and large angle of impingement indicates that will have different characteristics depending on the material used. If a particle is coming at a low angle, then to resist the wear or reduce the wear, the hardness of the surface must be higher than that of the particle. Looking at the second graph, if the angle of impingement is higher, then a softer material will be required to absorb the shear stress. Softer material refers to ductile or rubber material. Therefore, wear will be reduced in this case compared to harder material which will fracture on the surface [17].

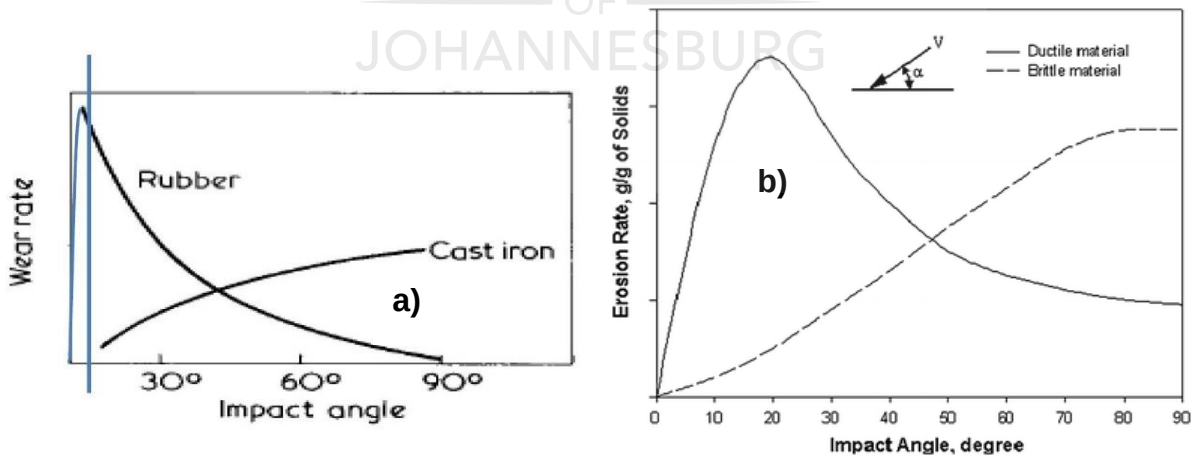

Figure 2 - 5:a) rubber vs. cast iron material illustrating rate of wear due to angle of impingement; and b) ductile vs. brittle material illustrating rate of wear due to angle of impingement [17].

By studying a softer material in Figure 2-5a which is the rubber, the graph indicates that this material can absorb energy and wear is very high at a lower angle due to a very low cutting resistance, but it can easily be chipped away. The layer of softer material can resist much more compression force compared to the shear force.

Impact angle cannot be necessarily defined from a distance away from the contact surface but is the angle of implementation just before the impact onto the affected surface. It has been indicated that the impact angle is the angle between eroded surfaces, the surface which is going to rotate and trajectory the particle immediately before the impact. If the impact angle is primarily very high or low but it changes as particles approach the eroded surface, then the angle at the last moment just before the collision shall be named impingement angle [17].

Research by Bayer [13], mentioned that it has been recognized that the angle at which the stream impinges the surface affects the rate at which material is detached from the surface and that this dependence is also influenced by the nature of the wearing material. This can be realized by considering the impact of a single particle with a surface. This angle defines the virtual magnitude of the two velocity components of the impact, namely the component parallel to the surface and the one normal to the surface. The normal component will define how long the impact will last in contact time (t_c) and the load. The product of the tangential velocity component determines the amount of sliding that takes place. The tangential velocity component also provides a shear loading to the surface, which is in support of the normal load that the normal velocity component formed. Therefore, as this angle changes, the amount of sliding that is produced also changes and as does the nature and magnitude of the stress system. Both of these characteristics influence wear [13].

These changes have indicated that different types of material would demonstrate different angular dependencies. As can be seen in Figure 2-5b, the result of the impact angle determining erosion rate is proven to be different for ductile and brittle materials, mostly at the peak erosion rate. These differences can be understood in terms of the main modes of damage related to these types of materials. As mentioned, the brittle fracture tends to increase the abraded wear volume over that

initiated by cutting or ploughing (plastic deformation). It was quantified that this could be as much as 10 times. As a basic rule, brittle materials are more likely to fracture under normal impact conditions (i.e. impacting velocity upright to the surface) than ductile materials. Consequently, as the erosive condition changes from a more grazing situation to a more normal impact, brittle materials would experience a greater tendency to undergo brittle fracture, which tends to cover the ductile or cutting contributions. For brittle materials, the erosion rate would then be expected to monotonically increase with the angle [17].

More research has been conducted by other researchers such as Finnie and co-workers [19] and discovered that for ductile materials the maximum erosion occurs at an impingement angle of approximately 20° whereby normal impact is estimated to be 90°. The experiment was done by considering abrasive cutting using a rigid angular particle in the surface of a ductile material. A constant ratio of normal to tangential force was expected with a force vector of constant direction. For this theory, the volume of material removed as a function of the mass impacting with a velocity of impact squared, the angle of impact and inversely proportional to the horizontal component of flow pressure and is related to the hardness between the particle and the material. This model of research did not describe the erosion of ductile materials at high impingement angles greater than 45° adequately. However, an improved analysis was conducted by Bitter [19] that described the erosion process to be consisting of two simultaneous processes. The two processes are as follows, cutting wear which dominates at low angles and deformation wear which dominates at high angles.

Tilly and co-workers [20] experiment described a two-stage process where large particles after impact produce small fragments that contribute to additional erosion. The fragmentation and outward flow of particle fragments caused additional erosion at 90°. Kanhere and Sheldon [21], investigations have shown velocity exponents of 2.3 and greater whereby increased fragmentation at higher velocities was used to explain this theory. This fragmentation included the particle size effect which had been observed experimentally where larger particles were found to be more prone to fragment and produce additional damage than fine particles. The investigation of the

role of particle embedment on the steady-state erosion of ductile materials by Ives and Ruff [22] found the embedded particles to be much smaller than the incident particles resulting from fragmentation upon collision. The investigated model for energy balance between the kinetic energy of the particle and the work expended during indentation which relates the erosion resistance of the material impact at 90° to Vickers's hardness to the power of 0.667 [23].

Concerning the erosion of ductile materials where erosion is maximum at an impingement angle between 20° and 30°, the erosion of brittle materials is found to be maximum at 90° which refer as normal impact. Brittle material is normally referred to materials such as ceramics, glasses and thermosetting polymer matrices in composite materials. Hertzian theory of impact [24, 25, 26, 27] has been used by numerous researchers to investigate the impact of solid particles on brittle materials to analyse the collision of elastic bodies in an elastic half-space. Even though the quasi-static stress distributions from this investigation were not accurate at moderate impact velocities, considerably wider applicability of the estimates for sizes of contact areas durations of impact has been found than would be expected based on the assumptions of the theory. Hertzian theory impact assumed that the cone and ring cracks which are formed intersect and with a sufficient number, this will result in mass loss occurring on the surface by a breakout of chunks of material. Radial cracking occurs and results in strength degradation, Adler [25], also confirmed this process experimentally by expanding the analysis. Evans, Gulden, Eggum and Rosenblatt [27] have produced an alternative theory to the Hertzian analysis which was based upon dynamic plastic indentation which has the features of plastic deformation of the contact area between the particle and the target material where radial cracks presumed to be propagating outward from the contact area and lateral cracks that initiated beneath the contact area and propagate between the radial cracks on planes nearly parallel to the surface.

There are five different types of erosive formation, namely, solid particle, liquid impact, liquid erosion, slurry erosion, and cavitation.

2.11.1. Solid Particle Impact Erosion

Solid particle impact erosion refers to damage on a surface caused by impingement of the solid particle transported by gas. The degree of damage is generally a function of the mass of particle impacting a surface with sharp corners at a given angle of impingement with a velocity [1]. This form of wear normally occurs in particle carrying systems such as fans and cyclone separators. Standard test method of conducting erosion tests by using solid particle impingement using a gas jet is ASTM G 76 [1].

As per ASTM G 76, Air jet erosion test system controls a repeated impact erosion approach containing a small nozzle delivering a stream of gas having abrasive which impacted the surface of test specimen [28]. The quantity of weight loss per unit of time signifies the erosion or wear rate providing laboratory-scale erosion measurements under a range of situations [28]. The test arrangement may be used to rank the erosion resistance of a material, weldments, coatings, plating's, epoxies, paints sprays and similar products under the controlled surroundings of the test. The system uses dry air of 689KPa max and a nozzle tube to control particle velocity and a variable media feed nozzle to control the particles fed rate of the abrasive impacting the test sample. An adjustable test sample holder controls the angle of incidence from 15° to 90° [28].

A particle within the gas approaches the surface with a rotational movement when impacted on the surface and behave as tiny cutters to form chips. Material is then subjected to fatigue mechanism, where particle forms a crater and repeated strikes hit the extended material around the crater until the lips eventually fracture. As stated, the effectiveness of larger grains can be less influenced by surface roughness and debris clogging effects than smaller grains. With naturally arising particles it is frequently difficult to separate sharpness and size. Therefore, it has been recommended that in certain cases that the larger particles may just be sharper. As with most characteristics of wear all of these effects probably contribute to the overall tendency with some being more important than others in particular conditions [13].

This tendency is shown in Figure 2-6. In all circumstances, there appears to be an almost linear relationship between wear and sizes up to approximately 100 μm, but above that size wear start to be independent of particle size. However, it has been suggested that in addition to the characteristics mentioned, particle loading could also take a role. As for size increases, the number of particles involved at any instant may change probably decreasing. As a result, the load per particle would increase. These two effects would be likely to offset each other. Under certain circumstances, they could cancel and stable wear behaviour as a function of size results [13].

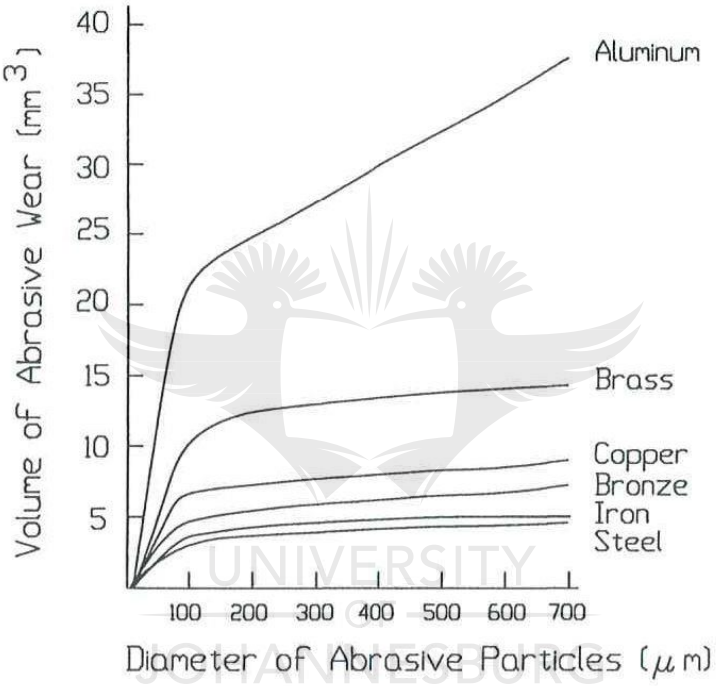

Figure 2 - 6: The influence of abrasive particle size and wear [13].

2.11.2. Liquid Droplet Impact Erosion

This form of erosion is formed by impingement of liquid droplets on a solid surface. A test can be performed by following test standard, ASTM G 73. Test for liquid impingement erosion test uses a sample at the end of a propeller that can rotate at a certain speed. The propeller rotates in an artificial rain field and damage to the specimen is measured as a volume loss versus time [1].

2.11.3. Slurry Erosion

Material removal caused by slurry motion over the solid surface. This form of erosion mainly occurs in pump handling drilling, mine water, and other conveying slurries in pipelines. Test standard, ASTM G 75 state a guide to ability of a material to resist erosion. The rate of wear is similarly affected by the same factors affecting solid particle erosion, the mass of particles that impact the surface, shape of the particle and its velocity. The phenomenon of slurry erosion is like that of solid particles. However, slurry systems usually involve parallel flow and the action of the particles is close to scratching [1].

2.11.4. Liquid Erosion

This form of wear is identified by subtraction of material by the action of liquid impingement or moving along the surface of a solid. This normally takes place inside piping made from materials that depend on a passive oxide layer for corrosion resistance. Materials that do not depend on passive oxide films such as plastics and ceramics are immune to this form of erosion. This erosion has limits that are based on a level of velocity. Therefore, regulating velocity to a lower value eliminates the occurrence of erosion [1].

2.11.5. Cavitation

Cavitation erosion is a result of damage to a solid surface, due to the formation of bubbles within a moving liquid or around a body which is in relative motion to the liquid. The bubbles are formed due to a sudden drop in pressure relatively to vaporization of the liquid. When bubbles move to the high-pressure area, liquid droplet collapse rapidly and cause shock pressure and explodes near the surface. The shock pressures cause material damage by a surface fatigue mechanism. When a bubble collapses, the surrounding liquid rushes in to fill the void. A jet is established which can develop stresses that can exceed the yield strength of materials. The mechanism of material removes is a microscopic fracture to form pits [1]. There is no universally applicable model to describe the influence of material properties on cavitation erosion resistance. Increasing hardness, the strain energy to

induce fatigue or tensile fracture, as well as a mechanism for absorbing cavitation energy, such as work hardening, have all been shown to be desirable properties for different materials. The most successful approach to limiting cavitation damage is through appropriate engineering design [1].

2.12. Wear Behaviour

Wear behaviour, Raymond G Bayer [29, 30], stated that wear behaviour is primarily built around wear mechanisms and wear phenomena. This provides an overview of wear and its complexity that is an essential value to the design engineer. The scientist is directly concerned with the identification and understanding of the mechanisms involved. The material engineer is concerned with the association of material properties to these mechanisms so that materials can be designed and developed to withstand these mechanisms. On the other side, the designer tends to view the wear state in terms of operational parameters and has the objective to select or establish a design that has the desired wear life. Consequently, treatment of wear behaviour in terms of operational parameters would be directly useful to the designer. This can be established by considering the relationship between three major operational characteristics to wear behaviour, namely:

- The nature of the impact
- The type of motion-related with the contact
- The environment surrounding the contact

In terms of the nature of the contact, it is useful to consider two comprehensive classifications. First, is two-body contact, this covers the contact among two solid bodies. The other common grouping is a single body in contact with a fluid or stream of particles. It is also useful to classify and define several broad classifications of motion that can be related to the two types of contact.

For the two-body contact condition, there are sliding rolling and impact motions. On the contact among fluid and single body, typical classifications are non-cavitation flow or cavitation, turbulent flow or streamline, and low angle or high angle particle impingement. These are a few major environmental groupings which are useful to consider for common design purposes. Among these are environments with and

without hard particles (abrasive and non-abrasive environments), lubricated and non-lubricated environments, and hostile or non-hostile ambient environments. The last type would include temperature as well as gaseous elements.

Before looking at wear behaviour in terms of these classifications, it is worthwhile to consider some of the more general characteristics of behaviour in relationship to design and design practices. Design methodologies to wear must identify the following characteristic of wear:

2.12.1. Wear is a system problem and not a material problem.

2.12.2 Materials can wear by variation of mechanisms and combinations of mechanism and subject on the Tribosystem in which it is used.

2.12.3 Wear behaviour is regularly nonlinear.

2.12.4. Transitions can occur in wear behaviour as a function of a wide selection of parameters.

The complexity of this condition can be decreased to a substantial degree by classifying wear situations according to operational aspects.

2.13. Particles Sizes

The dust particles are of different sizes because of their actual mode of origin such as crushing, weathering, abrasion, grinding and growth. The size also fluctuates around a mean value. Thus, the factor to be measured is not the particle size but the particle size distribution. The measurement process is therefore termed grain or particle size analysis and involves two stages, namely, measurement of the particle size arising and determination of the particle size distribution (volume proportions). For dealing with the methods for making these measurements shall base the analysis on two types of processes, namely, Particle analysis under the microscope and laser diffraction analysis.

For survey of particle sizes analysis methods, as stated earlier, particle size analysis involves measurement of the particle sizes and determination of the particle size

proportions. These two operations necessitate some separation of the particles present as a function of microscopic size of the particles.

In microscopic particle size analysis, the size of the particles is measured in the micrograph and the proportion is found by counting with reference to the size. In this method, the particles are treated collectively but in counting they are dealt with individually one after the other. Microscope analysis is a direct measurement method applicable to all particle sizes in the optical and electron microscope ranges. This method therefore covers the size range of all dust particles encountered. Another method of analysis is to use an Analysette 22 MicroTec Plus, an analysing device for particle measurement of suspensions, emulsions and solid matters that utilizes laser diffraction.

The device has central measuring unit and a dispersion unit. An ultrasonic water bath comprises the wet dispersion unit and can bring vibration at the power output of 50W of and deliver frequency of 40 kHz to the liquid. The laser diffraction method makes use of a laser light which is scattered by suspensions particles that are passing through. Depending on the size and optical properties of the particles, the light scattered at three-dimensional angle. A Fourier lens concentrates the scattered light into the focal plane of a detector array which measures the light intensity distribution due to the light scattering. Based on the light distribution obtained, the size distribution of particles is calculated.

Another two analysing methods that can also be used but not considered in this research are Sieve analysis and sedimentation methods. Sieve analysis, suitable movement of the dust on these sieves permits statistical comparison with the size of the holes and removal. In this method, the collective is split up into various categories with combined particle size measurement and removal with "n" sieves (n + 1) particle size categories will be obtained. Granular material with particle sizes is graded into size categories, almost exclusively by sieving methods. The grading or separation is affected by sieves, which are sets of surfaces containing uniform size holes and by suitable movement of the granular material relative to the sieves. The particles larger than the holes remain on the sieves, whereas the finer particles pass

through it. The two components thus produced are called the residue and the passage respectively.

On experimental mechanical sieving, generally several sieves are arranged in series. The material to be separated is placed on the top sieve and after complete separation the only particles remaining on the individual sieves are those larger than the holes in all sieves.

Sedimentation analysis, this method is one of the traditional methods of particles size analysis applicable to particles between 0.02 μm to 200 μm. The method determines the particle size indirectly from its sedimentation rate when exposed to gravity or centrifugal force in either liquid or gaseous environment.

2.14. Effect of Particle Velocity

Many authors have carried laboratory tests for wear erosion, to understand the cause and formation of the phenomenon. The research has been performed to understand the effect of erosion wear concerning impact angle and particle velocity. Their research revealed that the rate of erosion is dependent velocity and impact angle [30].

Some of the researchers performed the tests, their summary of the research are as follows:

- Lindsley and Marder, – investigated the effect of velocity on the solid particle erosion rate of alloys. “Their results revealed that erosion rate is dependent on velocity” [18].
- Matsumura, - investigated the effect of surface damage at a different impacting angle. Finding was “peak erosion rate occurs between 30° and 50° on ductile material” [31].
- Finnie, - - performed similar research as Matsumura. Results reveal that “peak erosion and wear rate occurred between 15° and 40° for ductile material” [32, 33].

- Stackwick and Batchelor, - also conducted a test using brittle material, results indicated that “erosion and wear rate increase with increasing impact angle reaching the peak at 90°” [34].
- Islam and Farhat, - conducted a test and their results presented that at low abrasive feed rate, “erosion rate decreases with increasing impact angle. Increased particle velocity resulted in increased erosion rate [35].

Another test was carried by Axinite, using a standard test method for conducting erosion tests by solid particle impingement using gas jets – ASTM G76-13. The test was carried over four different velocities and impact angle of 30° and 90°. These are common angles which many authors based their tests. For ductile material, the erosion rate is high at 30° and low at 90° [36].

“The results indicate that impinging surface at 30° and different velocities headed to increasing weight loss compared with impinging the specimens at 90°. It is proven that weight loss at 30° is much higher than that at 90° impact angle at the same testing velocities and period in terms of time, presenting the influence of impact angle in material loss. There is an indication that erosion rates of all ductile material increased with increasing particle velocity for the two-impact angle when ductile materials impinged with solid particles. The results also display that the erosion rate of eroded surface impinged at 30° is higher than that impinged at 90°. The theory explained further by using Figure 2 - 7 [30].

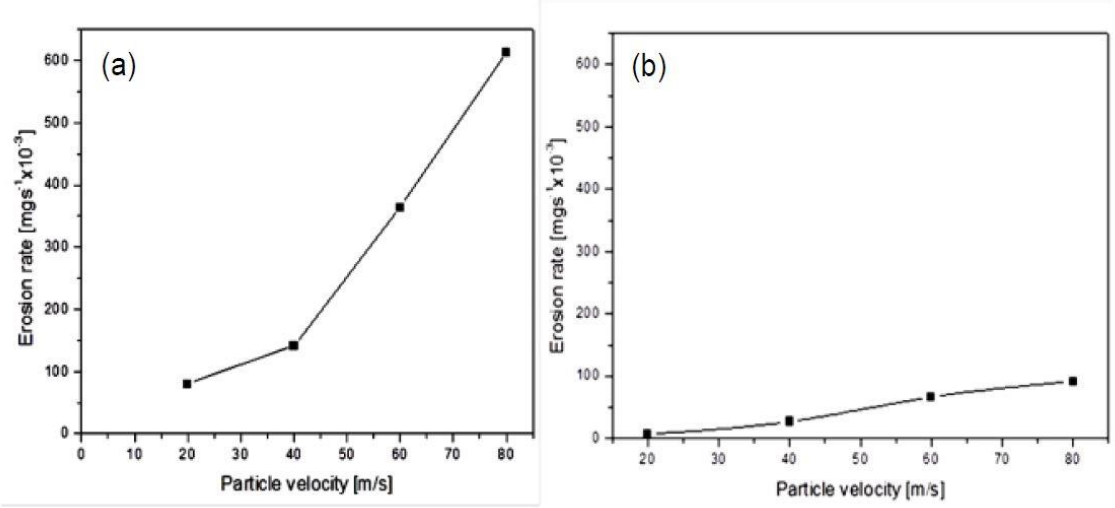

Figure 2 - 7:Erosion rate vs. particle velocity for 30° impact angle. b) Erosion rate vs. particle velocity for 90° impact angle [30].

2.15. Hardfacing

Metal components which are subjected to wear may be protected or repaired by welding a suitable alloy onto its surface. Choice of weld metal will depend upon the following factors:

1. Composition of original components.
2. Amount of metal to be replaced.
3. Type of wear conditions encountered in service.
4. Economic lifetime expected of component.
5. The economic justification for repairing rather than replacing.

The above five mentioned factors can be elaborated in the following manner [37]:

1. The material must be weldable and metallurgically compatible with proposed weld metal.
2. The weld metal must meet the mechanical requirements of the application. Too many layers of hard weld metal may crack and fracture under load. Buffer weld metal may be required before final hardfacing. The buffer weld refers to layers that are smeared when the base material has low weldability or to moderate the dilution when welding highly alloyed

consumable. For example, austenitic buffers will discontinue cracks from progressing into the base metal.

3. The relationship between impact, abrasion, corrosion, and erosion must be established before a suitable welded alloy can be identified.
4. Over-engineering should always be avoided, and hardfacing with an expensive material which outlasts the rest of the unit is not desirable. If components are in contact with others it may be beneficial for the one which is more easily replaced to wear preferentially to the other one. Care should be taken in choosing the wear resistance of the alloy to be welded onto such components and the use of hard alloys which may increase the wear of the other component should be avoided.
5. If the cost of repairing is greater and the expected economic life does not exceed that of the original part, then there is little point in welding the component. Yes, there may be some exceptions to this such as the non-availability of replacement parts.

After establishing the most suitable alloy for a certain application, the most economical method of welding should be identified. A major factor governing the cost of welding is the deposited rate. Low rates necessitate high labour costs which invariably exceed the cost of the weld consumable. However, if deposit quantities are small, this may not be such an important factor and a highly flexible process may be applicable. Inspection and understanding of wear mechanisms as well as knowledge of the response of alloys to these mechanisms will help to identify the type of alloy best required for an application [37].

2.16. Computational Fluid Dynamics

Computation fluid dynamics is a methodology that is used to solve the distinct solution of real engineering fluid flow problems [38]. This is a tool that can be used to provide a quantitative prediction of fluid flows through mathematical modelling, numerical methods, pre-processing and post processing utilities [39]. Governing equations for fluid motion under mathematical formulation are fundamental principles of mass, momentum and energy conservation. Computation fluid dynamics tool

requires boundary conditions and initial conditions to be specified to setup and initial computation. Boundary conditions that are required by governing equations depend on the equation itself and the form that it has been quantified. Common boundary conditions are classified either in terms of numerical values that must be set or in terms of the physical type of the boundary condition [40].

The physical boundary conditions that are required to be identified in the fluid problem solving are a solid wall, inlet, symmetry boundaries, periodic boundaries, pressure boundary condition, outflow boundary condition, opening boundary condition, and free surface and interface. After constituting all required physical boundary conditions, fluid flow simulation computation is run from the adequate computer [39].

Computation fluid dynamics simulation results are depended on the degree of uncertainty and the cumulative effect of various errors. Validation of results depends on evaluating computational results with analytical and numerical solutions. The desired goal of validating results is to ensure that the computation fluid dynamics produces reasonable results for a certain range of acceptance.

2.17. Summary

This Chapter has identified most of the types of wear that have been discovered by other researchers in the past years. Most of the discoveries were proven through tests in the laboratory and later related to actual existing problems on-site, but it appears that not many researchers have correlated their research with centrifugal fans installed in sugar mill plants to understand the formation of wear. Given that the technology has improved and there are fluid computations simulation programs that can be used to simulate fluid flow pattern inside the centrifugal fan, this dissertation will focus more on investigating wear taking place in sugar mill plants fans and correlate with CFD results.

CHAPTER 3: METHODOLOGY

3.1. Theoretical Approach

CFD analysis shall be used to determine the angle of impingement. The expectation underflow simulation is that the angle of impingement on ductile material should be between 10° and 55° to have an impact on influencing the wear that is taking place on the impeller and brittle material should be between 60° and 90°only if the rate of wear is abnormal. However, if the rate of wear between the two materials is occurring at the same rate, then the angle of impingement will be impacting onto the impeller at an angle of 55° according to Figure 2 – 5b.

At a low angle between 0° and 10°, the expectation is that the reaction of wear on brittle material (Hardox 500) will be slower than that of ductile material (Weldox 700) on the blade leading edge. Therefore, this implies that the adequate material construction of the impeller should be brittle. This theory is referring to Figure 2 – 5b. Correct data such as those stipulated in Table 5 - 4 shall be used to conduct a simulation to achieve appropriate air velocity pattern during impact taking place on the impeller. Impingement angle will be determined and measured as illustrated in Figure 3 - 1. Dotted lines with arrows represent the direction of the air motion passing through the impeller. Tangential lines parallel to the flow will be projected starting from the inner surface of the backplate to the inlet of the impeller to determine and measure impingement angles with a datum line taken from the impeller backplate. The angle of attack will be represented by D_1, D_2, D_3 and D_4 as indicated on the schematic layout under Figure 3 - 1.

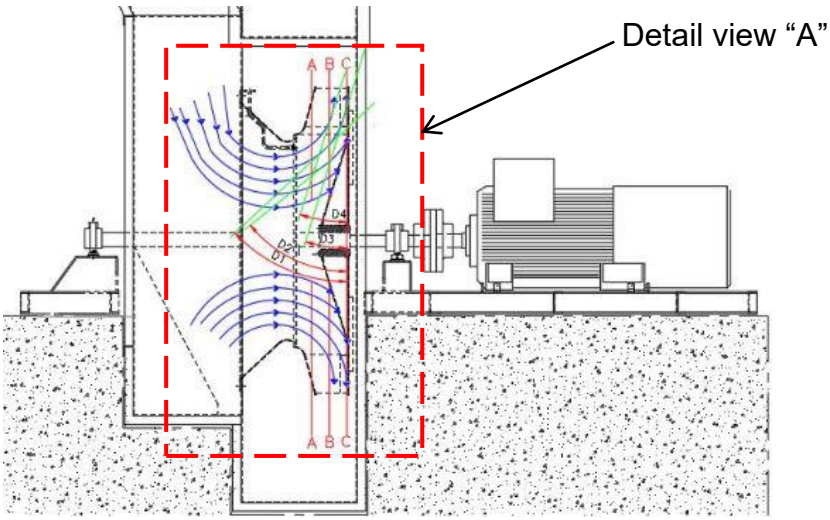

Figure 3 - 1: Fan sectional view illustrating impingement angle of attack to be measured on the simulation

After determining the impingement angle and the area in which particles are striking on the surface of the impeller. A comparison between the way particles strike the surface and the way wear has formed itself on the impeller will be investigated. The way wear has been formed on the impeller has been indicated on pictures under appendices section A. A comparison will be part of assisting in validating flow simulation results.

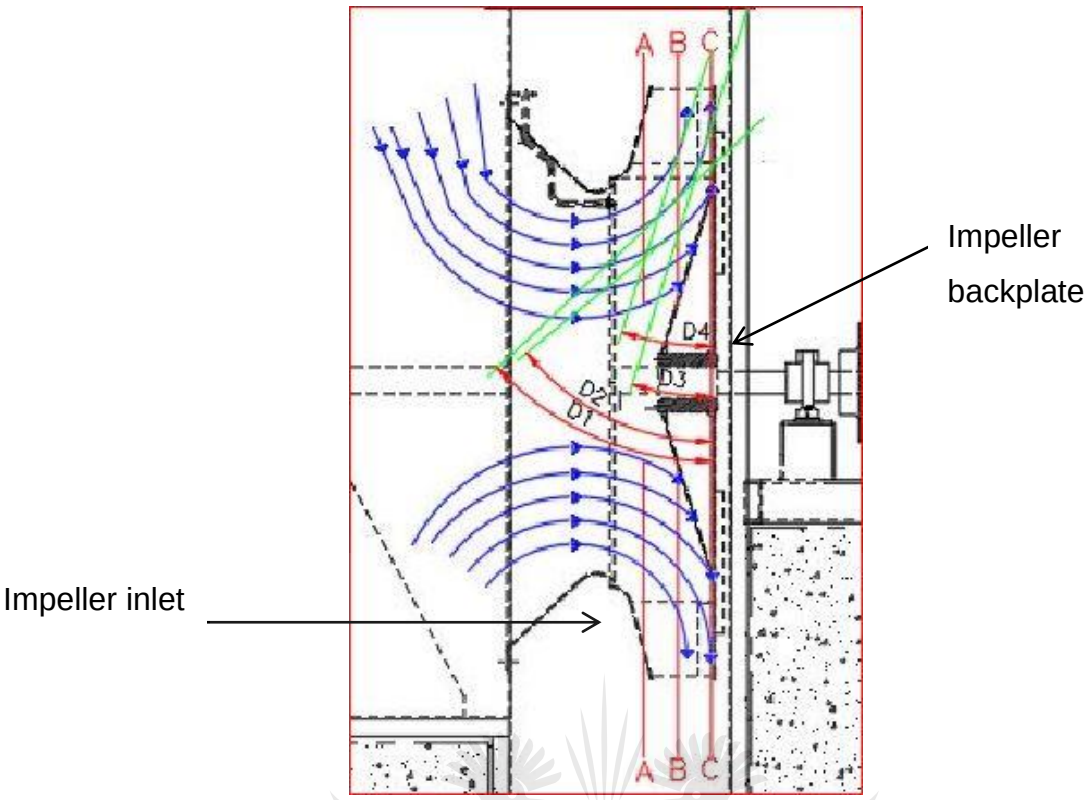

Figure 3 - 2: Detail view "A" showing enlarged measuring points of impingement angle taken the from fan section view in Figure 3-1.

Plane A-A, B-B and C-C shall be equally split along the width of the impeller. These planes are going to be set as datum lines to allow consistency of measuring on same points to make sure that appropriate degree of control, appropriate measurements, and analysis techniques are implemented. Width 'W' of the impeller shall be reference from the impeller inlet to the inner surface of the backplate. The 'W' will be divided to achieve 3 equal distances. Actual impeller width is 438mm, this will result in 3 equal distances of 146mm. Provision on plane C-C can be made by offsetting the plane by 3mm away from the backplate to be able to measure the angle of attack and particle velocity just before the impact.

Materials used in the construction of the impeller will normally plan an important role during wear formation. The material used for impeller construction is Weldox 700 and this base material has ductility properties compared to Hardox 500 material which was used to wear liners construction that is welded onto the impeller. Therefore, is very crucial to understand material property, whether ductile or brittle. Jan Drotsky [41] stated that materials may be classified as being either ductile or

brittle. The classification can be elaborated as follows, if a ductile material is subjected to an increasing tensile load it will elongate considerably and after the ultimate strength has been reached a large reduction in the cross-section will occur in the region of failure. Ductile materials fail due to shear and if the specimen is cylindrical, the fracture will be of the cup-cone type. A specimen with a rectangular cross-section will fail on a plane at 45° to the line of action of the applied force. Brittle materials undergo little or no plastic deformation and failure occur on a plane perpendicular to the axis of the specimen. This coincides with the plane on which the maximum direct stress occurs. Steel with a percentage elongation less than 13% or with a Brinell hardness greater than 300 may be classified as being brittle.

By applying theory stated by Jan Drotsky to classify which material is ductile or brittle between Weldox 700 and Hardox 500 First, comparison between Brinell hardness of the two materials is done to find out which material is rated above 300 Brinell hardness. After the comparison has been done, we found that Weldox 700 [8] ranges from 260 – 310 Brinell hardness. Hardox 500 [9] is found to be ranging from 470 – 530 of Brinell hardness. The second comparison was based on elongation between the two materials. Weldox 700 is found to have an average elongation of 14% which is sitting at the boundary of brittle material [8], while Hardox 700 has an average elongation of 10% [9]. This coincides with the theory and thus concludes that Weldox 700 is classified under brittle material because Brinell hardness is up to a maximum of 310BH and elongation is close to 13% while Hardox 500 is also classified under brittle material because Brinell hardness is above 300 and elongation is below 13%.

3.2. Velocity of Solid Particles

Under the same flow simulation with the same data used to initiate simulation under 3.1.1, velocity induced through the impeller shall be measured in the manner as illustrated in Figure 3 - 3. Velocities shall be measured along with the impeller, across the planes indicated on the schematic layout. The first point of velocity measurement will be on plane A-A from the side of the impeller inlet, second measuring point to be on plane B-B and the last measuring point to be on plane C-C.

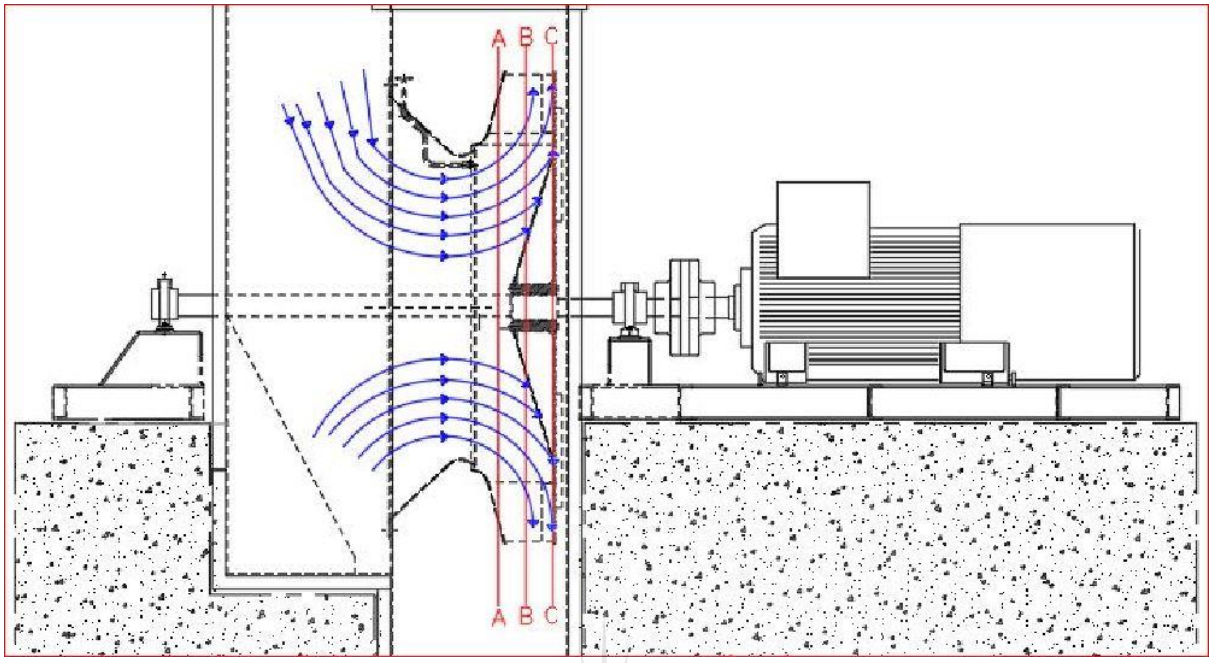

Figure 3 - 3: Fan sectional view illustrating velocity air motion to be measured on the simulation.

3.3. Shape and Size of Solid Particle

Solid particle inside gas substance approaches the eroded surface with rotational movement at certain velocity and angle. As particles impact the surface abrasion wear is formed. Particles erode the surface with a rotational movement during the impact or sliding effect. Therefore, identification of the solid particle's shape and size is essential. Shape and size of the solid particle will be determined under a microscope. Solid particle shall be evaluated under the microscope to analyse and observe the structural sharp edge shape. Several different methods can be used to measure the size of particles according to their basic physical properties. Under the micrographs of these particles, the expectation is that the shape of the particles could have contained sharp edges that are able to cut out material surface through rotational movement during the impact or sliding effect.

3.4. Summary on effect and wear formation

This Chapter will focused on an investigation to understand fluid flow pattern to be able to construct impingement angles as the flow become in contact with the impeller. In order to construct impingement, angles must be determined from the velocity vectors. This does not leave out the size and shape of the particles, a clear understanding of particle sizes to follow the fluid pattern was researched including edges of the particles because they have effects when they impact on the impeller.

CHAPTER 4: BAGASSE AND SCRUBBER ANALYSIS

4.1. Introduction

This Chapter stipulates how the bagasse ash particles were analysed in the laboratory to determine size and shape. The particles will be analysed by visualization as well as analysing the particles sizes and shapes. The particles have been analysed on a microscope to identify shapes and geometry. A Sieve Analysis Screen was also used to identify particles sizes. The analysis method also covered investigation on the cause of scrubber poor performance resulting in inadequate filtration. As for scrubber analysis, the ineffectiveness of the scrubber will be based on evidence and factors accumulated during site visit inspection for the wet scrubber.

4.2. Testing Methodology

The dust particles are of different sizes because of their actual mode of origin such as crushing, weathering, abrasion, grinding, and growth. The factor to be measured is not the particle size but the particle size distribution. The measurement process is therefore termed grain or particle size analysis and involves two stages, namely, measurement of the particle size arising and determination of the particle size distribution (volume proportions). For identification of sizes measurements and shapes, two types of processes have been used, namely, Particle analysis on the microscope and sieve analysis [13].

For a survey of particle size analysis methods, as stated earlier, particle size analysis involves measurement of the particle sizes and determination of the particle size proportions. These two operations necessitate separation of the particles present as a function of microscopic size.

In microscopic particle size analysis, the size of the particles is measured in the micrograph and the proportion is found by counting with reference to the size. Microscope analysis is a direct measurement method applicable to all particle sizes

in the optical and electron microscope ranges. This method, therefore, covers the size range of all dust particles encountered [13].

Another method of analysis is to use a set of surfaces each containing identical size holes in succession known as sieve analysis. Suitable movement of the dust on these sieves permits statistical comparison with the size of the holes. In this method, the collective is split up into various categories with combined particle size measurement and removal with "n" sieves (n + 1) particle size categories will be obtained. Granular material with particle sizes is graded into size categories, almost exclusively by sieving methods. The grading or separation is affected by sieves, which are sets of surfaces containing uniform size holes and by the suitable movement of the granular material relative to the sieves. The particles larger than the holes remain on the sieves, whereas the finer particles pass through it. The two components thus produced are called the residue and the passage respectively.

Experimental mechanical sieving are generally several sieves that are arranged in series. The material to be separated is placed on the top sieve and after complete separation, the only particles remaining on the individual sieves are those larger than the holes in all sieves [13].

4.3. Particle Size Analysis

Bagasse and coal ash together with water samples were collected from inside of the venturi wet scrubber after the scrubber being switched off for over a month for maintenance purposes. These samples were sent to a laboratory to analyse chemical composition. The aim of this test was to determine particles sizes, a composition of mass percentage, element and mass of a chemical or contaminate per unit volume of water. Picture of the sample is shown in Figure 4 - 1, this looks like black powder or sand. These particles have a variety of shapes and sizes.

Figure 4 - 1: Bagasse ash sample taken inside the venturi wet scrubber.

Particulate matter emissions were placed under a microscope to determine the shape and size of the fine particles. Figure 4 - 2, shows a bagasse ash particle under a microscope x50 magnification. Particles observed under a microscope have round ball shape, while most of the particles have irregular shapes with sharp edges with a metallic texture (probably iron) and others look like a molten glass or rock. Visualising the pictures 0441 and 0442, it can be seen that there are clear coloured glassy particles and they are quite a few of them and have sharp edges, this can be associated with 66.4% of SiO2 stated under Table 4 - 1. Particles look like charcoal were observed together with metal oxide (rust), but this is difficult to tell exactly what their individual composition is when using the microscope. Figure 4 - 2, indicates pictures of particles taken under a microscope

When counting different types of particles shapes from picture 0441 until 0477 and average these numbers of the sizes, round shapes are significantly less than the irregular shapes and most of the particles with sharper edges are more and larger. As stated earlier, the effectiveness of larger grains can be less influenced by surface roughness and debris clogging effects than smaller grains. As the particles appear, it

is difficult to separate size and sharpness. Therefore, it has been suggested that in certain cases the larger particles may be sharper.

Figure 4 - 2: Bagasse ash sample pictures after being taken placed under microscope and magnified to x 50. This Figure illustrates types of particles found inside wet scrubber.

A further test was performed to work out sizes and the shape of the particles by cutting a cross-sectional view through samples. Figure 4 - 3, shows bagasse ash after being magnified to x 100 and gives approximate sizes of particles to support results given in Figure 4 – 4 and Figure 4 – 5 and Figure 4 – 2 to Figure 4 – 3, reveals that there are two major shapes found under microscope, round shape and sharp edges. Measuring of sharp edge angles could not be achieved due to the equipment and instruments capabilities. In this regard, actual angles of the sharp edge have been disregarded.

As seen in Figure 4 – 2 to Figure 4 – 3, the majority of the particles are the glassy coloured particles and most of these particles have sharp edges. These particles can

be associated with 66.4% of SiO2 stated in Table 4 - 1. These particles due to shape and quantity might be responsible for most of the wear taking place on the impeller. The brown particles can be associated with stones that are fed in the system as part on the soil stuck on the sugar cane roots. Soil aspects such as particle size can affect the amount of particulate matter emissions from the boiler. If the sugar cane is inadequately washed or imperfectly prepared, this can also affect the bagasse ash content [7].

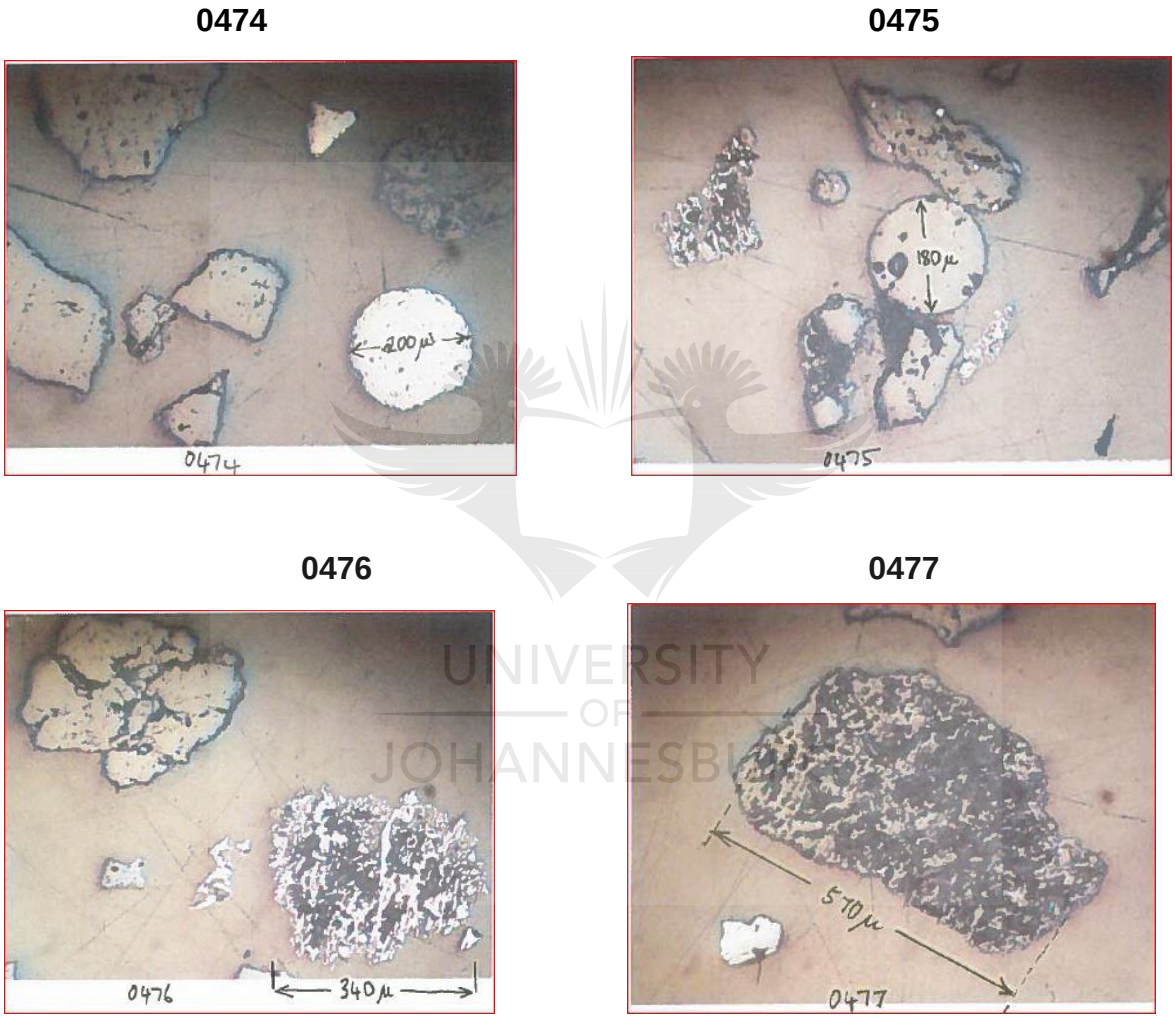

Figure 4 - 3: Bagasse ash sample pictures after being taken placed under microscope and grinded to view sectional view with magnification of x 100. This Figure illustrates sizes of particles found inside wet scrubber.

By analysing of laboratory results shown in Figure 4 - 4, this shows that particles found inside the venturi wet scrubber start from 14.5 μm. Common particles sizes found in the boiler fly ash range from 1µm to over 100µm.

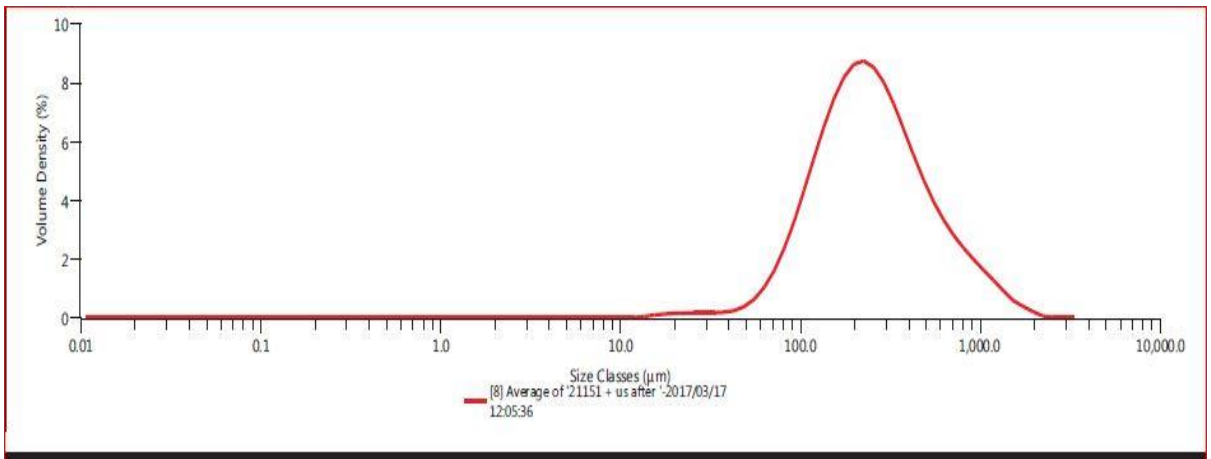

Result

Size (µm)	% Volume Under	Size (µm)	% Volume Under	Size (µm)	% Volume Under	Size (µm)	% Volume Under	Size (µm)	% Volume Under	Size (µm)	% Volume Under	Size (µm)	ılume Under
0.0100	0.00	0.0771	0.00	0.594	0.00	4.58	0.00	35.3	0.84	272	57.18	2100	99.97
0.0114	0.00	0.0876	0.00	0.675	0.00	5.21	0.00	40.1	0.98	310	63.89	2390	100.00
0.0129	0.00	0.0995	0.00	0.767	0.00	5.92	0.00	45.6	1.18	352	69.97	2710	100.00
0.0147	0.00	0.113	0.00	0.872	0.00	6.72	0.00	51.8	1.48	400	75.34	3080	100.00
0.0167	0.00	0.128	0.00	0.991	0.00	7.64	0.00	58.9	1.99	454	79.95	3500	100.00
0.0189	0.00	0.146	0.00	1.13	0.00	8.68	0.00	66.9	2.82	516	83.85		
0.0215	0.00	0.166	0.00	1.28	0.00	9.86	0.00	76.0	4.14	586	87.14		
0.0244	0.00	0.188	0.00	1.45	0.00	11.2	0.00	86.4	6.09	666	89.90		
0.0278	0.00	0.214	0.00	1.65	0.00	12.7	0.00	98.1	8.82	756	92.24		
0.0315	0.00	0.243	0.00	1.88	0.00	14.5	0.02	111	12.42	859	94.21		
0.0358	0.00	0.276	0.00	2.13	0.00	16.4	0.10	127	16.96	976	95.87		
0.0407	0.00	0.314	0.00	2.42	0.00	18.7	0.19	144	22.40	1110	97.22		
0.0463	0.00	0.357	0.00	2.75	0.00	21.2	0.31	163	28.64	1260	98.28		
0.0526	0.00	0.405	0.00	3.12	0.00	24.1	0.43	186	35.50	1430	99.04		
0.0597	0.00	0.460	0.00	3.55	0.00	27.4	0.57	211	42.72	1630	99.51		
0.0679	0.00	0.523	0.00	4.03	0.00	31.1	0.70	240	50.04	1850	99.82		

Figure 4 - 4: Bagasse ash particle sizes.

Average particle sizes were determined by working out volume against the majority of particle sizes. A portion of particles was mixed with water under a screening mechanism to determine particle sizes of specific volume. What transpired on the screen, particles are placed on the screen and get filtered through in different sizes. The graph indicated in Figure 16, is plotted in terms of sizes versus volume of density. The high peak on the graph indicates that about 50% of the volume of the particles was found to be 240 μm. in size. It was observed that particle sizes start from 14.5 μm with 99.98% of volume density and up to 2100 μm with 0.03% of volume density. Three average sizes indicated from the laboratory results are shown in Figure 4 - 5, are 102 μm, 240 μm and 669 μm.

Result		Result	
Concentration	0.0760 %	Span	2.367
Uniformity	0.741	Result Units	Volume
Specific Surface Area	30.43 m^2/kg	Dv (10)	102 µm
D [3,2]	188 µm	Dv (50)	240 µm
D [4,3]	328 µm	Dv (90)	669 µm

Figure 4 - 5: Bagasse ash average size particles.

Particulate discharges from boilers fired using bagasse are considered to be abrasive and can cause erosion within the mechanical accumulator. As mentioned under literature review that, large particles greater than 1µm are more easily collected by inertial impaction because these particles have more inertial momentum to resist change in gas path and therefore, impact the droplets. Small particles < 1µm are more difficult to collect by inertial impaction because they remain in the flow lines of the gas due to the predominance of the fluid drag force [6].

Table 4 - 1 shows elements composition extracted from samples. In this table, all elements which are part of making bagasse ash particles are weighed with a mass percentage. This will give a clear understanding of what chemical reaction might take place during the impact of a particle onto the impeller with water acting as a catalyst. The table shows Silicon Oxide being the highest at 66.4%, following by elements that contain a majority of percentage as per the following sequence, 9.31% of Aluminium, and 8.43% of Iron, 5.68% of Carbon, 2.92% of Calcium and 2.89% of Titanium. These elements added together to make 92.74% of elements composed inside bagasse and coal ash. During oxidation, the elements may react to form compounds which are reported to exist in Table 4 – 1. Silicon found to have the highest mass percentage. When reacting with oxygen from H2O forms SiO2 also known as quartz. This compound is found to be classified amongst aggressive particulate matter [22].

Table 4 - 1: Elements Composition Mass Percentage.

ELEMENT	Reported As	Composition in Mass %
Carbon	C	5.68
Sulphur	S	0.071
Manganese	MnO	0.17
Phosphorus	P_2O_5	0.45
Silicon	SiO_2	66.4
Chromium	Cr_2O_3	0.06
Nickel	NiO	≤ 0.01
Copper	CuO	≤ 0.01
Aluminium	Al_2O_3	9.31
Vanadium	V_2O_5	0.075
Titanium	TiO_2	2.89
Cobalt	CoO	0.006
Calcium	CaO	2.92
Magnesium	MgO	1.84
Iron	FeO	8.43
Sodium	Na_2O	0.93

Particle Size Distribution certificate SDS 1779 attached

Table 4 -2 shows the chemical composition of elements extracted from the water sample. Particle density has been determined during the laboratory analysis and was found to be 2615 kg/m^3. From the water sample, Silicon is found to be the second highest element with 37% of mass content.

Table 4 - 2: Elements Composition in Mass Percentage.

Element Found	Reported as	Mass Percentage	Element Found	Reported as	Mass Percentage
Silver	Ag	≤1	Sodium	Na	33
Aluminium	Al	≤1	Niobium	Nb	≤1
Arsenic	As	≤1	Nickel	Ni	≤1
Boron	B	≤1	Phosphorous	P	≤1
Barium	Ba	≤1	Lead	Pb	≤1
Beryllium	Be	≤1	Sulphur	S	2
Bismuth	Bi	≤1	Antimony	Sb	≤1
Calcium	Ca	≤1	Selenium	Se	≤1
Cadmium	Cd	125	Silicon	Si	37
Cobalt	Co	≤1	Tin	Sn	≤1
Chromium	Cr	≤1	Strontium	Sr	≤1
Copper	Cu	≤1	Tantalum	Ta	≤1
Iron	Fe	≤1	Tellurium	Te	≤1
Potassium	K	10	Titanium	Ti	≤1
Magnesium	Mg	33	Vanadium	V	≤1
Manganese	Mn	≤1	Tungsten	W	≤1
Mercury	Hg	≤1	Zinc	Zn	≤1
Molybdenum	Mo	≤1	Zirconium	Zr	≤1

4.4. Scrubber Analysis

Many venturi scrubbers have a variable throat to allow for a change in load. As the throat is decreased in size, velocity increases resulting in increasing pressure drop and better efficiency in removing submicron particles is achieved. Venturi scrubbers use several methods to atomize the scrubbing water. In the case of Ubombo Sugar Mill venturi scrubber, the liquid is sprayed through jets across the venturi throat. This provides effective removal of submicron dust, fumes, and mist particles. This is the first choice for many applications [7].

The second phase of particles entrapment is created by passing the gas and water streams simultaneously through the extremely small throat section on a venturi. As

the velocity is increased in the throat, the liquid breaks up into extremely fine drops. High-velocity range makes the relative velocity between gas and liquid high enough to cause good liquid atomization and particle collection. The liquid drops collide with and remove the particles in the gas stream and the drops then agglomerate for separation from the gas [7]. Wet scrubbers can offer continuous reliable service when they are operated properly and maintained frequently. Poor design or operation and maintenance leads to component failure. Most scrubber failures result from abrasion, corrosion, solids build-up and wear of rotation parts.

4.4.1. Failure due to Corrosion

Corrosion frequently arises in wet scrubbers when the gases being washed contain acid-forming compounds or soluble electrolytic compounds. The combustion of fossil fuels, especially coke, coal and residual fuel oil, yields oxides of sulphur which can produce sulphuric acid in scrubbing liquors. Acids and electrolytes are corrosive to carbon steels. Chlorides are corrosive to many stainless-steel materials and fluorides are harmful to nearly all stainless steel materials except certain specially formulated high nickel alloys. Avoidance of corrosion is handled through correct choice of materials of construction and through pH control.

4.4.2. Failure due to Abrasion

Abrasion can transpire where gases or scrubbing liquors containing high concentrations of abrasive particulates are in the turbulent mode or are subjected to unexpected change in flow direction. Usual wear areas in scrubbing systems include venturi throats, walls of centrifugal vapour accumulators near the inlet duct and elbows in the ductwork. Solutions to abrasion wear include the use of pre-cleaning devices and the use of large radius turns in ductwork.

4.4.3. Failure due to Solids Build-up

Solids build-up is a common problem to wet scrubbers and one that is frequently difficult to control. The two types of solids build-up are sedimentation and chemical

scaling. Sedimentation happens when a layer of particles becomes attached to a surface or settles in areas of low turbulence. Sedimentation can lead to ploughing of pipes and ducts or build-up on internal parts. Chemical scaling is an outcome from a chemical reaction of two or more kinds of substance to form a precipitate on the surface of scrubber components. Solids build-up may transpire in piping, sumps, scrubber packing, and instrumentation lines or ductwork and may lead to decreased scrubber efficiency and major equipment failure. Solution is to apply a method to control scaling include increasing the liquid-to-gas ratio, controlling pH providing greater residence period in the holding tank and adding other chemical agents such as dispersants.

During a site research visit to Ubombo Sugar Limited, the inspection revealed that other parts were malfunctioning before the scrubber being switched off. Malfunctioning of these components can be associated with scrubber failure that can be caused by the three mentioned causes of failure stated in 4.4.3.1 to 4.4.3.3.

Three factors that were investigated on site that are expected to be the cause of scrubber inefficiency are,

4.4.3.1. Particle settling in the reservoir

During inspection, from discussed facts with some of the Ubombo Sugar Mill employees, there was a great concern about settling of particles in the reservoir before water is recycled to the venturi wet scrubber. Concern was that the time allocated to recycle water back to the scrubber is not adequate, reason being that water is recycled while the mixture is still too dense with solid particles prior particle settling at the bottom of the reservoir.

4.4.3.2. Worn out spray nozzles

Most of the spray nozzles have been worn out inside the venturi chamber. This indicates that atomization of water droplets or mist was no longer effective during plant operation. As the size of the droplets is reduced closer to the size of the

particles, there is a higher probability of collision improvement. Effective scrubbing requires atomizing the liquid to a finesse related to particle size to afford maximum contact with the particles to be captured. Pictures taken during the inspection to support that other parts of the venturi wet scrubber were malfunctioning are illustrated in Figure 4 – 6.

Position of welded nozzle connecting pipe before wear occurs.

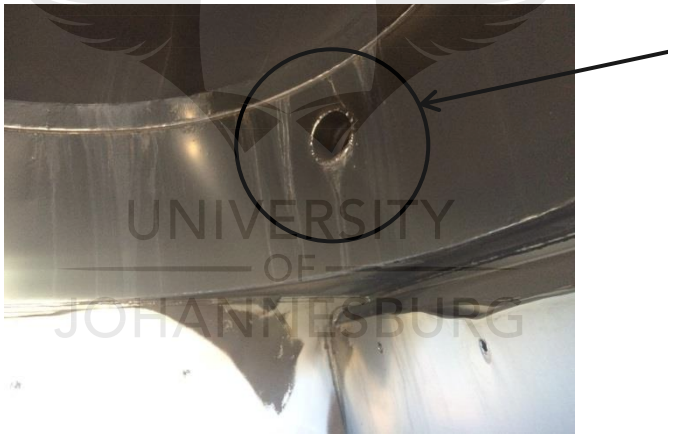

Position of welded nozzle connecting pipe after wear occurred.

Figure 4 - 6: Picture inside the venturi chamber, on the top shows spray nozzle connecting rod and the bottom shows spray nozzle connecting rod that is worn out.

4.4.3.3. Ceased throttling damper doors

Throttling damper doors on the neck of the venturi chamber were unable to throttle discharged water, this might be a resultant from an actuator which has stopped working or damper doors pivot bars are unable to rotate due to particles trapped between the pivot bars and the bore on the throttling damper housing. The doors remain fully opened while the throat area stacked on the highest opening position.

Picture taken during the inspection to support ceased throttling damper statement that other parts of the venturi wet scrubber were malfunctioning is illustrated in Figure 4 – 7.

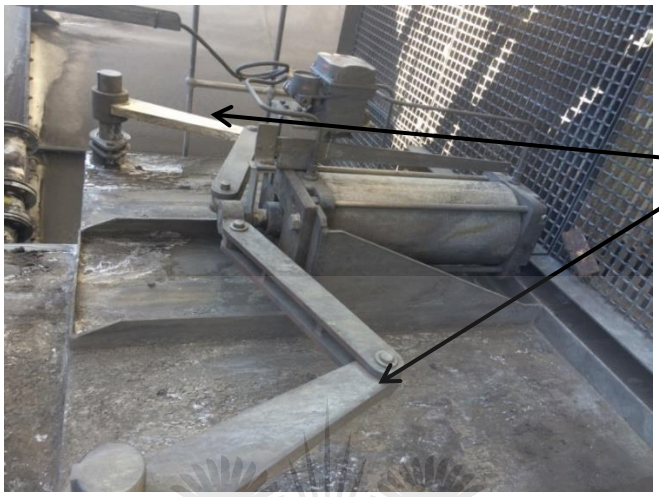

Figure 4 - 7: Venturi damper doors stacked at maximum fully opened position.

4.5. Summary

This Chapter focused on investigating the cause of wear by studying particle shapes, sizes, and inefficiency of the scrubber. With the aid of laboratory tests, particle shapes were observed and found that the majority of the particles have sharp edges and such shape frequently results in accelerating wear. Majority of particles sizes were above 100 μm with an average size of 240 μm , this indicates that such particle size when impact on the surface will discharge significant kinetic energy onto the surface and big particles irregularly break into smaller particles during impaction and this will result in accelerating rate of wear.

The research has indicated that malfunctioning of the wet scrubber has resulted in causing scrubber inefficiency. Aggressive substances that are coming from the boiler into the wet scrubber worn out spray nozzle system leave the scrubber vulnerable because no atomization of droplets is taking place to entrap particles. The results in this Chapter showed that bagasse ash particles passing through the impeller are one of the main causes of wear due to particles quantity and sharp edges. A scrubber

has been found to be ineffective due to malfunctioning of components, which thus cause failure in the filtration system. No calculations performed due to wet scrubber data restriction from Consultant Company that was busy working out a proposal to improve wet scrubber efficiency.

CHAPTER 5: SIMULATION ANALYSIS

5.1. Introduction

This Chapter is explaining how the simulation of what is occurring on the impeller during the operation was conducted and how parameters were achieved. The simulation will show how air particles are conveyed through centrifugal fan airways. The Chapter covers all the calculations that are required to provide parameters to be used in the simulation package to conduct fluid flow analysis.

5.2. Calculations

Referring to Figure 1 -1 in Chapter 1, the wet scrubber and ID fan are linked through ducting of 2.6m in diameter. The ducting has been connected to transition piece which changes the shape from round to rectangular to interlock with a rectangular shape of inlet damper. A reducer was constructed with a diameter of 2.6m on the inlet side and 0.873m x 2.9m rectangular shape on the discharge side of the damper. The two mentioned shapes are going to be used to work out the area to calculate the velocities in the ducting and on the inlet cone discharge. The inlet cone discharged air directly to the impeller.

Table 5 - 1 and Table 5 - 2, give ID fan technical data which used to select the fan. The fan was selected to operate with two application conditions, first condition was based on firing bagasse inside the boiler and the second was based on firing coal. The fan was designed to have three different operational conditions. The conditions are stipulated in the following sequence,

a. MCR initial duty
b. MCR final duty
c. Design duty

Calculation and simulation are based on two sets, first set was based on application where bagasse is fired inside the boiler and the second set is referred to coal firing. Design duty was not considered in this exercise because this was incorporated

during the fan selection to build factor of safety in case the gas inside the fan raises to 190°C or if there is a need to operate the fan for short period under this condition.

Table 5 - 1: Fan operating duty for bagasse firing in the boiler.

Bagasse Firing	Units	Design Duty	MCR-Final	MCR-Initial
Volume Flow (σ)	m^3/s	82.5	63.5	60.1
Static Pressure (P_S)	Pa	3179	2483	2388
Operating Temperature (T)	°C	70	70	69
Air Density (ρ)	kg/m^3	0.927	0.927	0.927
Barometric Pressure on site (P_B)	Pa	102 000	102 000	102 000

Table 5 - 2: Fan operating duty for coal firing in the boiler.

Coal Firing	Units	Design Duty	MCR-Final	MCR-Initial
Volume Flow (σ)	m^3/s	51.5	42.9	40.9
Static Pressure (P_S)	Pa	3586	3336	3284
Operating Temperature (T)	°C	54	54	54
Air Density (ρ)	kg/m^3	1.040	1.040	1.040
Barometric Pressure on site (P_B)	Pa	102 000	102 000	102 000

5.2.1. Bagasse Firing

Calculating velocity pressure inside the round ducting of diameter 2.6m is as follows:

Duct area $(A_1) = \frac{\pi}{4} \times D_1^{\,2}$ (5.1)

$$= \frac{\pi}{4} \times 2.6^2$$

$$= 5.309 m^2$$

Velocity $(V_1) = \frac{\sigma}{A_1}$ (5.2)

$$= \frac{63.5}{5.309}$$
$$= 11.96 m/s$$

Velocity Pressure $(P_{v1}) = \frac{1}{2} \times \rho \times V_1^2$ (5.3)

$$= \frac{1}{2} \times 0.927 \times 11.96^2$$
$$= 66.3 Pa$$

As mentioned in Section 5.1, the round duct is connected to the round inlet of the transition piece and the outlet of the transition piece is connected to the rectangular shape of the fan inlet damper. This requires calculating the area of the transition piece.

Transition piece area $(A_2) = L \times W$ (5.4)

$$= 0.873 \times 2.9$$
$$= 2.532 m^2$$

Inlet Damper Velocity $(V_2) = \frac{\sigma}{A_2}$ (5.5)

$$= \frac{63.5}{2.532}$$
$$= 25.08 m/s$$

Velocity Pressure $(P_{v2}) = \frac{1}{2} \times \rho \times V_2^2$ (5.6)

$$= \frac{1}{2} \times 0.927 \times 25.08^2$$
$$= 291.54 Pa$$

Area of the fan inlet cone discharging into the impeller is smaller than the area at the fan inlet. This implies that the velocity of the particles that are impacting on the impeller surface will be higher than the velocity at the fan inlet, this result in increase of velocity pressure. The velocity pressure will be also affected by the change in

density due to air being compressed. Before calculating velocity pressure inside the fan, a compression factor (f) must be determined.

To calculate compression factor, two variables must be determined, variables absolute inlet pressure and total pressure rise. Absolute inlet pressure can be achieved from subtracting inlet static pressure from barometric pressure. Total pressure rise is achieved by adding pressure losses of all necessary fan components at the fan inlet and outlet. Table 5 - 3, gives loss coefficients that are used to calculate pressure losses. Calculations to indicate how values of these two variables are calculated,

Table 5 - 3: Losses coefficient [46]

Description	Units	Loss Coefficient	Loss Coefficient Values
Fan Inlet damper loss (P_{dmp})	Pa	ξ_{dmp}	0.4
Fan Inlet box losses (P_{inlet})	Pa	ξ_{inlet}	0.55
Fan outlet diffusor losses (P_{diff})	Pa	ξ_{diff}	0.31

Calculating fan pressure losses [46]:

$$\text{Inlet damper losses}(P_{dmp}) = P_{v2} \times \xi_{dmp} \quad (5.7)$$
$$= 291.54 \times 0.4$$
$$= 116.6Pa$$

$$\text{Inlet box losses}(P_{inlet}) = P_{v2} \times \xi_{inlet} \quad (5.8)$$
$$= 291.54 \times 0.55$$
$$= 160.3Pa$$

$$\text{Outlet diffusor losses } (P_{diff}) = P_{v2} \times \xi_{diff} \quad (5.9)$$
$$= 291.54 \times 0.31$$
$$= 90.38Pa$$

Fan shaft losses calculation [46]:

Affected area $\left(A_{shft}\right)=\left(d_s^2-d_n^2\right)\times\frac{\pi}{4}$ (5.10)

$$=\left(1.7226^2-0.155^2\right)\times 0.7854$$
$$=2.33m^2$$

Diameter ratio $(\delta)=\frac{D_{imp}}{d_s}=\frac{2.490}{1.7226}=1.445$ (5.11)

Shaft loss coefficient $\left(\xi_{shft}\right)=\delta^{\left(\frac{1}{3}\right)}\times\left(\frac{d_n}{d_s}\right)^2$ (E5.12)

$$=1.445^{\frac{1}{3}}\times\left(\frac{0.155}{1.7226}\right)^2$$
$$=0.009153$$

Fan shaft losses $\left(P_{shft}\right)=\left(\frac{\sigma}{A_{shft}}\right)^2\times\frac{\rho}{2}\times\xi_{shft}$ (5.13)

$$=\left(\frac{63.5}{2.33}\right)^2\times\frac{0.927}{2}\times 0.009153$$
$$=3.15Pa$$

Fan total pressure rise $(\Delta P_T)=P_T$ + Total Losses (5.14)

Fan total pressure $\left(P_T\right)=P_S+P_{v2}$ (5.15)

$$=2483+291.54$$
$$=2774.54Pa$$

Total losses = $P_{dmp}+P_{inlet}+P_{shft}+P_{diff}$ (5.16)

$$=116.6+160.3+3.15+90.38$$
$$=370.4Pa$$

Fan total pressure rise $(\Delta P_T)=2774.54+370.4$

$$=3144.94Pa$$

Absolute inlet pressure calculation $\left(P_{AB}\right)=P_B-P_S$ (5.17)

$$=102000-2483$$
$$=99517Pa$$

Isentropic exponent / Kappa [47] $(\kappa)=\frac{c_p}{c_v}=1.4$ (5.18)

For air Kappa is a constant value [46].

Compression factor $(f) = \frac{\kappa}{\kappa - 1} \times \frac{P_{AB}}{\Delta P_T} \times \left[\left(\frac{P_{AB} + \Delta P_T}{P_{AB}} \right)^{\frac{\kappa-1}{\kappa}} - 1 \right]$ (5.19)

$$= \frac{1.4}{1.4-1} \times \frac{99517}{3144.94} \times \left[\left(\frac{99517 + 3144.94}{99517} \right)^{\frac{1.4-1}{1.4}} - 1 \right]$$

$$= 0.989$$

Density inside the fan $(\rho_f) = \frac{\rho}{f}$ (5.20)

$$= \frac{0.927}{0.989}$$

$$= 0.937 kg/m^3$$

Area of the discharge inlet cone $(A_3) = \frac{\pi}{4} \times D_3^{\,2}$ (5.21)

$$= \frac{\pi}{4} \times 1.687^2$$

$$= 2.235 m^2$$

Velocity at the Inlet Cone $(V_3) = \frac{\sigma}{A_3}$ (5.22)

$$= \frac{63.5}{2.235}$$

$$= 28.4 m/s$$

Velocity Pressure $(P_{v3}) = \frac{1}{2} \times \rho_f \times V_3^2$ (5.23)

$$= \frac{1}{2} \times 0.937 \times 28.4^2$$

$$= 377.9 Pa$$

Calculating Reynolds number at the highest velocity point, which is at the inlet cone discharge. This value requires determination of kinematic viscosity [47].

Kinematic viscosity $(\nu) = (17.1 + 0.048 \times (273.15 + T)) \times 10^{-6}$ (5.24)

$$= (17.1 + 0.048 \times (273.15 + 70)) \times 10^{-6}$$

$$= 33.57 \times 10^{-6} m^2/s$$

Reynolds number $(\mathrm{Re}) = \frac{V_3 \times d}{\nu}$ (5.25)

$$= \frac{28.4 \times 1.687}{33.57 \times 10^{-6}}$$
$$= 1.427 \times 10^{6}$$

Fan tip speed calculation $(V_{Tip}) = \frac{\pi \times D_{imp} \times N_{imp}}{60}$ (5.26)

$$= \frac{\pi \times 2.6 \times 629}{60}$$
$$= 94.2 m/s$$

Calculated density $(\rho_B) = \frac{P_{AB}}{RT}$ (5.27)

$$= \frac{99517}{287 \times (273.15 + 70)}$$
$$= 1.010 kg/m^3$$

5.2.2. Coal Firing

Calculating velocity pressure inside the round ducting of diameter 2.6m:

Duct area $(A_1) = \frac{\pi}{4} \times D_1^{\,2}$ (5.28)

$$= \frac{\pi}{4} \times 2.6^2$$
$$= 5.309 m^2$$

Velocity $(V_1) = \frac{\sigma}{A_1}$ (5.29)

$$= \frac{42.9}{5.309}$$
$$= 8.1 m/s$$

Velocity Pressure $(P_{v1}) = \frac{1}{2} \times \rho \times V_1^{\,2}$ (5.30)

$$= \frac{1}{2} \times 1.040 \times 8.1^2$$
$$= 34.12 Pa$$

Transition piece area $(A_2) = L \times W$

(5.31)

$$= 0.873 \times 2.9$$
$$= 2.532 m^2$$

Inlet Damper Velocity $(V_2) = \frac{\sigma}{A_2}$ (5.32)

$$= \frac{42.9}{2.532}$$
$$= 16.94 m/s$$

Velocity Pressure $(P_{v2}) = \frac{1}{2} \times \rho \times V_2^2$ (5.33)

$$= \frac{1}{2} \times 1.040 \times 16.94^2$$
$$= 150 Pa$$

Calculating fan pressure losses:

Inlet damper losses $\left(P_{dmp}\right) = P_{v2} \times \xi_{dmp}$ (5.34)

$$= 150 \times 0.4$$
$$= 60 Pa$$

Inlet box losses $\left(P_{inlet}\right) = P_{v2} \times \xi_{inlet}$ (5.35)

$$= 150 \times 0.55$$
$$= 82.5 Pa$$

Outlet diffusor losses $\left(P_{diff}\right) = P_{v2} \times \xi_{diff}$ (5.36)

$$= 150 \times 0.31$$
$$= 46.5 Pa$$

Fan shaft losses calculation:

Affected area $\left(A_{shft}\right) = \left(d_s^2 - d_n^2\right) \times \frac{\pi}{4}$ (5.37)

$$= \left(1.7226^2 - 0.155^2\right) \times 0.7854$$
$$= 2.33 m^2$$

Diameter ratio $(\delta) = \frac{D_{imp}}{d_s} = \frac{2.490}{1.7226} = 1.445$ (5.38)

Shaft loss coefficient $\left(\xi_{shft}\right) = \delta^{\left(\frac{1}{3}\right)} \times \left(\frac{d_n}{d_s}\right)^2$ (5.39)

$$= 1.445^{\frac{1}{3}} \times \left(\frac{0.155}{1.7226}\right)^2$$
$$= 0.009153$$

Fan shaft losses $\left(P_{shft}\right) = \left(\frac{\sigma}{A_{shft}}\right)^2 \times \frac{\rho}{2} \times \xi_{shft}$ (5.40)

$$= \left(\frac{42.9}{2.33}\right)^2 \times \frac{1.040}{2} \times 0.009153$$
$$= 1.61Pa$$

Fan total pressure rise $(\Delta P_T) = P_T$ + Total Losses (5.41)

Fan total pressure $\left(P_T\right) = P_S + P_{v1}$ (5.42)

$$= 3336 + 150$$
$$= 3486Pa$$

Total losses = $P_{dmp} + P_{inlet} + P_{shft} + P_{diff}$ (5.43)

$$= 60 + 82.5 + 1.61 + 46.5$$
$$= 190.6Pa$$

Fan total pressure rise $(\Delta P_T) = 3486 + 190.6$
$$= 3677Pa$$

Absolute inlet pressure calculation $\left(P_{AB}\right) = P_B - P_S$ (5.44)

$$= 102000 - 3336$$
$$= 98664Pa$$

Kappa $(\kappa) = \frac{c_p}{c_v} = 1.4$ (5.45)

For air Kappa is a constant value.

Compression factor $\left(f\right) = \frac{\kappa}{\kappa - 1} \times \frac{P_{AB}}{\Delta P_T} \times \left[\left(\frac{P_{AB} + \Delta P_T}{P_{AB}}\right)^{\frac{\kappa-1}{\kappa}} - 1\right]$ (5.46)

$$= \frac{1.4}{1.4 - 1} \times \frac{98664}{3677} \times \left[\left(\frac{98664 + 3677}{98664}\right)^{\frac{1.4-1}{1.4}} - 1\right]$$
$$= 0.987$$

Density inside the fan $(\rho_f) = \frac{\rho}{f}$ (5.47)

$$= \frac{1.040}{0.987}$$
$$= 1.054 kg/m^3$$

Area of the discharge inlet cone $(A_3) = \frac{\pi}{4} \times D_3^{\,2}$ (5.48)

$$= \frac{\pi}{4} \times 1.687^2$$
$$= 2.235 m^2$$

Velocity at the Inlet Cone $(V_3) = \frac{\sigma}{A_3}$ (5.49)

$$= \frac{42.9}{2.235}$$
$$= 19.19 m/s$$

Velocity Pressure $(P_{v3}) = \frac{1}{2} \times \rho_f \times V_3^2$ (5.50)

$$= \frac{1}{2} \times 1.054 \times 19.19^2$$
$$= 194.2 Pa$$

Kinematic viscosity $(\nu) = (17.1 + 0.048 \times (273.15 + T)) \times 10^{-6}$ (5.51)

$$= (17.1 + 0.048 \times (273.15 + 54)) \times 10^{-6}$$
$$= 32.80 \times 10^{-6} m^2/s$$

Reynolds number $(\mathrm{Re}) = \frac{V_3 \times d}{\nu}$ (5.52)

$$= \frac{19.19 \times 1.687}{32.80 \times 10^{-6}}$$
$$= 0.987 \times 10^6$$

Calculated density $(\rho_B) = \frac{P_{AB}}{RT}$ (5.53)

$$= \frac{98664}{287 \times (273.15 + 54)}$$
$$= 1.051 kg/m^3$$

Table 5 - 4, was established to compile all parameters required to be used as boundary conditions during flow simulation. Flow simulation was performed using SolidWorks software. After running simulation, results comparison between bagasse and coal firing to take place.

Table 5 - 4: Parameters used in Computation Fluid Dynamics (CFD)

Description	Units	Bagasse Firing	Coal Firing
Volume Flow (σ)	m^3/s	63.5	42.9
Barometric Pressure (P_B)	Pa	102000	102000
Static Pressure (P_S)	Pa	2483	3336
Velocity Pressure (P_{V2})	Pa	291.5	150
Total Pressure (P_T)	Pa	2774.5	3486
Fan Pressure Rise $\Delta(P_T)$	Pa	3145	3677
Operating Temperature (T)	°C	70	54
Air Density (ρ_f)	kg/m^3	0.937	1.054
Velocity at Inlet Box (V_2)	m/s	25.08	16.94
Fan Speed	rpm	649	615
Impeller Tip Speed	m/s	91.9	81.5
Reynolds number (Re)		1.427×10^6	0.987×10^6

5.3. Flow Simulation

5.3.1. Simulation

Confirmation on what is transpiring on the impeller during operation has been validated by setting up two CFD models to determine gas path angle of impingement and velocity that contribute to wear formation. Two project simulations were set up in flow simulation package, the first project was based on bagasse firing and the second project was based on coal firing inside the boiler.

The parameters used for CFD were as per Table 5 – 4, on each project a fan speed was applied in the rotating regions and the boundary condition, the volume flow rate is set on the fan inlet. A total fan pressure rise is applied on the fan discharge side. Fan inlet static pressure and fluid temperature at fan inlet were used under initial conditions. Goals such as fluid density, velocity, and static pressure were set to compute the simulation.

5.3.2. Simulation Results

Both simulations were run on efficient CFD package and results were achieved. The focus of the simulation was to determine angles of impingement on the blades and backplate of the impeller. Angle of impingement was achieved after completing simulation. However, another factor that is contributing to wear forming was observed. Velocity was found to be the second factor that is contributing to forming wear and this was indicated from highly colour dense area on the blade viewing on the sectional views in Figure 5 – 2.

5.3.2.1. Bagasse Firing Simulation Results

Several cut plots were taken from CFD results to indicate the flow profile as the air passes through the impeller entering from the fan inlet side and leaves at fan discharge side. These two openings were used as boundary conditions to compute CFD. Figures 5 – 1, illustrate velocity profile with arrows entering and leaving the impeller under simulation performed considering bagasse firing. Figure 5-1 also gives ranges of radial velocities up to a maximum of 75.77m/s with different colours

to indicate the location of ranges. Cut plot also indicates that there are areas on the blade that experience high radial velocity marked with dark orange colours ranging from 51m/s to 63m/s.

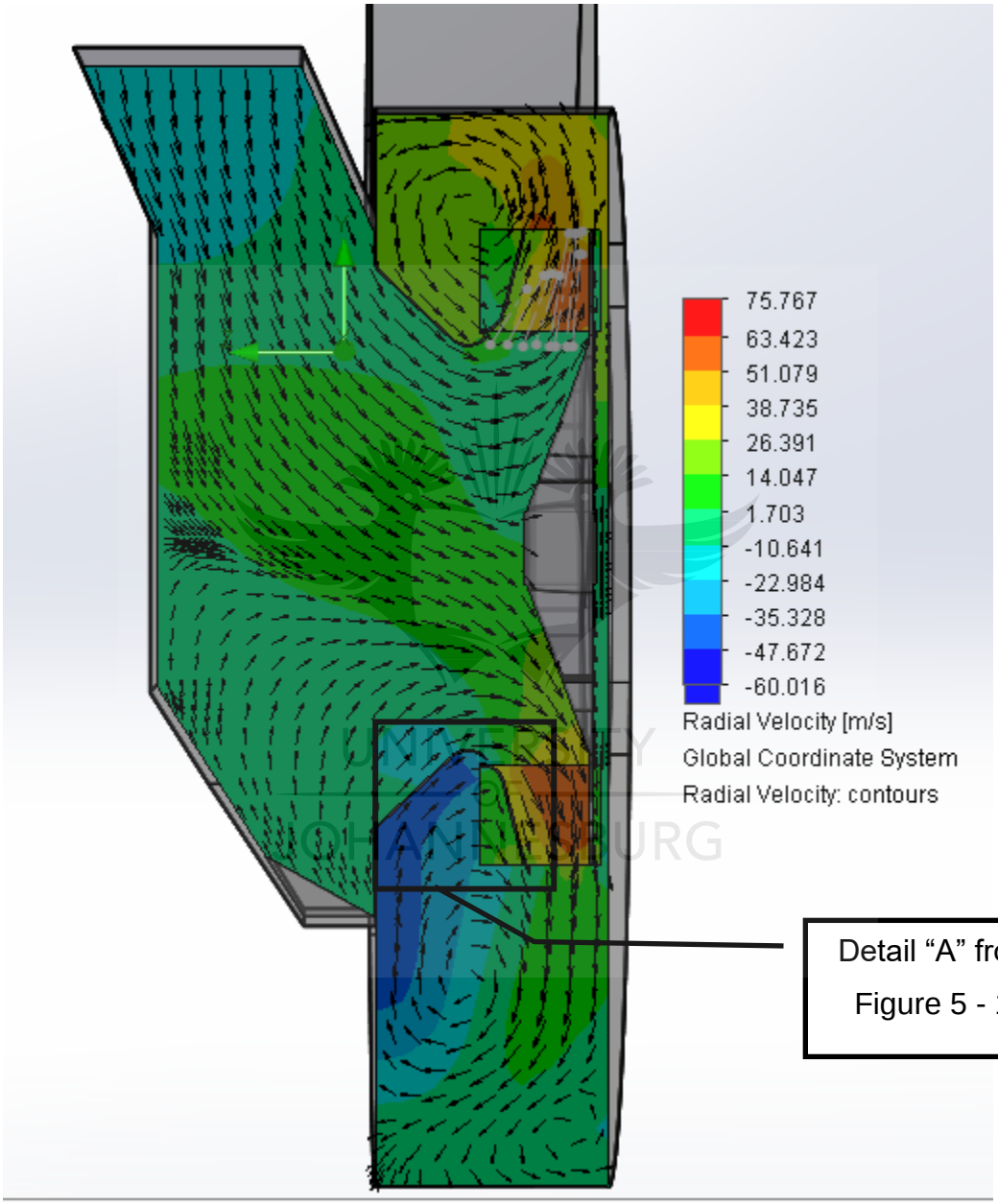

Figure 5 - 1: Radial velocity cut plot through ZY plane under bagasse firing.

Figure 5 – 2, illustrates cut plot of velocity profile of the air entering and leaving fan distributed inside the fan casing and passing through impeller. Velocities range from 0m/s to 95.5m/s at maximum. Highest velocity is found to be on the inner side of the

impeller shroud marked with dark orange colour which ranges from 81m/s to 88m/s. By studying the velocity profile at the fan inlet, it is observed that fan inlet velocity ranges from 13m/s to 27m/s and instantly increases as soon the fluid enters the impeller. This is the velocity traveling along the impeller inner surfaces.

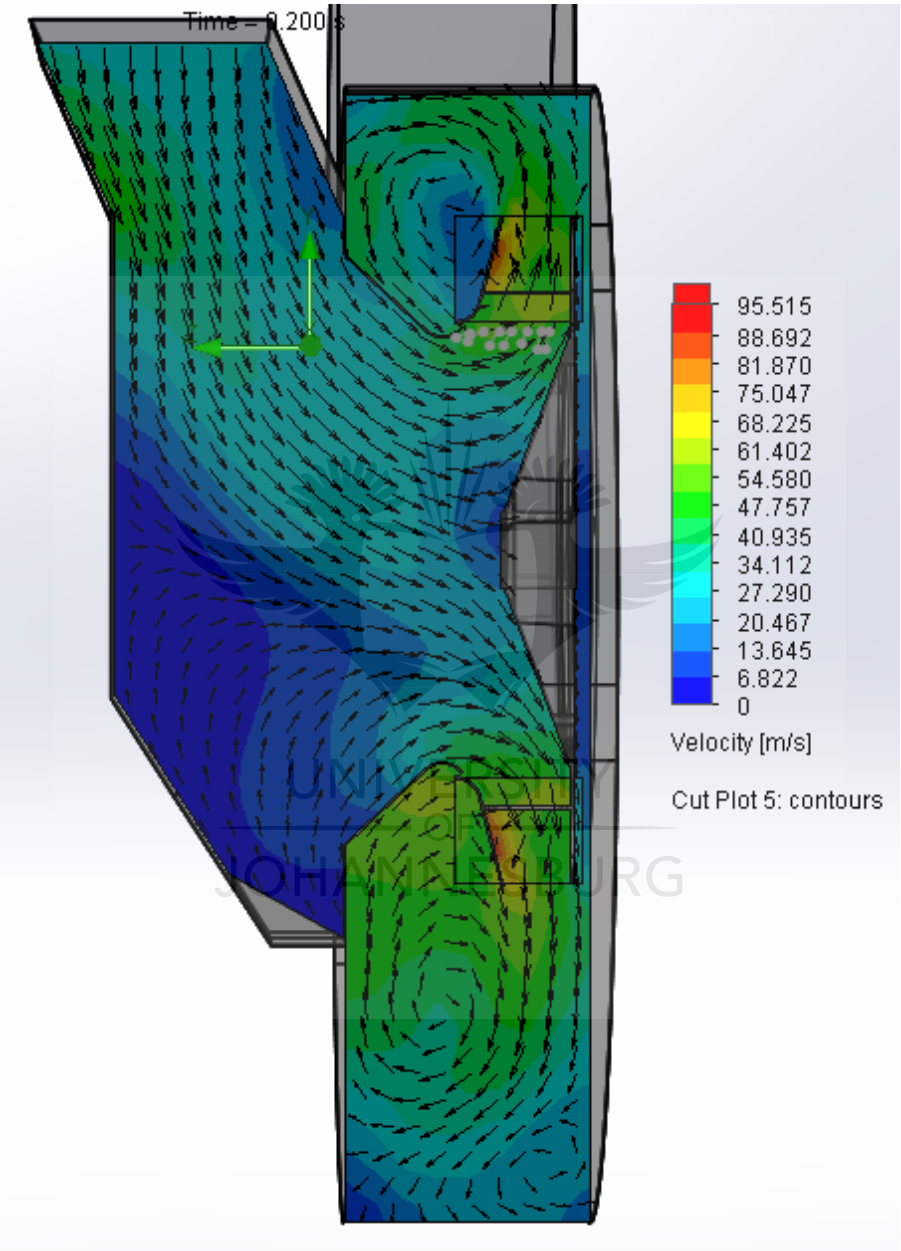

Figure 5 - 2: Velocity cut plot through ZY plane under bagasse firing.

Another illustration of the distribution of radial velocities that are like Figure 5 – 1, however in this case the flow direction is represented by using streamlines instead of vectors (arrows). This scenario is indicated in Figure 5 – 3 which clearly indicates

flow pattern distributions how air is conveyed inside the impeller prior entering the fan casing volute. This Figure 5 – 3 is used to illustrate angles of attack onto the impeller.

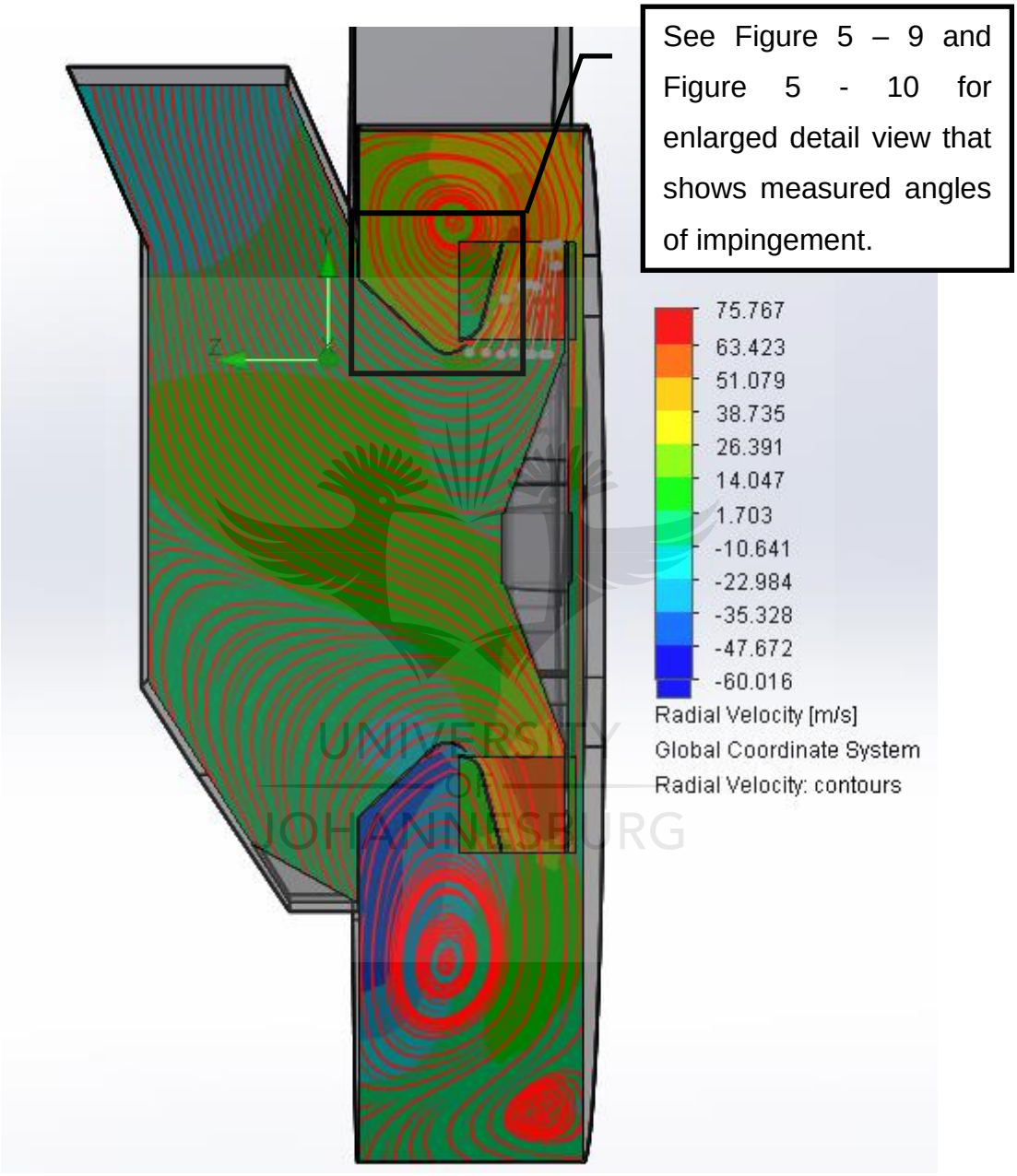

Figure 5 - 3: Radial velocity cut plot through ZY plane under bagasse firing represented by streamlines.

On the XY plane, as seen in Figure 5 – 4, another cut plot is taken to illustrate air distribution inside the fan casing volute as the air leaves the impeller. This sectional view shows the highest radial velocity distribution ranging from 51m/s to 74m/s

tangential to impeller blades and also along the outer impeller surface. The upper volute shell with less surface area indicates that is extremely subjected to high radial velocity ranging from 39m/s to 63m/s.

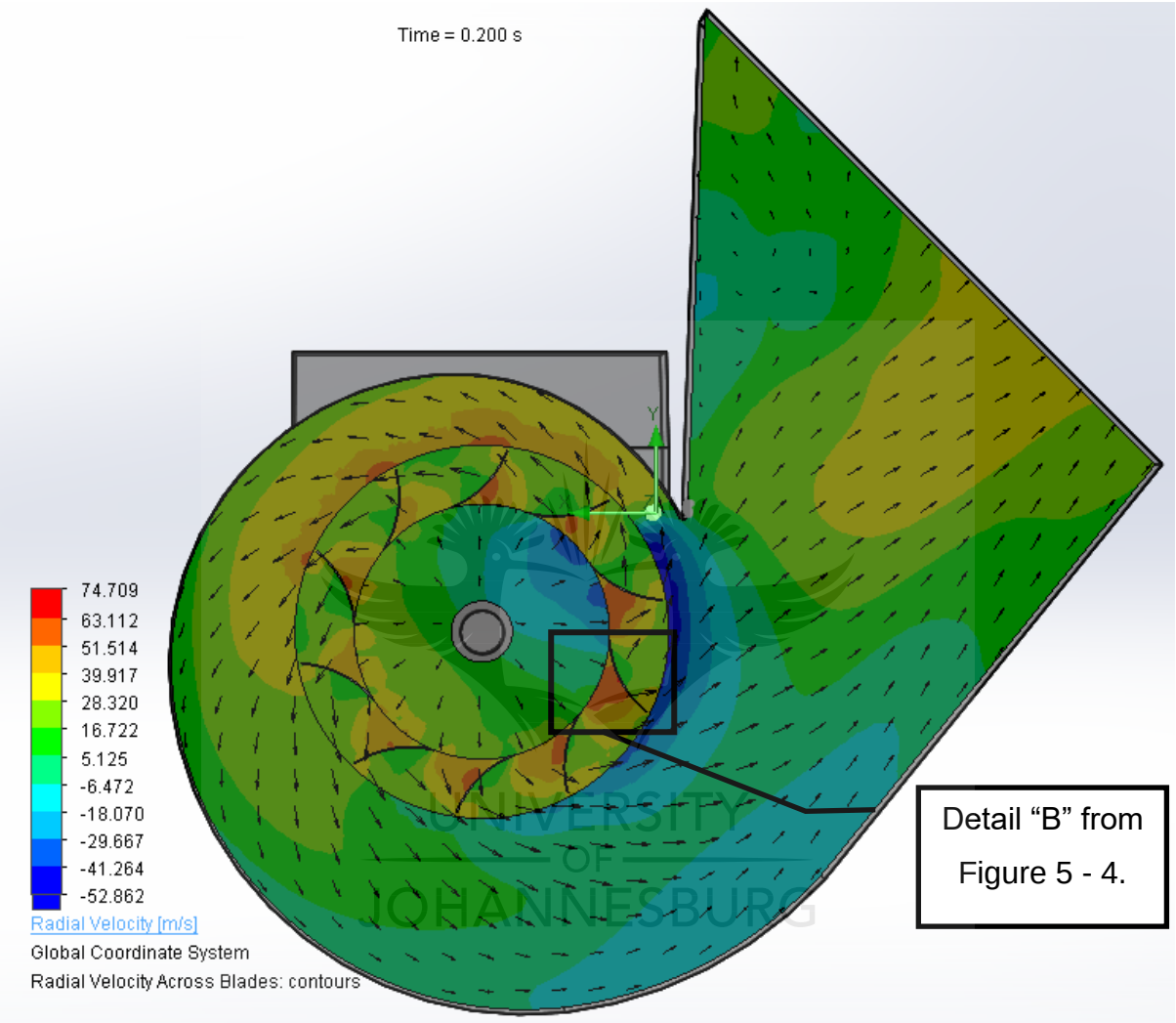

Figure 5 - 4: Radial velocity cut plot through XY plane under bagasse firing.

5.3.2.2. Coal Firing Simulation Results

Figure 5 – 5 illustrates the velocity profile with arrows entering and leaving the impeller under simulation performed considering coal firing. This gives ranges of radial velocities up to maximum of 83.6m/s with different colours coding to indicate the location. Cut plot indicate that the highest radial velocity spot is on the top side of the volute outside impeller. The cut plot for coal firing condition indicates that has

highest velocities than bagasse firing condition. However, the highest radial velocity spot is not within the impeller surface,

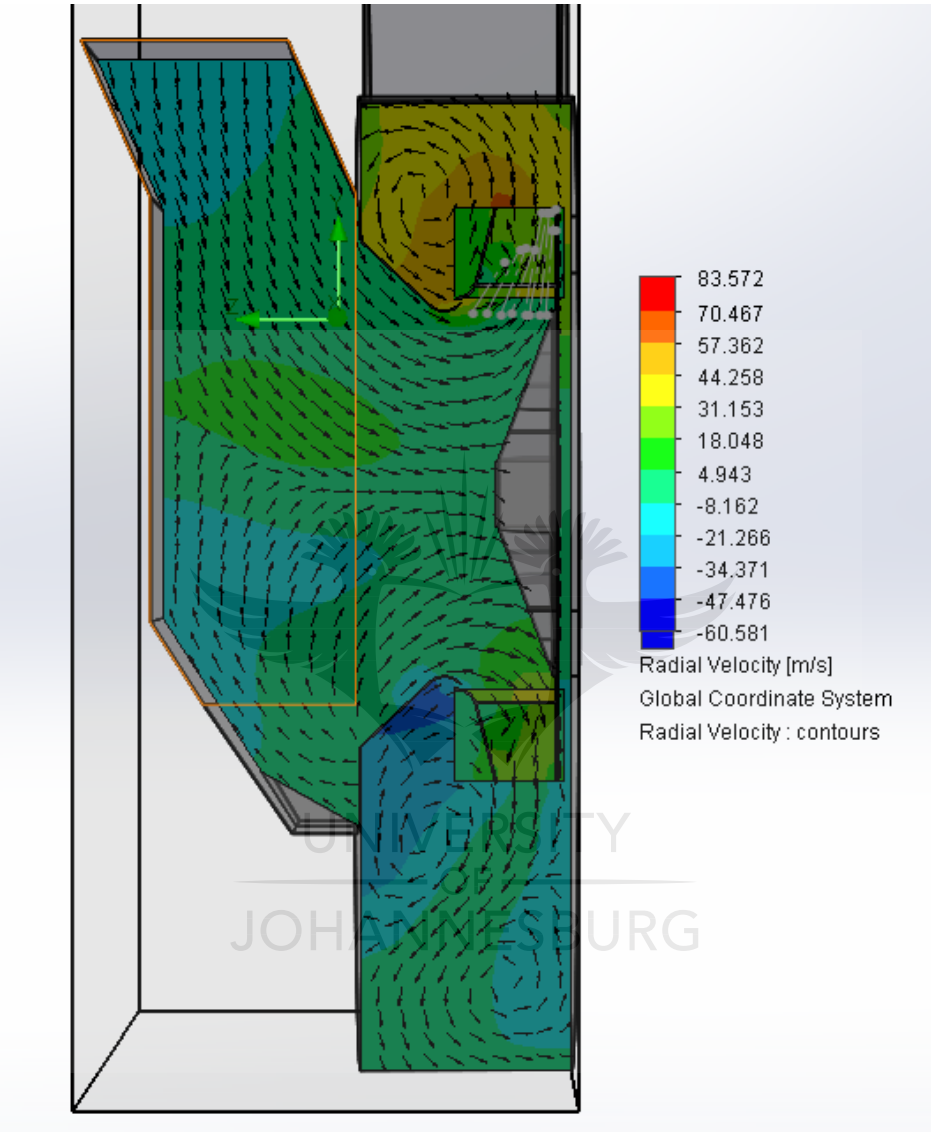

Figure 5 - 5: Radial velocity cut plot through ZY plane under coal firing.

Similarly, Figure 5 – 2 under bagasse firing condition, Figure 5 – 6 illustrate cut plot velocity profile of air entering and leaving fan distributed inside the fan casing and passing through the impeller. Velocities range from 0m/s to 93m/s being the maximum value, this velocity is less than the one under bagasse firing condition. The highest velocity is also found to be on the inner side of the impeller shroud marked with dark orange colour coding which ranges from 75m/s to 88m/s. By studying the

velocity profile at the fan inlet, it is observed that fan inlet velocity ranges from 15m/s to 31m/s and also increase when air is about to exit the impeller.

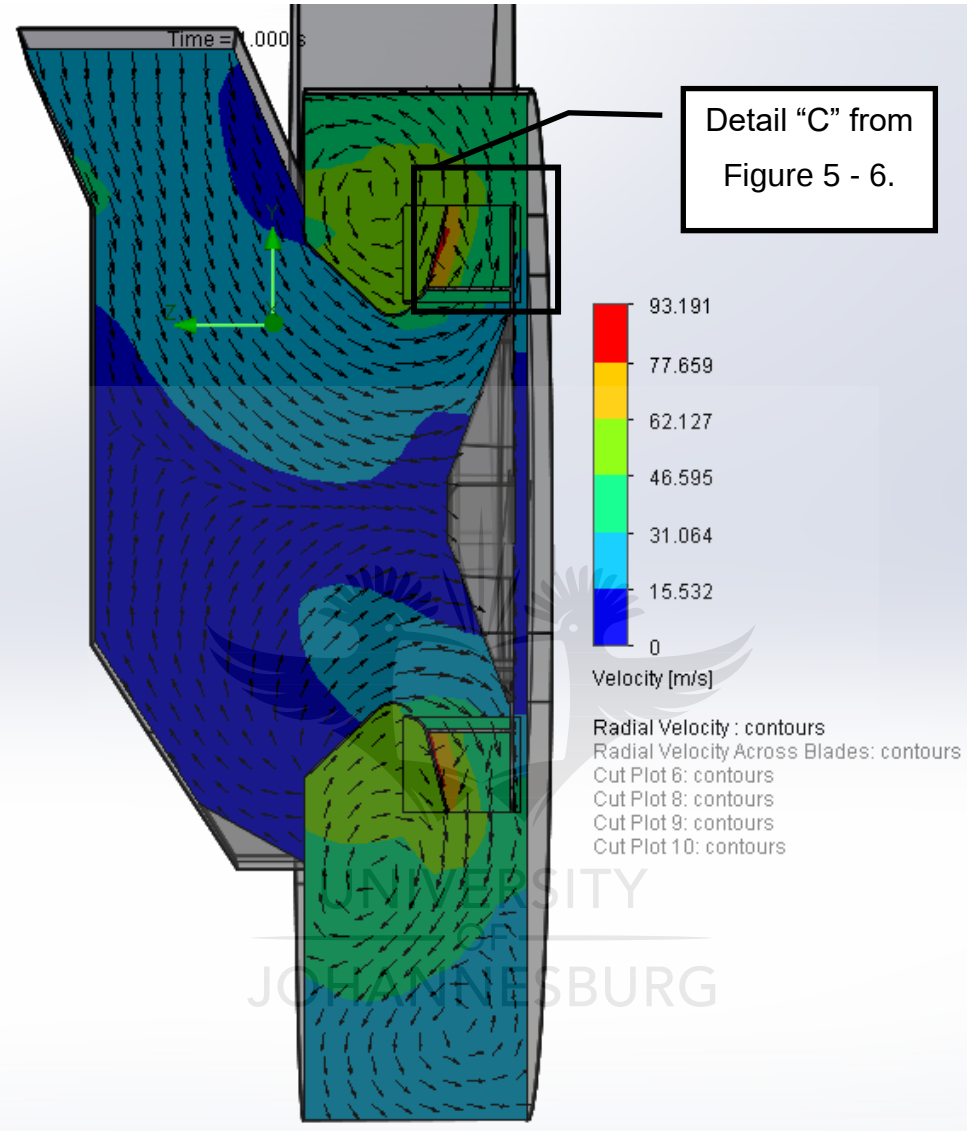

Figure 5 - 6: Velocity cut plot through ZY plane under coal firing.

Representing a similar cut plot as Figure 5 – 5, where radial velocities are similar, however, in this case, the direction flow is also represented by using streamlines instead of vectors (arrows). Figure 5 – 7 will be later used to illustrate angles of attack onto the impeller. The figure also indicates flow pattern distribution on how air is conveyed inside the impeller prior entering the fan casing volute.

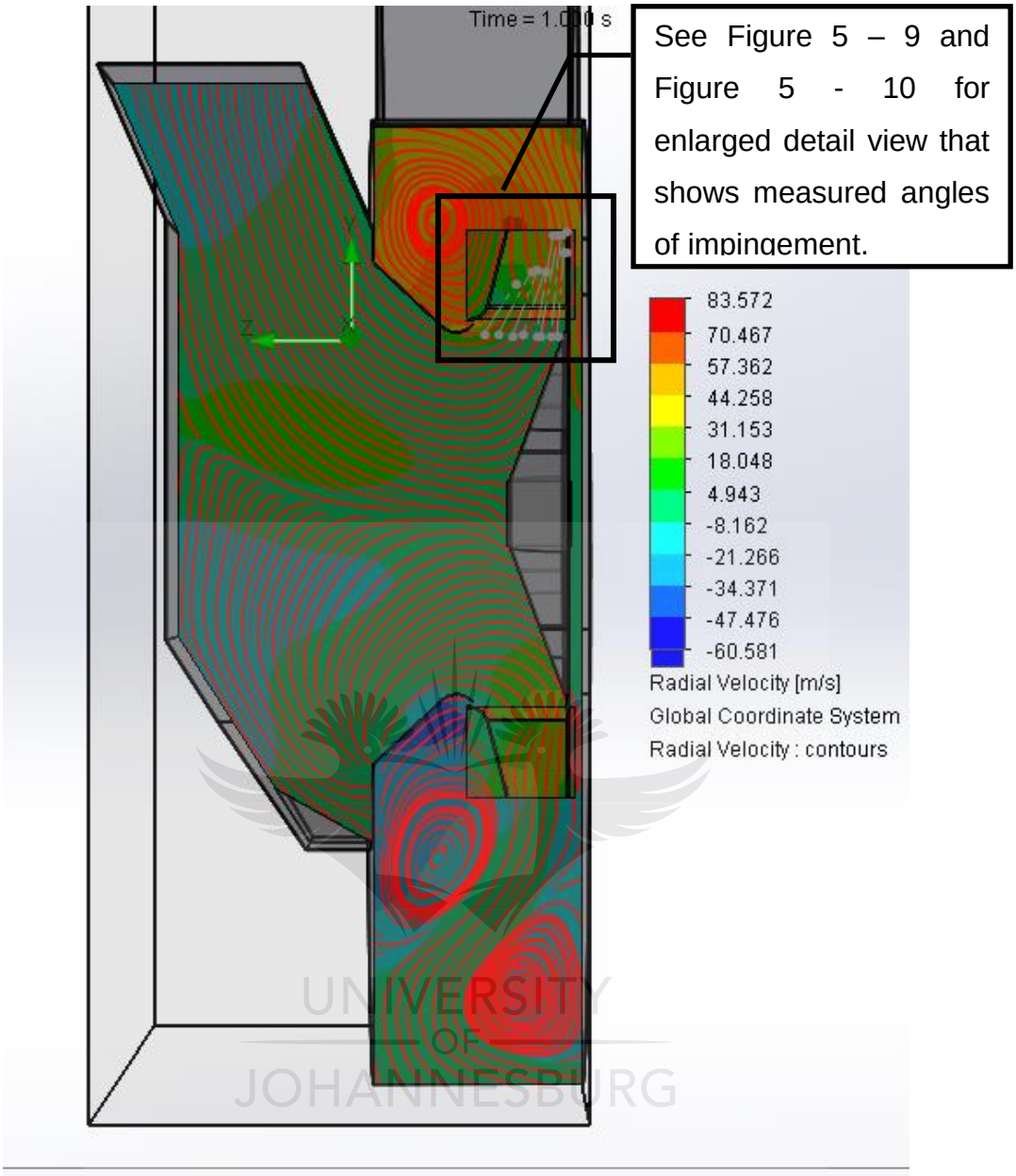

Figure 5 - 7: Velocity cut plot through ZY plane under coal firing represented by streamlines.

On the XY plane, as seen in Figure 5 – 8, another cut plot taken to illustrate air distribution inside the fan casing volute as the air leaves the impeller similar to Figure 5 - 4. This sectional view shows highest radial velocity distribution ranging from 58m/s to 71m/s tangential to impeller blades and also along the outer impeller surface. The upper volute shell with less surface area indicates that is extremely subjected to high radial velocity ranging from 32m/s to 58m/s. All values for coal firing condition are found to be higher than bagasse firing condition.

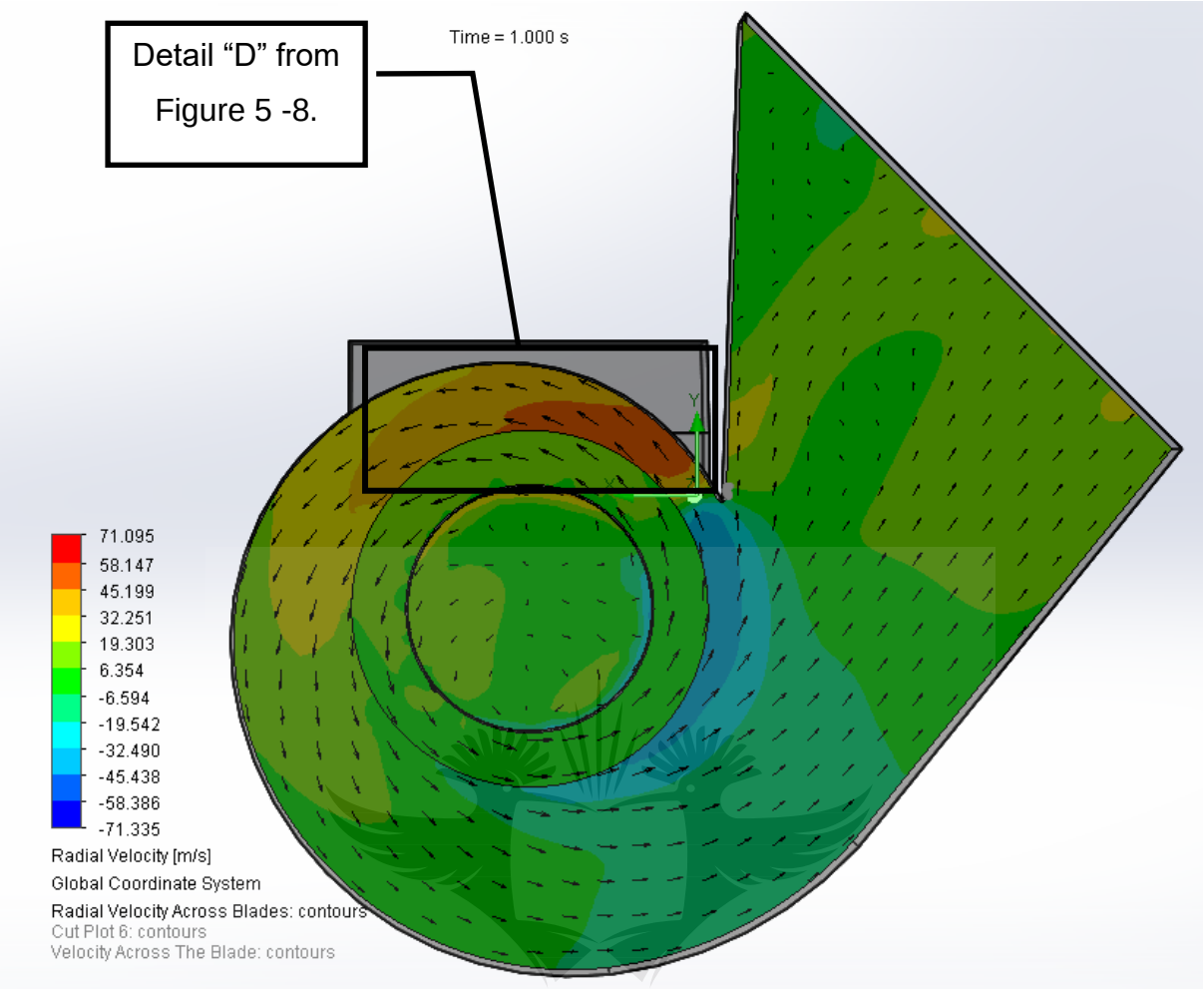

Figure 5 - 8: Radial velocity cut plot through XY plane under coal firing.

5.3.2.3. Impingement Angles Measurements

Angles of impingement in this study measured from vertical plane of impeller blades. Projection angles are represented by lines that are drawn over the streamlines of air path projected tangential to streamlines. Streamlines are represented by continuous red lines at impeller inlet and leaves the impeller chamber. Figure 5 – 9, illustrate angles of attack at the blade leading edge under bagasse firing condition. These are angles measured just before particles in the air path impact on the blade. These are critical angles because they shall reveal what effect they have on the blade leading edge.

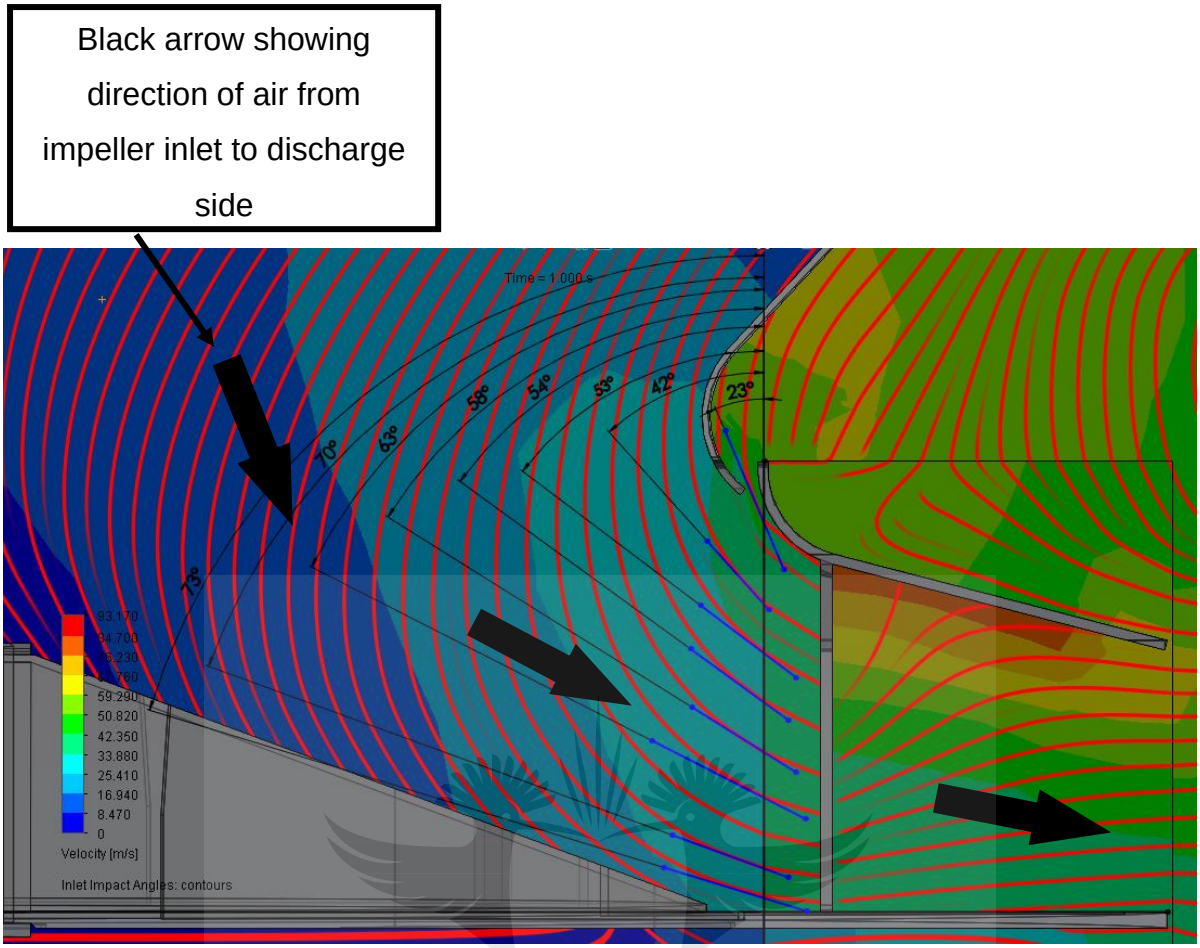

Figure 5 - 9: Angle of impingement at the blade leading edge under bagasse firing.

Repeating measurements of angles in Figure 5 – 9 but measuring on coal firing condition. Angles of attack at the blade leading edge are found to be within the same range between coal firing and bagasse firing condition. Figure 5 – 10 illustrate angles measured under coal firing condition. As mentioned, these angles are crucial to understanding their effect, it is also very important to compare Figure 5 – 9 with Figure 5 – 10. This will give a clear view of the effects between two different firing conditions. By comparing the two figures, it can be concluded that angles of impingement on the blade leading edge seem to be within the same range for both conditions.

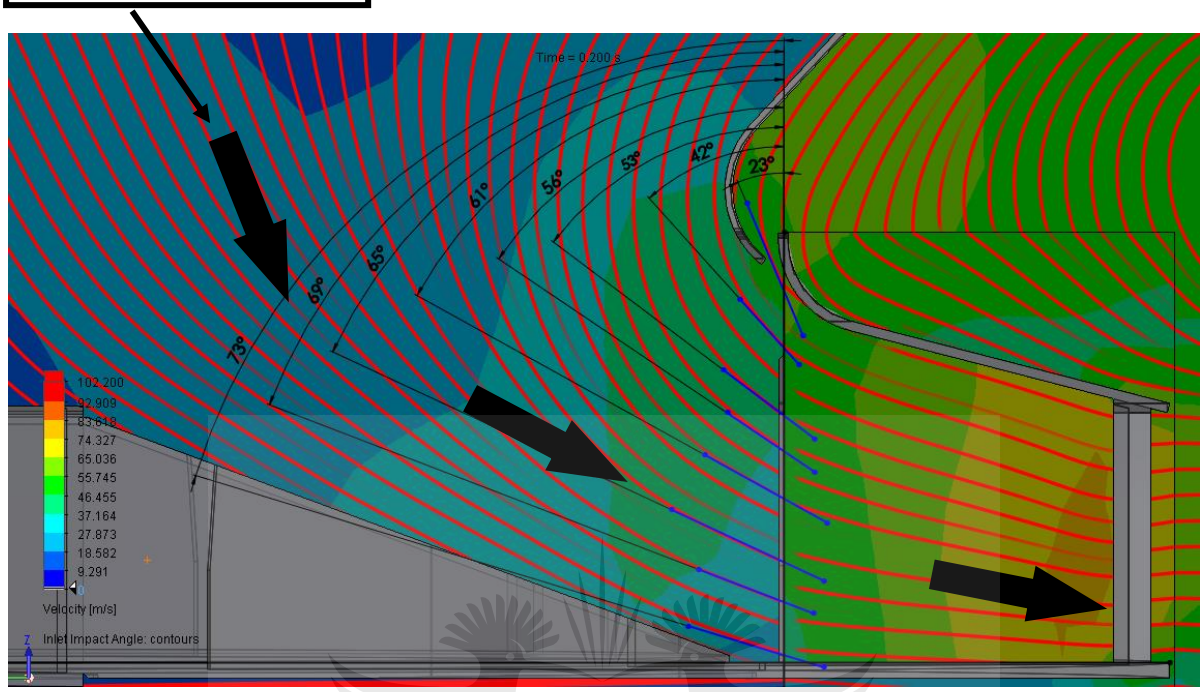

Figure 5 - 10: Angle of impingement at the blade leading edge under coal firing.

A crucial factor to be considered when analysing particles flow path is that not all particles sizes are able to follow the fluid flow stream. Particles that are classified as small have the ability to follow air stream curvatures as the flow hit the impeller leading blade edge. Small particles are particles from 300µm and less. However, these small particles are highly turbulent. With higher velocity and increase in mass of particles, particles can only follow the streamline curvature in a limited way but will highly follow the impeller centrifugal and inertia forces resulting in small impingement angles. Particles with sizes approximately 300µm and more, will fly somewhat the in a straight path impacting the impeller backplate and reflected, eventually colliding with incoming particles and tumbling along the backplate with reduced velocity at impingement angle close to 90° or less on the leading-edge depending on the leading-edge inclination relative to the backplate [48].

Regarding this theory, a relation can be made between the theory and the pictures taken on site. The impeller hub cone and part of the backplate show the effect resulting on large particles impacting from a straight path as indicated in Appendix A.

5.3.3. CFD Results Analysis

Analysis of results is a very crucial aspect in research which requires the understanding of findings that leads to the conclusion of the theory stated under literature review. However, prior analysing the results a relation between achieved calculated values and results achieved by CFD simulation must be validated. This assures that CFD results underflow simulation section is valid and acceptable. This relation was given in the form of a table of results that contains data information requested, calculated values and parameters taken from CFD results. This included parameters used for the boundary and initial conditions for simulation. Table 5 – 5 illustrates what was used to validate results and it has been proven that CFD results were found to be close to calculated values.

Table 5 - 5: Validation of results

Description	Units	Given Data- Bagasse	Given Data- Coal	Bagasse Calculated	Coal Calculated	Bagasse - CFD	Coal - CFD
Volume Flow	m^3/s	63.5	42.9	-	-		
Barometric	Pa	102000	102000	-	-		
Static Pressure	Pa	2483	3336	-	-		
Velocity Pressure	Pa	-	-	291.5	150		
Total Pressure	Pa	-	-	2774.5	3486		
Pressure Rise	Pa	-	-	3145	3677	-	-
Operating Temp.	°C	70	54	-	-	70.35	69.7
Air Density	kg/m^3	0.936	1.054	1.010	1.051	1.03	1.06
Velocity at Inlet	m/s	-	-	25.08	16.94	25.4	16.64
Fan Speed	rpm	649	615	-	-	-	-
Tip Speed	m/s	-	-	91.9	81.5	86.2	81.7
Reynolds number		-	-	1.427×10^6	0.987×10^6	-	-

After CFD was performed, a correlation between results and pictures taken on site was necessary to be implemented. The relation was based on studying CFD results and identified areas that relate to literature as stated in this dissertation. This is

focused on impact angle by relating what was obtained on the actual blade on site where the impact angle is high and closer to 90° and what transpired where the impact angle is lower and closer to 0°.

By comparing angles of impingement at the blade leading edge in Figure 5 – 9 and Figure 5 – 10, with blade pictures photographed on site, as shown in Figure 5 – 11. The rate of wear was higher on the blade leading edge where the angle of impingement is between 20° and 45° and where angles of impingement are more than 45°, the rate of wear was less but took place in a uniform pattern. Both bagasse and coal firing conditions had identical patterns of an angle of impingement. Figure 5 – 11 illustrated a spot on the blade where wear was taking place at a high rate. This was the same area where CFD results revealed that the angle of attack was very low and closer to 0°. By studying CFD results it was found that under bagasse firing condition the lowest angle of impingement is 23° and under coal firing condition the lowest angle of impingement is also 23°.

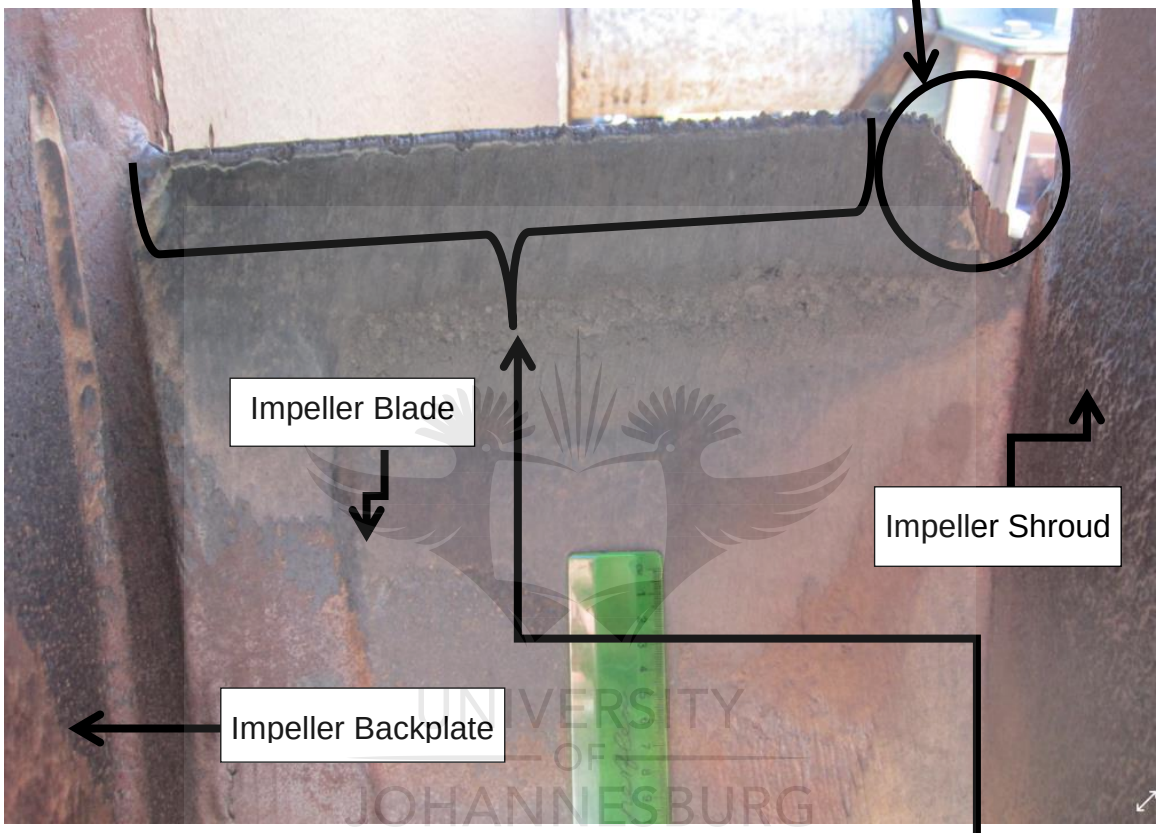

Figure 5 - 11: Worn blade leading edge picture taken on site.

Figure 5 – 11, also shows an area where rate of wear transpired at a uniform rate. Wear at this location on the blade was generated in different pattern and this wear formation can be related to angles of impingement higher than 45° as indicated in Figure 5 – 9 and Figure 5 – 10 for both firing conditions.

Another factor which has been exposed through studying CFD results and found to be contributing to a major role in wear formation on the impeller is the rotational velocity. Rotational velocity is the flow of particles with the rotating movement of all particles about their centre of an axis in the air stream. With the high rate of velocity and larger particles passing through the impeller, it was found that the quantity of particles impacting the blade back surface results in wear formation. As indicated by the sizes and shapes of the particles sample taken on site in Figure 4 – 2, that these particles due to shape and quantity might be responsible for major wear taking place on the impeller. It is also stated that some brown particles can be associated with stones that are fed into the boiler as soil stuck on the sugar cane roots. As stated, *the Nalco Water Handbook* [45], soil characteristics of such particle size can affect the magnitude of particulate matter emissions from the boiler. The number of particles found inside the fan casing on site confirms that there are large quantities of particles passing through the fan, Figure 5 – 12 shows Picture of particles found at the bottom of the fan casing after the fan casing has been opened for service.

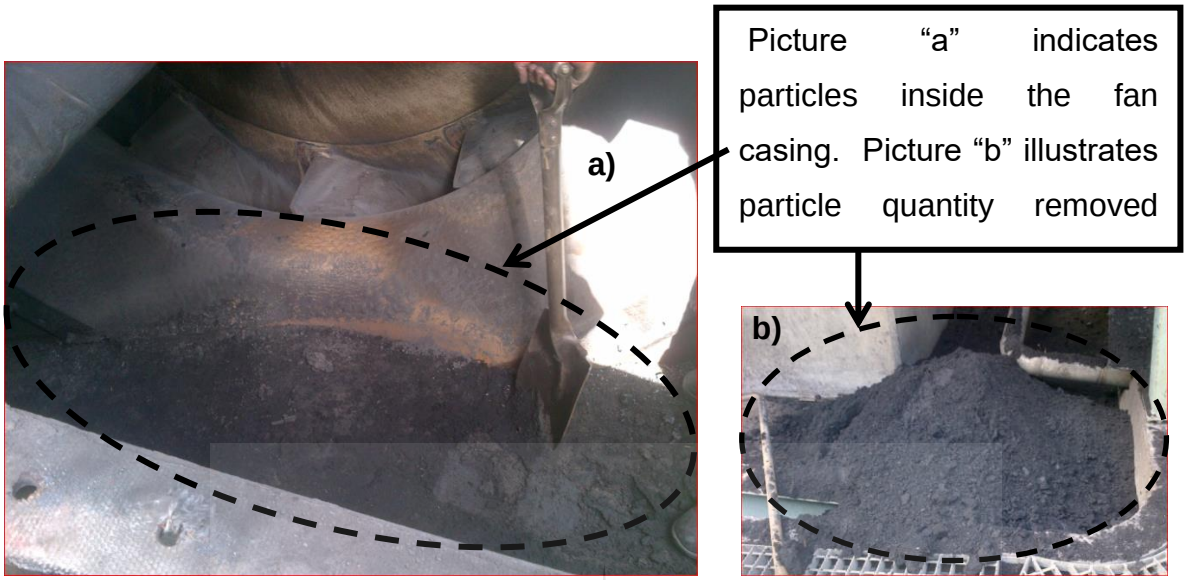

Figure 5 - 12: a) Particles found inside fan inlet box. b) Particles quantity removed inside fan inlet box.

In literature review, it was stated that a common feature of all abrasive wear process is the indentation of the wearing surface by the abrasive particles, resulting in the formation of continuous grooves. In general, the abrasive wear rate is therefore strongly dependent on the hardness of the wearing material relative to the hardness of the abrasive [7].

It was also stated that erosive wear is a function of particle velocity, impingement angle (known as impact angle) and size of roughness. Either solid or liquid particles or a combination of both come with velocity and impinge on a solid surface and impart some kinetic energy to the surface, where an angle of impact will be an important parameter. The main factors in wear formations are the mass of particles as well as velocity particles. By increasing the particle size, increase wear rate, increasing the velocity will increase the wear rate and impact angle irrespective of the type of material being used [7].

Therefore, an appropriate analysis CFD results achieved during simulation must be done to understand the effect of particles sliding over the eroded impeller surfaces. This analysis of particles has been inspired by the different in velocity levels observed on the different parts of the impeller that has been revealed by the CFD

results. There are two types of velocities that can be plotted from CFD simulation results, the first one is rotational velocity and the second type is a normal velocity that is conveying fluid without rotation of particles.

Correlation of results was first based on particles rotational velocity from CFD results comparing to a blade picture taken on site in Figure 5 – 13 in relation to detail “A” in Figure 5 – 1 and detail “B” in Figure 5 – 4. Figure 2 – 5a and Figure 2 – 5b indicates that the rate of wear increases with velocity increase and velocity is high when the angle of impact is lower and closer to 0°. Impact angle is close to 0° when particles slide over the eroded surface and this provides a valid reason why there was wear over the blade surfaces. CFD results indicate high-velocity area at the back of the impeller blade on the same area where wear is observed on the picture in Figure 5-13. From the picture, there was slight wear established at the back of the impeller blade where no work to convey the fluid is done on the blade. The high-velocity area seen on the CFD results correlates with the slight wear seen at the back of the blade picture.

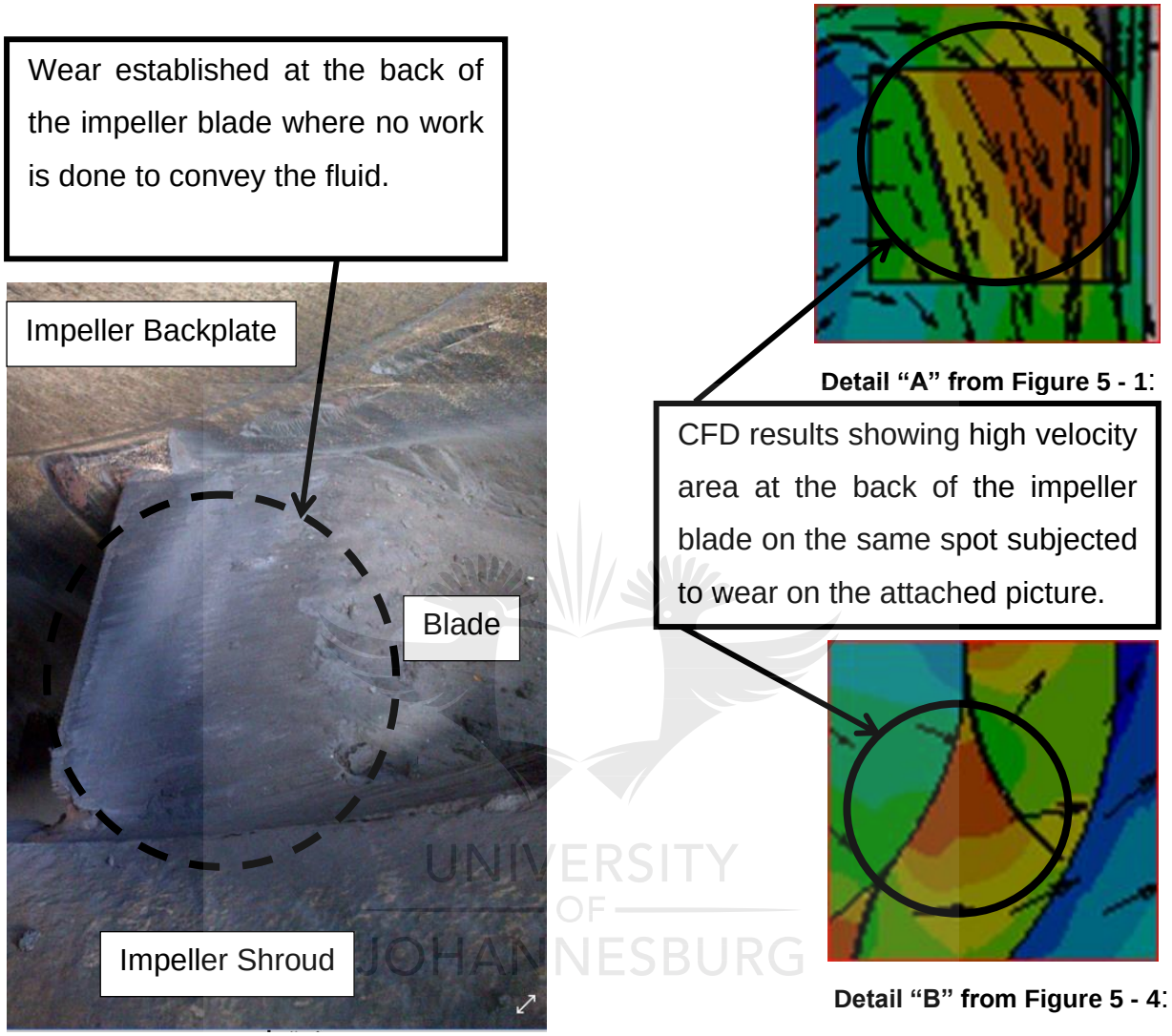

Figure 5 - 13: Picture showing blade wearing at the back surface of the surface that is not doing work.

Similar observations on the surface of the impeller blade that was doing the work to convey air have been observed on the CFD results where velocity is too high, and results correlate with the picture of the blade taken on site. It was found that the blade surface closer to the trailing edge of the blade was subjected to a high rate of wear. According to CFD results, high velocity on the inner surface of the blade only occurs when selecting air flow velocity and not radial velocity on the CFD software.

This wear formation pattern can be related to literature view statement state that “increasing in velocity will increase wear rate”. Figure 5 – 14a indicates CFD results showing high velocity area at the inner blade surface on the same spot subjected to wear on the attached blade picture. This high velocity spot is related to CFD results as per detail “C” in Figure 5 – 6. There was enormous wear seen on the surface of the blade as seen in pictures shown in Figure 5 – 14a, the cause of this wear can be related to damages caused by rebound of particle onto blade surface. This led to correlates CFD results to wear pattern seen on the impeller by investigating the effects of velocity and rebound impact angle has on wear formation.

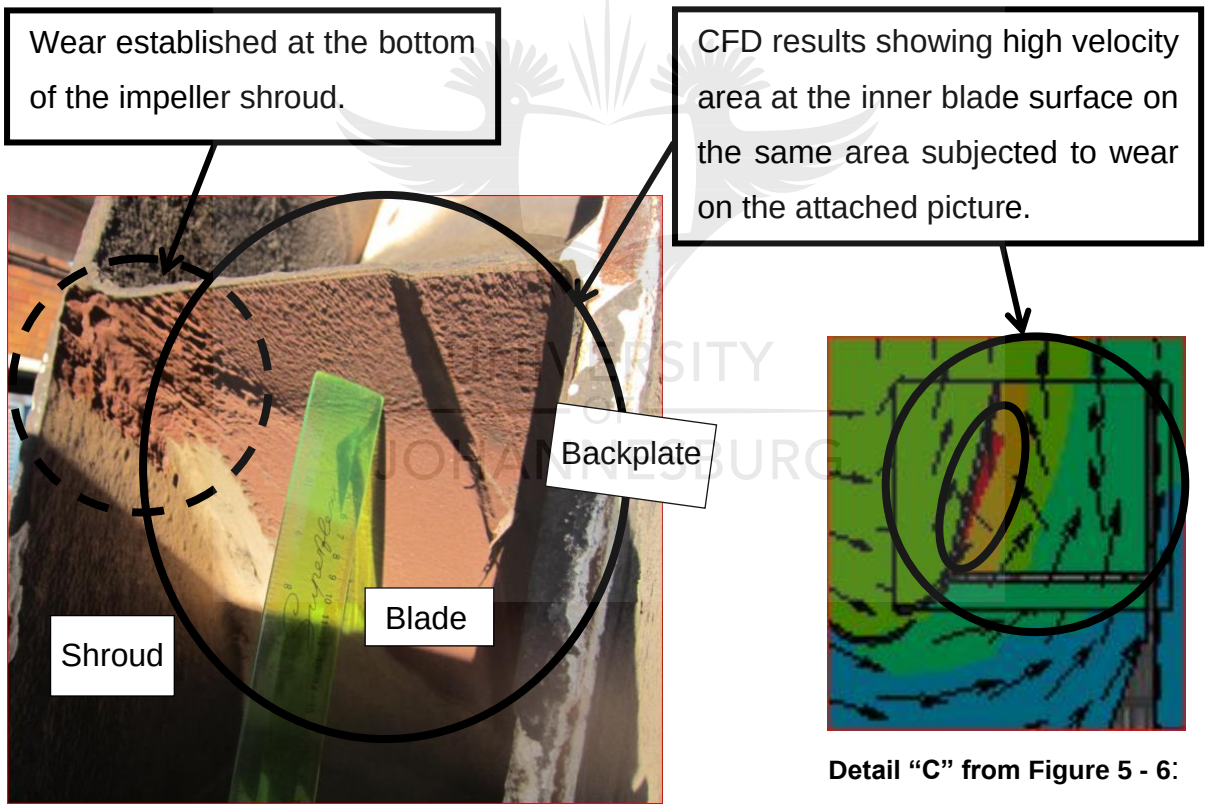

Figure 5 - 14a: Picture showing blade wearing at the front surface of the surface that is doing work.

The wear pattern on the blade indicates that wear formation is occurring on the blade at different rates, this is indicated by different thickness levels observed from the impeller shroud to the back plate. The circle on the picture indicate high erosion wear

occurring on the shroud and the same area subjected to wear correspond to high velocity area shown in red colour at the inner side of the impeller shroud taken from CFD results. By relating wear on the blade compared to CFD results, the observation is that rate of wear is higher closer to the impeller shroud and getting less and less toward the impeller backplate where the ruler in the picture is pointing. However, there is a huge difference in thickness closer to the impeller blade. This is due to wear liner welded on the blade to reduce wear formation.

By analysing CFD results in Figure 5 – 6 looking at detail “C”, it is observed that impeller blade is consist of different velocities with the highest velocity indicated closer to the impeller shroud and reducing as it gets closer to impeller backplate. These gradients of velocity level correlate to the difference of blade thickness subjected to wear as illustrated in the picture in Figure 5 – 14a. This can validate that velocity has contributed to wear formation as shown from the pattern of erosion wear in detail “C”.

The last observation from CFD results is the high velocity area between the fan casing volute and the impeller where the air is discharged from the fan impeller to the fan casing volute. This area is subjected to dust particles pass through the impeller within fluid gas. Figure 5 – 8, indicates that the velocity in that area ranges from 45.2m/s to 58.2m/s, this is the highest velocity that is found inside the entire fan casing air path as seen on the simulation results and in this regard the volute surface will be subjected to particles approaching the surface at a kinetic energy created from high velocity particles.

Detail “D” in Figure 5 – 8 indicates the highest velocity inside fan casing volute which correlates with a picture taken on site in Figure 5 – 15. The motive is to find out what is occurring on the volute surface where CFD results reveal that there is high velocity. The findings support the concept that state “increasing the velocity will increase wear rate” and this will give a definite correlation to the theory that high

velocity areas correlate with the observed wear on the entire fan component. See the relation for this theory in Figure 5 – 15.

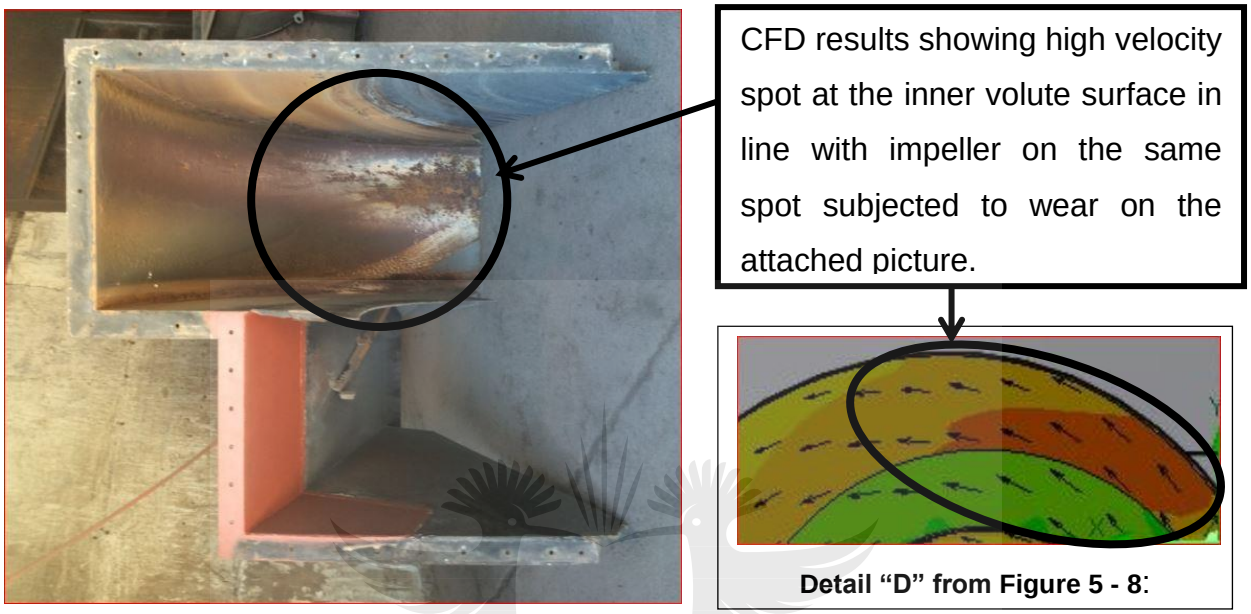

Figure 5 - 15: Picture showing wear at the top section of the fan casing.

The analysis of CFD results compared with wear found on the fan casing volute as per the attached pictures has again proven that particle velocity has a huge impact on wear formation. This is validated because the highest velocity area on the fan casing volute correlates with the highest wear found on the fan casing volute on site. The observed wear on the volute casing is not part of the research, however, this validates that CFD velocity pattern corresponds to wear observed on fan components.

5.3.4. Validation between two CFD Results

A third-party company from Germany namely TLT-Turbo was consulted to conduct CFD simulation to relate CFD results presented in this research. The aim of consulting this company was to make sure that results presented in this dissertation are correct and valid. TLT-Turbo is a company that specialize in doing research and development on improving reduction of wear formation on rotating components.

TLT-Turbo performed single flow simulation based on coal firing condition using PTC Creo Cad software versus SolidWorks Cad software used for CFD results presented in this research. There is a slight difference between the two CFD software's in terms of results accuracy and hence they will be always a slight difference in values. Figure 5 – 16 and Figure 5 – 17 relate CFD results in terms of velocity diagrams taken from both CFD simulations software. These two Figures indicate flow passing through the fan and discharged to the atmosphere. Velocity from TLT-Turbo which is Figure 5 – 16 ranges from 0m/s to 98m/s. On the other hand, Figure 5 – 17, velocity range from 0m/s to 93m/s. The difference of values resulted from the difference in accuracy of individual simulation software.

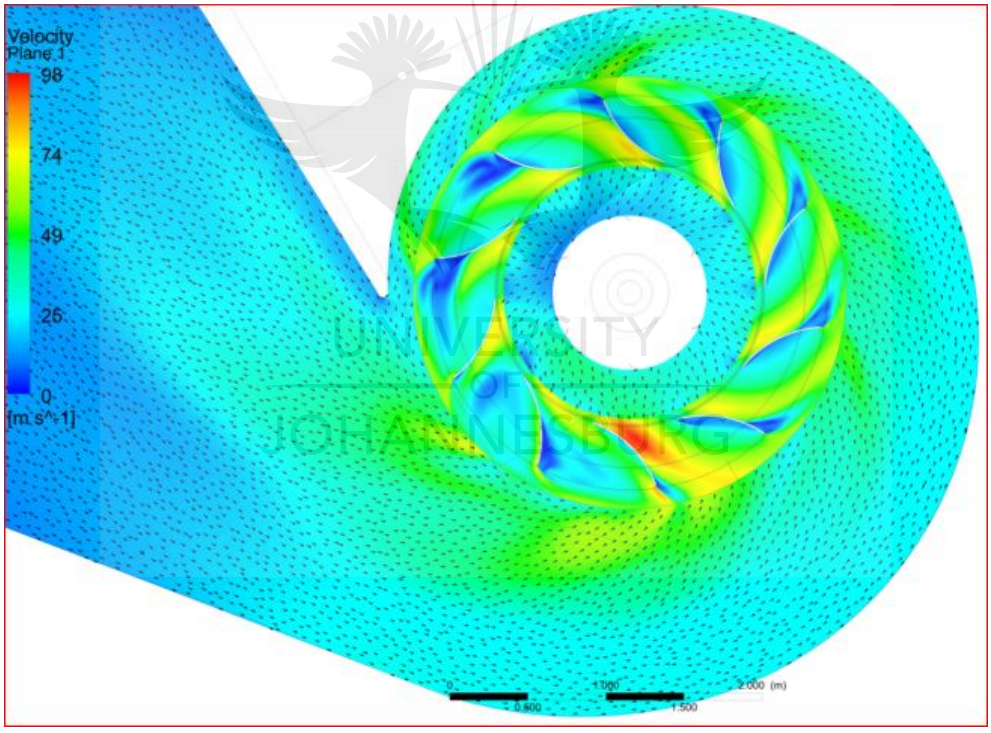

Figure 5 - 16: CFD results from TLT-Turbo.

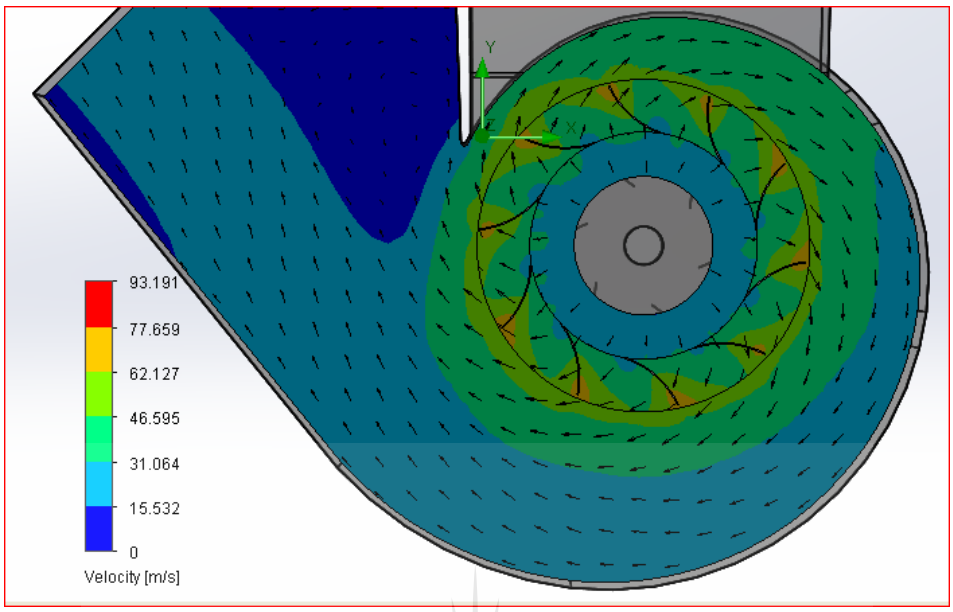

Figure 5 - 17: CFD results as presented on this thesis.

Other sets of pictures used to compare results from both simulations software taken on the inlet side of the fan and referred to velocities. These pictures illustrate flow entering fan inlet box and passing through the impeller and moved into the fan casing volute. Figure 5 – 18a present TLT-Turbo CFD results and Figure 5 – 18b present results used under this thesis to analyse flow pattern that has influence in causing wear. Again, velocity from TLT-Turbo which is Figure 5 – 18a ranges from 0m/s to 98m/s and in Figure 5 – 18b, velocity ranges from 0m/s to 93m/s.

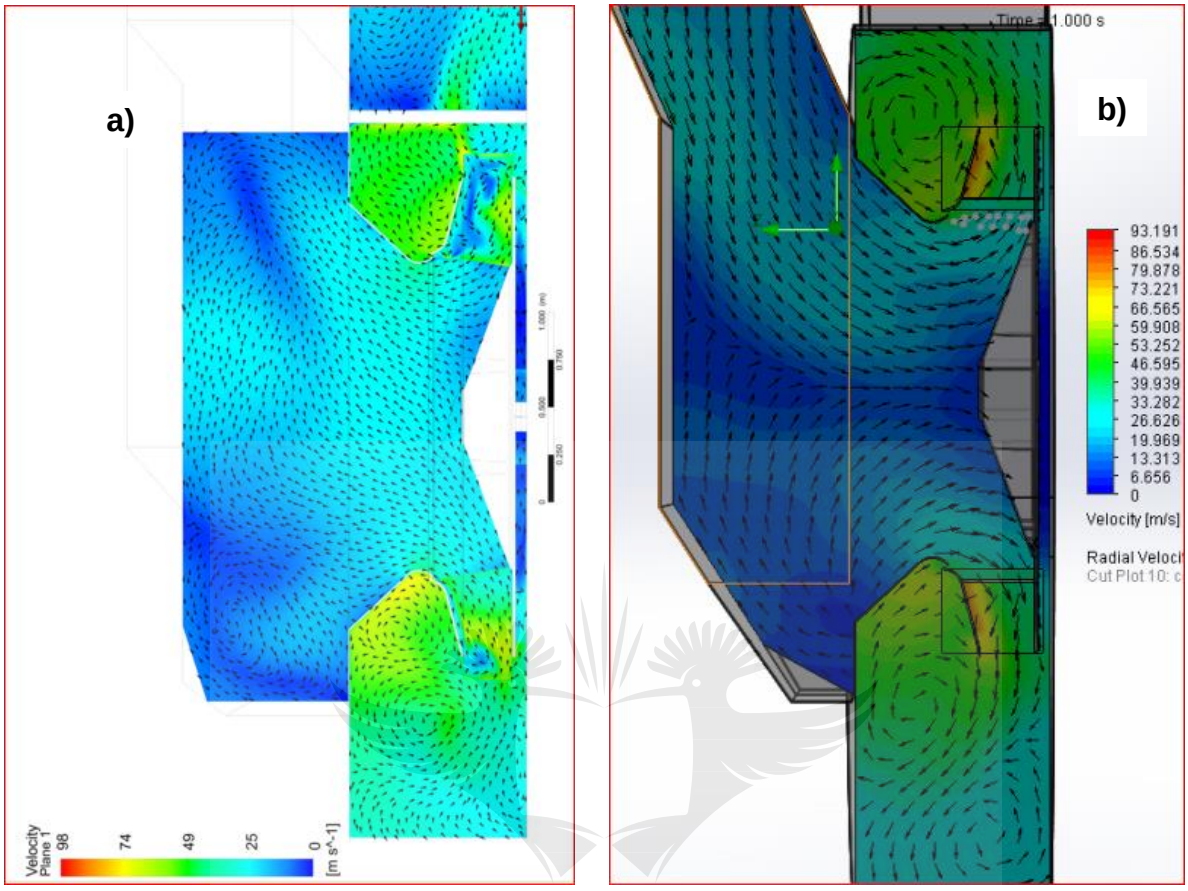

Figure 5 - 18: a) CFD results from TLT-Turbo. b) CFD results as presented on this thesis.

The correlating of results achieved between CFD performed by TLT-Turbo and CFD presented in this research report indicated that the results are very similar. However, viewing planes and colour coding presentations are not exactly same and that is why pictures are not the same. Results analysed from Figure 5 – 16, Figure 5 – 17, Figure 5 – 18a and Figure 5 – 18b have proven that all flow simulation results being used to analyse wear formation in this research are reliable.

5.3.5. Analysing Wear Rate on Different Materials

After the fan is installed and commissioned in 2009, the end user has been buying spare impeller every season to replace the eroded impeller that is in operation frequently. Sugar Mill Plant decided not to buy spare impellers anymore from OEM to reduce cost, in addition to that, they have decided to do reverse engineering and manufacture impeller on their own.

During reverse engineering the sugar mill took a decision not to manufacture impeller using Weldox 700 instead they used S355JR material to further minimize cost. The replacement of material has been done somewhere around the year 2015.

This has created an opportunity to compare wear formation of two different material grades. This analysis validates theory demonstrated by using Figure 2 – 3b between two ductile materials if correlates with an observation on site referring to erosion rate. Figure 5 – 19a) illustrate blade made of Weldox 700 and Figure 5 – 19b) illustrate blade made of S355JR material. Figure 5 – 19a) indicates that wear took place at the starting edge of the blade that is attached to the impeller side plate and wear was found to be very high at that position. The angle of impingement at that point was measured to be between 20° and 45°. While on the other hand, Figure 5 – 19b) indicates that wear took place between similar ranges as to blade leading edge, all angles are referred to Figure 5 – 9 and Figure 5 – 10.

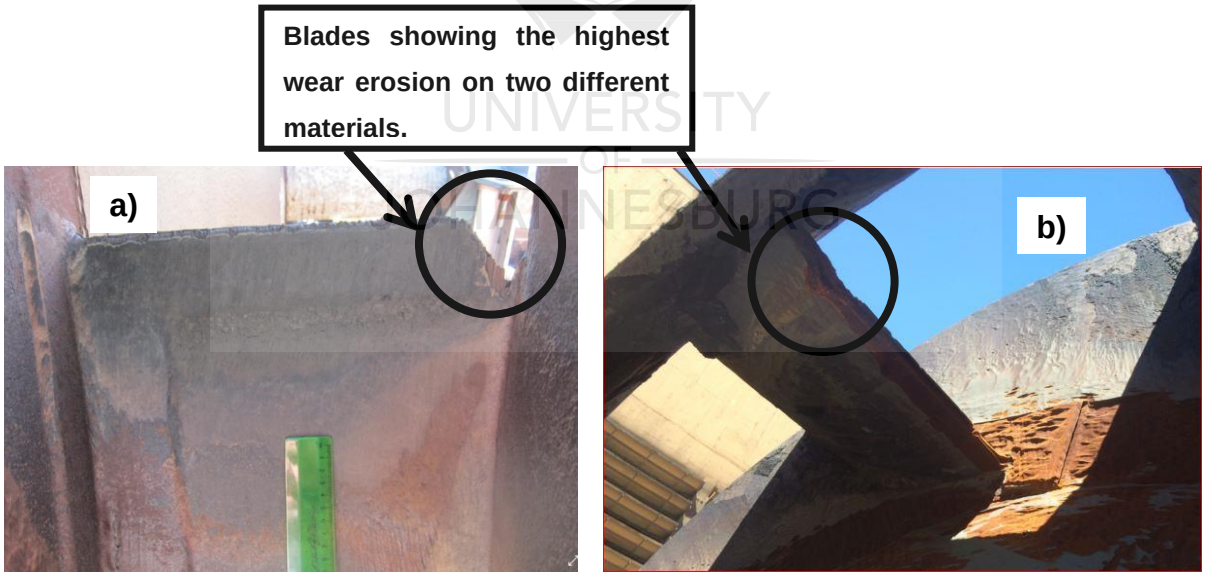

Figure 5 - 19: a) Blade made of Weldox 700 material. b) Blade made of S355JR material.

The remaining blades section leading edge of Weldox 700 toward the backplate, wear rate is occurring very slowly and uniformly. Like S355JR material blade, wear rate is occurring very slow and uniformly but lower rate when compared to Weldox 700 material. This can be explained by using tested erosion curves in Figure 5 – 20.

The test is conducted using S355J2 material which is equivalent to S355JR material and both grades have the same mechanical properties and chemical composition. The only difference is how the energy impact tests were conducted. S355J2 material erosion test is compared to S690QL material which is equivalent to Weldox 700. See Figure 5 – 20.

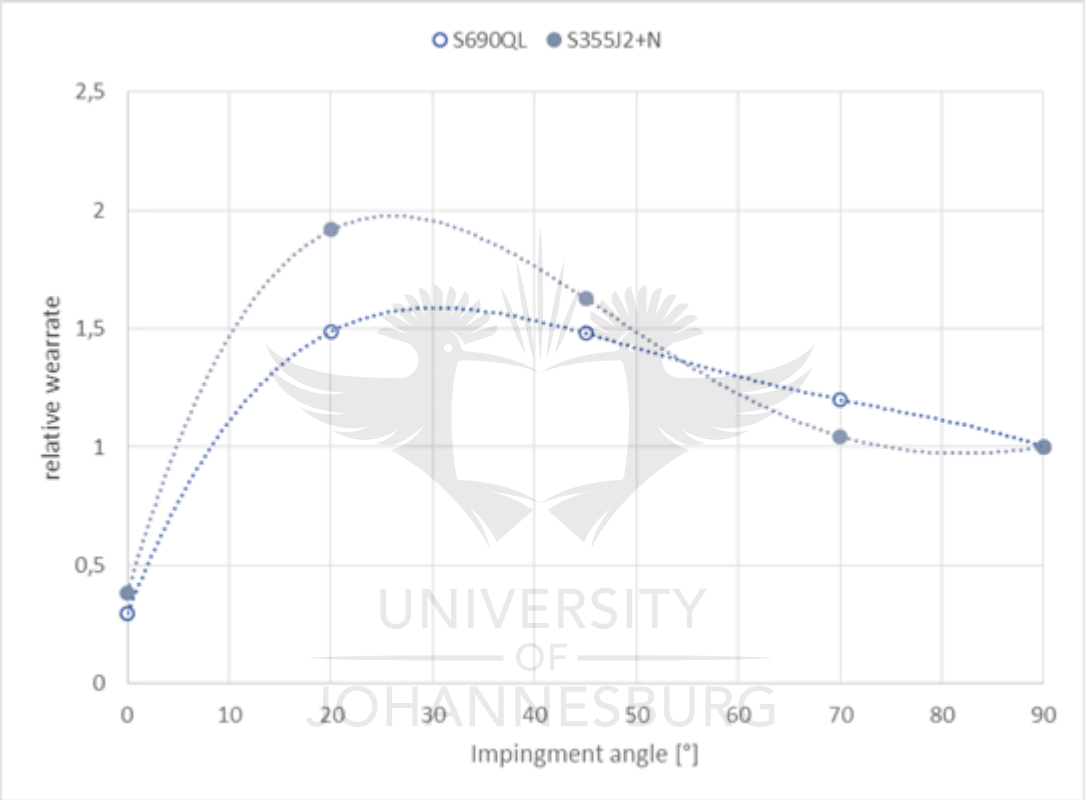

Figure 5 - 20: Ductile materials S690QL vs. S355J2+N illustrating rate of wear due to angle of impingement.

TLT Turbo in Germany has established this graph during their test. The test was conducted to determine the impingement angles which will have an effect on both materials. The results reveal that both materials follow a similar pattern with S690QL giving less wear rate between 0° to about 55° and gives a higher wear rate between 55° and 90°. The wear formation illustrated in Figure 5 – 11 is found to be higher at the starting point of the blade welded to shroud plate and lower and uniform on the rest of the blade leading edge section. The explanation is that wear formation is high between 20° and 45° for both materials since both materials have proven to be

ductile as per the test. The curve also explains the observation in Figure 5 – 19a) and Figure 5 – 19b), where it was observed that the rest of the blade leading edge of both material grades towards backplate are subjected to low wear formation with Weldox 700 material being subjected to higher rate formation compared to S355JR material.

Clarification of what is causing the difference of low wear formation on both blades leading edge grades can be understood using Figure 5 – 20, for angles between 55° to 90° the rate of wear decreases as the impingement angle approaches 90°. A pattern of wear formation shown in Figure 5 – 19a and in Figure 5 – 19b correlates with the test results as per Figure 5 – 20. Therefore, validate that wears formation on the impeller is correlating with theory as per graph in Figure 2 – 3b, which has been verified by using plotted graph established by TLT-Turbo Germany under Figure 5 – 20.

Another proven factor that correlates with the tested theory in Figure 5 – 20 and validate high velocity particles impacting on surface relating to Figure 2 - 5, this is based on a difference of wear formation on the inner surface of the blades. There is a difference of wear formation between Weldox 700 and S355JR material blade as seen in Figure 5 - 21a and Figure 5 – 21b.

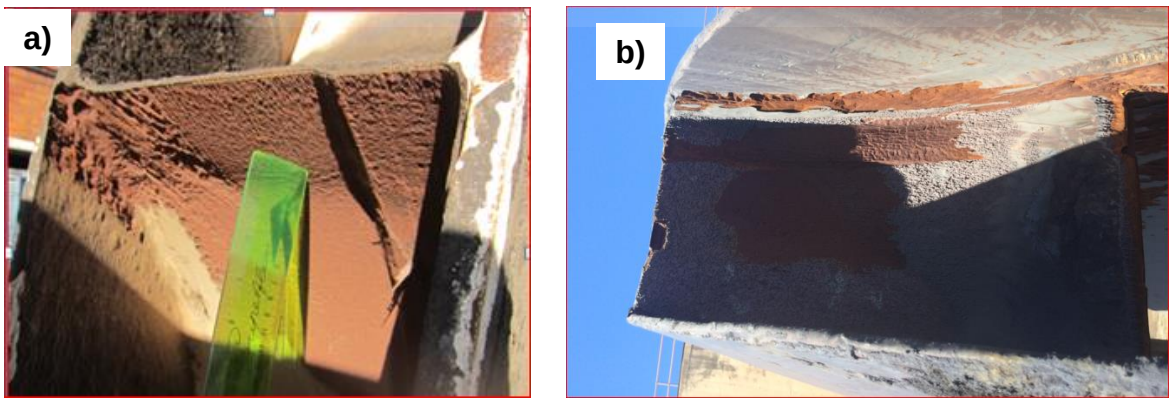

Figure 5 - 21: a) Inner surface worn blade made of Weldox 700 material. b) Inner surface worn blade made of S355JR material.

The research has shown that there is a difference in wear rate. Therefore, the correlation between theory and wear observed on site is very crucial. The correlation is based on Particle Flow Erosion at Ventilator Components Article by Dr. Dieter Holzdeppe [43]. The article shows the results of the total impact energy process with the assumption that particle is rigid, hard and does not split or rotates within the airflow when impacts on ductile material. During impaction, pressures in MPa can be induced in microseconds over the contact surface [43].

A continuous repeat of impact over the surface developed plastic deformation energy with kinetic re-bounce energy of the particle compromised. Re-bounce of particles happens into the inner surface of the blade when particles enter in the impeller and within the flow are hit by rotating impeller blades and results in re-bounce impact angle particles between 60° and 90° in relation to the impacted surface, prior deflected into fan casing volute. Figure 5 – 22a and Figure 5 – 22b represent the formation of plastic deformation and kinetic re-bounce energy.

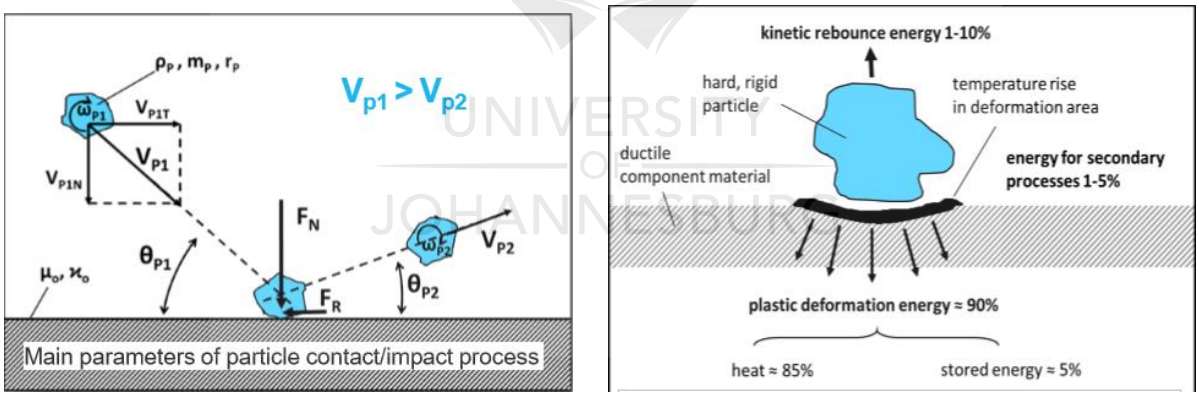

Figure 5 - 22: a) Particles approaching contacts surface. b) Particle showing energy balance during re-bounce [43].

Figure 5 - 21a and Figure 5 - 21b shows wear from different grades materials and this is due to continuous repeating impact whereby Weldox 700 has shown a higher rate of wear formation compared to S355J2+N material. This is due to high velocity impact and re-bounces particles above 60° and closer or equal to +/- 90°. Although both materials are ductile, they have responded differently since Weldox 700 has higher hardness compared to S355J2+N material. Harder material is susceptible to

fatigue and fracture at a higher angle and therefore will result in plastic deformation followed by micro-cracks and propagation to induced cracks will continuously grow until the blade is subjected to material loss. Particle velocity plays an important role in increasing wear formation because the research has proven that the higher the velocity the higher the rate of wear. The theory has proven that the velocity is not relative to the flow velocity in the impeller, but particles velocity is equal to the impeller rotating tip speed. Due to high velocities, the rate of wear is too high on the blades made of Weldox 700 and very low on blades made of S355JR material due to effective energy absorption characteristics.

5.4. Summary

The aim of this Chapter was to run a simulation to reveal what was taking place inside a centrifugal fan during operation and discover how erosive wear is established. The focus was on impingement angle and velocity effects on the impeller surface. Parameters used to perform CFD in this Chapter were found satisfactory judging from the results achieved. Calculations performed were found to be correlating with the CFD results achieved in a simulation. The damage patterns on an impeller were found to be correlating with the impingement angle patterns and high velocity zones indicated by the simulation results. Loss of materials due to wear was found to be correlating with the wear observed on site.

CHAPTER 6: CONCLUSIONS AND RECOMMENDATIONS

6.1. Introduction

This research aimed to investigate wear that is taking place on the impeller fan installed in sugar mill plant and to establish an understanding of what type of wear it is, and what causes it. The research is focusing on finding out particles path carried by gas passing through a fan.

The impeller was subjected to wear within a short period after being installed and commissioned. The first approach to conduct research was to collect particles samples site inside the scrubber to determine particles sizes and compound composition. Particles were assessed in a laboratory to determine the sizes and the particle's compositions. The second approach was based on performing a CFD simulation in SolidWorks 3D package to simulate what was happening inside the fan, but before commencing with CFD simulation, hand calculations were performed to work out parameter values to be used for boundary conditions. The third approach was to analyse venturi wet scrubber damages patterns to establish how the damage was encountered and what was the effects of these damages?

After laboratory experiments, the particles sizes were found to be more than common bagasse fly ash in the boiler and containing sharp edges. CFD results were corresponding as they correlate with the damages seen on the impeller. Therefore, the conclusion will be based on all gathered information about wet scrubber utilities and compared with wear formation from literature review as validated by other researchers who conducted tests to prove their theories. A comparison evaluating CFD results observed to prove theories and wear pattern on the impeller. As for wear formation in the wet scrubber will be judged by inefficiency, evidence, and factors observed during a site visit.

6.2. Conclusions

After the research, it was determined that the highest wear on the impeller was seen at the highest peak of the rate of wear graph determined through laboratory experiment. This dissertation on wear formation on a centrifugal impeller has revealed that erosive wear is the major type of wear that is taking place. This is a result of aggressive particulates impacting on the impeller coming from the boiler and passing through the scrubber unfiltered. Damages of spray nozzles inside wet scrubber proved that droplets are not generated to capture flying ash from the boiler and thus results in variation of particles size passing through the fan. The investigation also revealed that particles flow outline correlates with an experiment on studying impact angles on ductile materials. Comparison of literature review with patterns of wear damages found on the impeller has proven to be a success. The study is a success as computational fluid dynamics was performed to verify the angle at which particles are impacting on the impeller, has correlated with the erosive wear seen on the impeller and was in line with expected results. With the aid of actual angle of impact against wear test performed in a laboratory in Germany using the two involved materials on impeller design has supported the literature review and has established explanations on different wear formation on blade upper and lower leading edge.

This research study has shown that all investigated factors were able to be proven. This concludes that wear formation on the centrifugal impellers has been proven to be highly affected by the angle of impingement on the blade leading edge and material hardness on the blade surface. Therefore, the study conforms to wear tribology previously investigated by other researchers through tests. The study has revealed that impingement angles and high particles velocity plays an important role in accelerating rate of wear and these two factors are supplemented by the high rate of aggressive particles passing through the fan and therefore, the outcome of the findings verifies the stated hypothesis.

6.3. Recommendations and Possible Future Work

CFD analysis has indicated that there are different impingement angles of the blade leading edge and therefore different wear pattern formation on the blade leading edge is encountered, this requires different configuration approaches to manage wear minimization. This means that the leading-edge blade upper section can be protected by applying hardfacing with Vickers hardness greater than the particles impacting up to a transition where the effect of lower and larger impingement angle is the same as seen on tested erosive plotted curve using different materials. Then the rest of the blade leading edge bottom section to be protected by using hardfacing which has softer or lesser hardness compared to parent material used to construct the blades. A preferred material to be used for impeller construction after a comparison has been made between two different material used for impeller construction is Weldox 700 because of its ability to withstand wear formation on the blade surface. For reduction of particles impacting onto the impeller, end-user to consider consulting with wet scrubber specialist to look at redesigning the wet scrubber to have better filtration. Possible future consideration to investigate various particle constituent samples found amongst the bagasse ash using energy dispersive spectroscopy.

REFERENCES

[1] M. K. Bundinski and K. G. Bundinski, Engineering Materials Properties and Selection, Ninth Edition, New Jersey: Hamilton Printing Co., 2010.

[2] W. H. Encyclopedia, “Alexander Sablukov,” *Centrifugal Fan, Timeline of Russian Innovation, List of Russian Inventors,* vol. ID no: WHEBN0018067511.

[3] R. Thomson and D. Wong, “Boiler Induced Draft Fan Operation,” *Induced Draft Fan Selection, Boiler Fan Design, Sugar Mii Boilers,* vol. 32, pp. 665-678, 2010.

[4] E. Aul and E. H. Pechan, “Bagasse Combustion in Sugar Mills,” *Emisssion Factor Documentation for AP-42,* pp. Section 1.8, iii – xxxiii, 1993.

[5] J. T. A. P. Control, “Air Pollution Control,” *Wet Scrubbers,* 2015.

[6] U. E. P. Agency, “Wet Scrubber,” *Wet Scrubber,* pp. 5.4.1 - 5.4.38 Ch5*, 2002*.

[7] W. Shakespeare, “Wet Scrubber for Emission Control,” in *Environmental Engineer's Mathematics Handbook*, CRC Press LLC, pp. Ch 10, pg 249 - 286, 2005.

[8] S. O. AB, “Weldox Structural Steel Plate,” in *Data Sheet - Version 2005-10-15*, Sweden, p. 1, 2005.

[9] S. O. AB, “Hardox Wear Plate,” in *Data Sheet, Version 2008-05-10*, Sweden, p. 1. 2008.

[10] T. A. Rodil, “Edge Effect on Abrasive Wear Mechanisms and Wear Resistance in WC-6wt%Co Hardmetals,” in *Wear*, pp. 1-39, 2006.

[11] F. Goerge and J. Schmitt, “Liquid and Solid Particle Impact Erosion,” in *AFML-TR-79-4122*, pp. 1-74, 1979.

[12] P. K. Press, Material to Resit Wear, Swansea: Swansea University College, 1986.

[13] R. G. Bayer, Mechanical Wear Prediction and Prevention, Vestal, New York: MArcel Dekker, inc., 1994.

[14] G. W. Stachowiak, “Wear Materials,” *Mechanisms and Practice,* 2005.

[15] I. Hutching, “Tribology,” *Friction and Wear of Engineering Materials,* no. Department of Materials Science and Metallurgy Unviersity of Cambridge, pp.

164-165, 1994.

[16] Roberts,"Wear,"[Online].Available:http://www-sgroup.materials.ox.ac.uk/lectures/tribology/wear.pdf, 2003.

[17] H. Hirani, "Wear Mechanisms," *Lecture no. 09,* 2012.

[18] B. A. Lindsley and A. R. Marder, "The Effect of Velocity on the Solid Particle Erosion Rate of Alloys," *Wear,* pp. 510-516, 1999.

[19] J. G. Bitter, "Wear," *Wear,* vol. 6, pp. 5-21 and 169-190, 1963.

[20] G. P. Tilly, "Wear," *Wear,* vol. 14, pp. 63-79 and 241-248, 1969.

[21] A. Kanhere and G. L. Sheldon, "Wear," *Wear,* vol. 21, pp. 195-209, 1972.

[22] L. K. Ives and A. W. Ruff, "Electron Microscopy Study of Erosion Damage in Copper," *Erosion: Prevention and Useful Applications,* pp. 5-35, 1979.

[23] W. F. Adler, "The Mechanics of Liquid Impact," *Treatise on Material Science and Technology,* vol. 16, 1978.

[24] I. Hutchings, "Mechanisms of the Erosion of Metals by Solid Particles," *Wear,* pp. 59-76, 1979.

[25] W. F. Adler, "Analysis of Multiple Particles Impacts on Brittle Materials," *Wear,* no. Air Force Materials Laboratory and Wright-Patterson Air Force Base, 1974.

[26] P. A. Engle, "Impact Wear of Materials," in *Wear*, Amsterdam, Elsevier Scientific Publising Company, pp. 33-334, 1976.

[27] A. G. Evans, M. E. Gulden, G. E. Eggum and M. Rosenblatt, "Impact Damage in Brittle Materials in the Plastic Response Regime," in *Wear*, CA, International Science Center, 1976.

[28] M. Hadad and S. Siegmann, "Solid Particle Erosion Test at High Temperature," in *Coating Technology*, pp. 1-2, 2012.

[29] R. G. Bayer, Engineering Design for Wear, Vestal, New york, U.S.A: Marcel Dekker, 2004.

[30] P. C. Okonkwo, A. M. Mohamend and A. Ahmed, "Influence of Particle Velocities and Impact Angle on the Erosion Mechanisms," *Advanced Material Letters,* pp. 653-659, 2015.

[31] M. Matsumura, "Investigate the Effect Surface Damage at Different Impacting Angles Due to Impinging Silica Sand Particle," *ISIJ Internationl,* pp. 168-176, 1991.

[32] I. Finnie, “Peak Erosion and Wear Rtae Occurred Between 15° and 40° for Ductile Material,” *Wear,* pp. 87-103, 1960.

[33] I. Finnie, A. Levy and D. H. Macfadden, “Fundamental Mechanisms of the Erosive Wear of Ductile Metals by Solid Particles,” *Erosion: Prevention and Useful Applications,* pp. 36-58, 1979.

[34] G. W. Stackwick and A. W. Batchelor, “Erosion and Wear Rate Increase with Increase Impact Angle Reaching the Peak at 90°,” Boston, 2001.

[35] M. A. Islam and Z. N. Farhat, “Erosion Rate Decreases with Increasing Impact Angle and Increased Particle Velocity Resulted in Increased Erosion Rate,” *Wear,* pp. 180-181, 2014.

[36] D. A. Axinte, “Erosion Tests by Solid Particle Impingement Using Gas Jets,” *International Journal of Machine Tools and Manufacturing,* no. 49, pp. 797-803, 2009.

[37] K. Myles, Wear Control Principles and Practice, Northcliff, SA: Myles and Associates, 2016.

[38] S. F. Anwer, “Computational Methods in Engineering Application,” *Introductional to Computational Fluid Dynamics,* 2016.

[39] D. Kuzmin, “Computational Fluid Dynamics,” Institute of Applied Mathematics University of Dortmund, Dortmund, 1993.

[40] N. Ashgriz and J. Mostaghimi, “An Introduction to Computational Fluid Dynamics,” in *Fluid Flow Handbook*, Toronto, Department of Mechanical and Industrial Eng. University of Toronto, pp. 2-9, 2006.

[41] J. Drotsky, “Simple Stress and Strain,” in *Strength of Materials for Technicians*, pp. 31-32, 1985.

[42] N. Van der Westhuizen, Interviewee, *Hardox 500 Classification - SSAB Special Steel.* [Interview]. 28 August 2018.

[43] D. Holzdepper, “Basic Principle of Erosion and Materials/Coatings Resistant Against Particle Flow Erosion,” *Particle Flow Erosion at Ventilator Components,* pp. 19-20, December 2015.

[44] J. R. Laguna-Camacho, M. Vite-Torres, E. A. Gallardo-Hernandez and E. E. Vera-Cardenas, “Solid Particle Erosion on Different Metallic Materials,” in

Trbology in Engineering, pp. 63-77, 2013.

[45] “Wet Gas Scrubbing,” *The Nalco Water Handbook,* pp. 41.2-41.3, 1979.

[46] TLT-Turbo, “Basic Aerodynamic Centrifugal Fans,” in *Siemens Ltd. india Trianing*, Bad Hersfeld, Germany, 2016.

[47] I. O. f. Standardization, Industrial Fans - Performance Testing Uisng Standardized Airways, 2007.

[48] D. Holzdeppe, “Impingement Angle on Centrifugal Impeller Blades,” Dr.Ing Dieter Holzdeppe, Zweibrucken, Germany, 2018.

[49] AP-42, “Bagasse Combustion In Sugar Mills,” in *Boiler*, pp. 4-5, 2017.

APPENDICES A

Figure A: First picture showing wear on the backplate and hub plate.

Figure B: Second picture showing wear on the backplate and hub plate.

Figure C: Third picture showing wear on the backplate and hub plate.

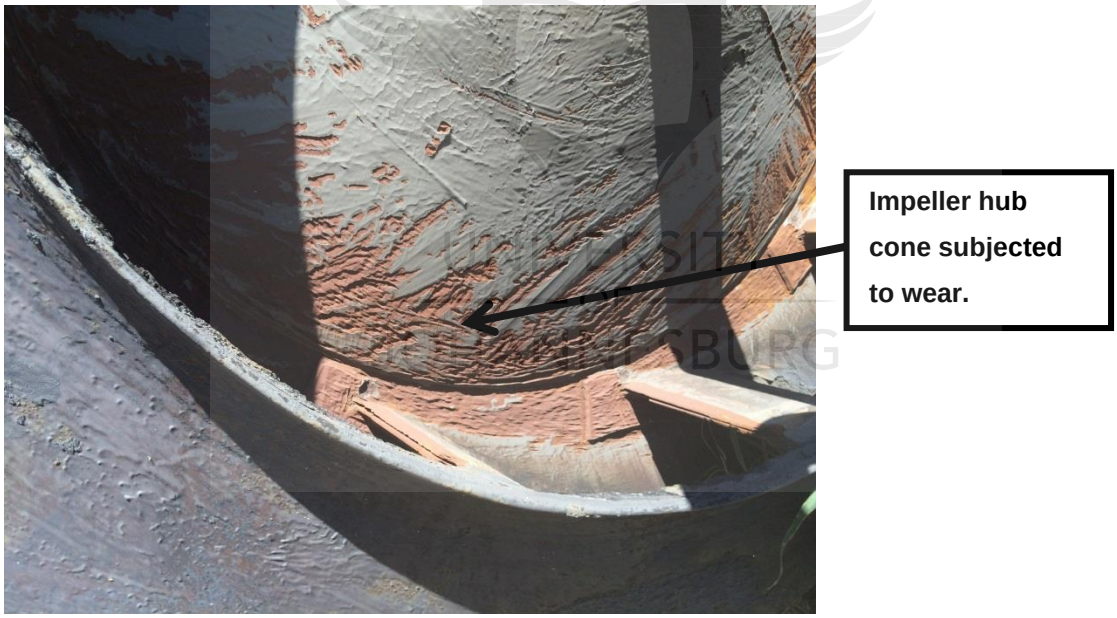

Figure D: Fourth picture showing wear on the backplate and hub plate.

APPENDICES B: CONFERENCE PAPER

Eleventh South African Conference on Computational and Applied Mechanics
SACAM 2018
Vanderbijlpark, South Africa, 17-19 September 2018

Investigation of Material Wear Formation on Centrifugal Fan Impeller

K.A. Mabunda[a] and P.M. Mashinini[b]

[a]*University of Johannesburg, Department of Mechanical Engineering and Industrial Technology, Doornfontein Campus, Johannesburg, 2094*

[b]*University of Johannesburg,Department of Mechanical Engineering and Industrial Technology, Doornfontein Campus, Johannesburg, 2094*

email address : aphas.mabunda@gmail.com[a], mmashinini@uj.za.ca[b]

Abstract

This paper reports the investigation of wear formation on centrifugal fan impeller which was exposed to bagasse ash particles in the sugar process plant and to simulate what took place as particles impact on the impeller surface. Computational Fluid Dynamics has been used as a tool to simulate impaction of flow around the impeller to determine the impingement angles and velocity particles. After performing simulation using SolidWorks, angle of impingement was found to be low at the impeller inlet and gradually increase angle toward 90°, in reference to the blade root. The lowest angle found after simulation was 23°. This angle correlate with the theory mentioned for ductile material, stating that ductile material is susceptible to wear formation when the impact angle is between 15° and 45° with a peak at 25°. Computational Fluid Dynamics using SolidWorks has been verified by using a third-party company that worked on Creo 3.0 simulation. Research has revealed that material selection based on particles impingement angle, is key as when applied to centrifugal fans and related applications.

Keywords: Wear, Centrifugal Impeller Fan, CFD, impingement angle

1. Introduction

Many industries such as sugar mill plant, power generation, mining, smelters, platinum, steel and minerals process plant have been facing a huge problem with wear formation. Most of these industries have been seeking for solutions on what causes wear and how to minimize it. Sugar industry has been one of the leading industry that kept questioning manufacturer of process plant ventilation fans on how can wear formation be control and nevertheless, there still a grey area of knowledge in terms of how wear is formed on the fan impeller. There are many types of wear that have been already discovered by many researches around the world. It has been determined that abrasive wear is one of the major wear that is highly subjected to fan impellers in sugar mill plant and is classified as erosive wear [1]. The biggest challenge of diagnosing wear is to understand the system, because wear is said not to be material problem but system problem [2]. The system is referred to the fluid substance that is conveyed inside the fan. Particularly in sugar mills, bagasse ash is the substance that is sucked from the boiler during combustion and pass through a filtration system where it gets entrapped and only clean air supposed to be discharged into atmosphere. Bagasse has been classified as fuel substance which is a by-product of sugar cane leaves, roots combined with soil and sugar cane stalk after being crashed to extract the juice [3]. It was found in the sugar mill that the study is based on that too much excessive quantity of bagasse ash is unfiltered in the venturi wet scrubber and passes through the fan. These bagasse ashes impact on the impeller and cause massive material loss. The study is about how bagasse ash impact on the impeller, at what velocity and what are the effects that are contributing to material loss that must be understood to mitigate the rate of wear on the impeller. Fig. 1 shows the schematic of the scrubber and centrifugal fan as well as the typical scrubber with a venturi to illustrate the working arrangement of the system.

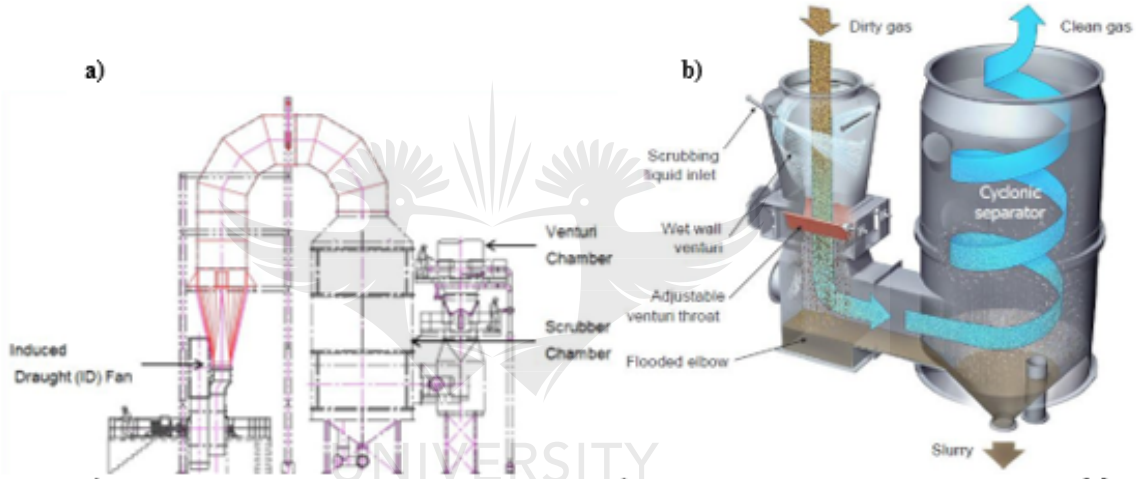

Fig. 1: a) Schematic diagram of scrubber and centrifugal fan and, b) Typical working arrangement of Venturi scrubber [4].

The main aim of this study was to perform a CFD and correlate the results to wear damages found in situ and to establish the uncertainty of what are the impingement angles in relation to impeller blades leading edges. The study of wear by other researchers has revealed that particles impact angles are one of the major factor that contribute to wear formation and these angles react differently to ductile and brittle materials [5,6]. The theory state thus, lower and higher angle will have different characteristics. When particle approach eroded surface at a lower angle, angle between 5° to 30° and collide with the surface, during collusion shape of particle will affect the wear rate by trying to graze the surface or cut the surface. During this process shape of particle does matter because particles work as a cutting tool and therefore wear takes part in a form of abrasion wear [6]. Basically, these are two surfaces rubbing each another and to resist wear rate, hardness of the component need to be higher. On the other hand, when angle of impingement is higher and is between 60° to 90°, to resist the wear, a ductile material will be required because most of the energy is transferred to the component and observes all this energy as a compressive load. By increasing the particle size will increase wear rate, increasing the velocity will increase wear rate and impact angle will affect in either way but, depend on what type of material being used [6].

2. Methodology

CFD simulation was computed by applying data used to select the fan operating duty, first condition was based on firing bagasse inside the boiler and the second was based on firing coal. This report will be focusing on bagasse firing condition. The first step to the simulation preparation was to create a 3D model and after creating the 3D model and

inlet extension piece was created to be used on the fan inlet to smoothen the flow during simulation. A set of calculations has been performed to establish extra parameters required to setup the CFD project. Parameters such as total fan pressure rise, Reynolds number, fluid density, Impeller tip speed and velocities at fan inlet. For CFD setup, a project was created with analysis type to be internal and exclude cavities without flow condition. Rotating type was selected with local region under sliding. Under initial and ambient conditions, thermodynamic parameters required settings for pressure and temperature, where pressure was set using total fan pressure rise of 3145Pa and temperature was set to a value of 70°C which is referred to inlet fluid temperature. On the input data under setup computational domain, the model was set to be within the boundary and under rotational region, fan rotating speed of 615rpm was applied to enable the simulation to recognise that the impeller is rotating. The next step was to apply boundary conditions, a flow rate of 63.5m^3/s was applied on the inlet of extension piece and since the fan is discharging to the atmosphere through a stacker, a barometric pressure of 102000Pa as taken from the data supplied by the client was applied on the discharge side of the fan. The final setup was to establish goals and the following goals were created; to global maximum fluid density, global and surface velocities, surface total pressure and outlet flow rate.

Prior running the simulation, global mesh setting was conducted and including a separate mesh that was conducted on the impeller only. After running a CFD, results were achieved and further analysed by creating cuts and surface plots. Since the study was focusing on velocities and how the fluid passes over the impeller blades and backplate, cuts plots on velocity were crucial factors and were plotted by using arrow pattern. To estimate projection of angle of attack, projected angles were represented by lines that are drawn tangential to the arrows of air path that are anticipated to be tangential to air streams. Angles of attack are measured between fluid streamlines and vertical plane of impeller blades leading edge. Streamlines are represented by black arrows moving in axial direction at impeller inlet and leaves the impeller chamber in radial direction. A CFD setup has been successfully done by setting up a project in SolidWorks package by using fan duty data provided by the consultant to establish boundary condition and goals needed to run simulation. Cut plots were plotted focusing on the flow pattern on the inlet of the impeller to determine impact angle and the second factor that was crucial to explore on the results was the highest velocity spots. Angles achieved from the CFD results were compared against erosion vs impingement angle curve established by TLT-Turbo R&D department [6]. The impeller was constructed from ductile material which is Weldox 700.

3. Results

Simulation was run, and desired results were achieved. The focus of the simulation was to determine angles of impingement of particles onto the blades and backplate of the impeller. Particles velocity also plays a major contribution on wear formation with aid of particles sizes, shape and quantity passing through the fan and therefore, study of velocity profile was a crucial factor to determine the cause of wear. Fig. 2, illustrates cut plot of velocity profile of the air entering and leaving fan distributed inside the fan casing and passing through impeller.

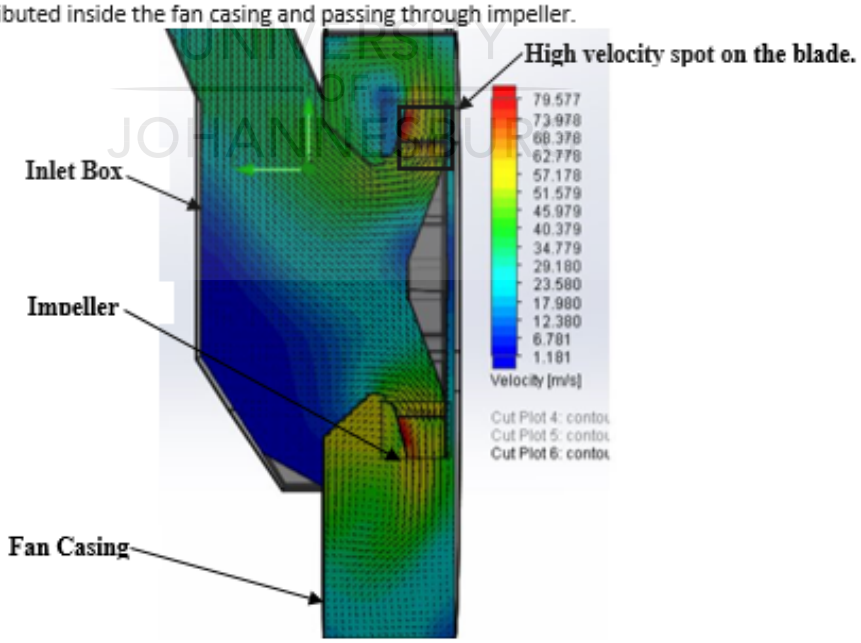

Fig. 2: Sectional view illustrating velocity profile as the air enter the fan

3

Velocities range from 0m/s to 95.5m/s maximum. Velocity at the fan inlet box ranges from 20m/s to 27m/s, velocity gradually increases on the upper side of the fan inlet cone while the bottom side remains the same as the velocity on the fan inlet box. As the air inters the impeller, the velocity dramatically starts to increase until the air leaves the impeller and discharged into the fan casing volute. High spot velocity discovered on the blade surface from CFD results has been indicated with high dense spots colour coding starting from green up to dark orange as marked on the blade viewing from the sectional view in Fig. 2 where velocity ranges from 44m/s to 78.5m/s maximum on the surface of the blade and this is the blade surface that is mostly exposed to high velocities.

When viewing Fig. 2 on a different plane as seen in Fig. 3, a second cut plot is taken to illustrate air distribution inside the fan casing volute and the impeller as the air leaves the impeller. Velocity values have been adjusted to reflect the highest velocity that is exposed to majority of blade surface. This sectional view shows the highest velocity on the blade as 79.6m/s and indicated by red spots and tangential to impeller outer surface of the velocity ranging between 53.5m/s to 66.5m/s. The volute shell area indicates to be subjected to velocity ranging from 14.3m/s to 53.5m. On the discharge side of the fan casing on the upper left section indicates that less air is being conveyed over that surface. This has been recognised by maximum velocity of 14.3m/s that is shown on that area.

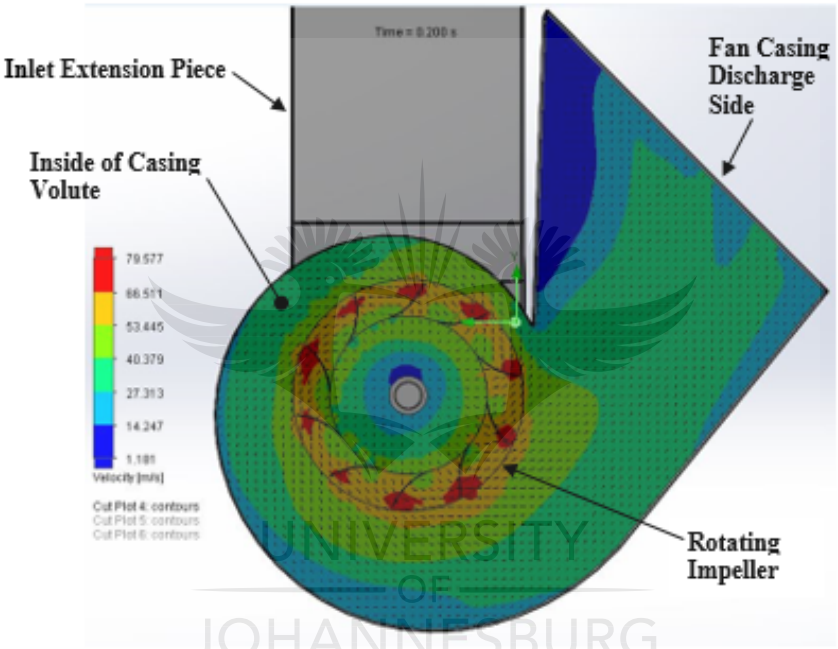

Fig. 3: Sectional view illustrating velocity profile as the air leaves the fan.

Erosive wear [6,7], is a function of particle velocity and impingement angle being supplemented by shape and size of conveyed particles. Either liquid or solid particles or combination of both comes with velocity and impinge on solid surface and convey some kinetic energy to the surface, during this stage an angle of impact will be an essential parameter. The main factors that takes part on wear formations is mass and hardness as well as velocity particle. Angles of impingement in this study have been measured from vertical plane of impeller leading edge blade represented by vertical black line and blue lines tangential to flow stream arrows. Fig. 4, illustrate angles of attack at the blade leading edge under bagasse firing condition and these are angles measured just before particles in the air path impact on the blade surface. It can be seen in Fig. 4 that impingement angle is low starting from the top blade leading edge and gradually increase toward the backplate with a maximum angle of +/- 75°. By taking a close look in Fig. 4, it can be observed that after the air has been discharged into the fan casing volute a swirl is formed outside the impeller on the side of the shroud. This swirl is indicated by arrows impacting on the outer surface of impeller shroud and when taking a close look using Fig. 2, it can be observed that these arrows go back into the impeller through a 12mm gap between the impeller inlet cone and shroud ring. This can be interpreted by saying that fine particles leaving the impeller are brought back into the loop through swirl process and these particles are repeating the impaction onto the upper blade leading edge.

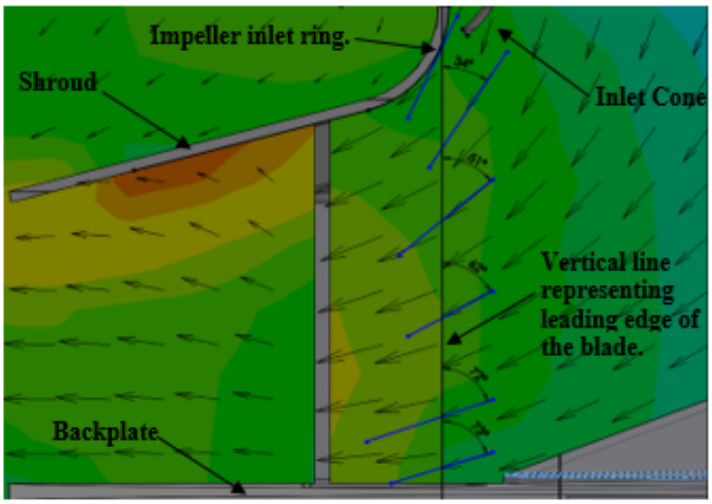

Fig. 4: Sectional view illustrating velocity profile as the air leaves the fan.

4. Analysis of CFD result

In erosive situations, particles that are normally entrained in a fluid can impact the wearing surface. The load between the particle and the surface, results from the momentum and kinetic energy of the particle [6,7,8,9]. The theory that has been tested by other researchers such as Dr. Dieter Holzdeppe from TLT-Turbo in Germany has been used to validate the CFD result [10]. The initial material construction of the impeller was Weldox 700 and it was later changed by the end user to S355JR. The theory was based on researching effects on different angle of attack against different types of materials. Dr. Dieter Holzdeppe [10] and his student has done a test on Weldox 700 and S355JR material to determine the effect due to different impact angles. The result reveals that both materials follow similar pattern with S690QL (equivalent to Weldox 700) giving less wear rate between 0° to about 55° and gives higher wear rate between 55° and 90° as compared to S355JR material. The graph explain that wear rate formation is high between 10° and 55° for both materials, since both materials have proven that are ductile as per the test. Fig. 5 illustrate the tested theory in full detail. With aid of comparison between CFD results from Fig. 4 and the graph in Fig. 5, it can be predictable that high rate of wear should be observed at the blade leading edge upper side of the impeller where angles ranges from 15° to 40° and with the increase in impact angles to maximum of +/-75° in Fig. 4, the expectation should be that from 40° up to 75° wear rate should be established at a lower rate and be uniform.

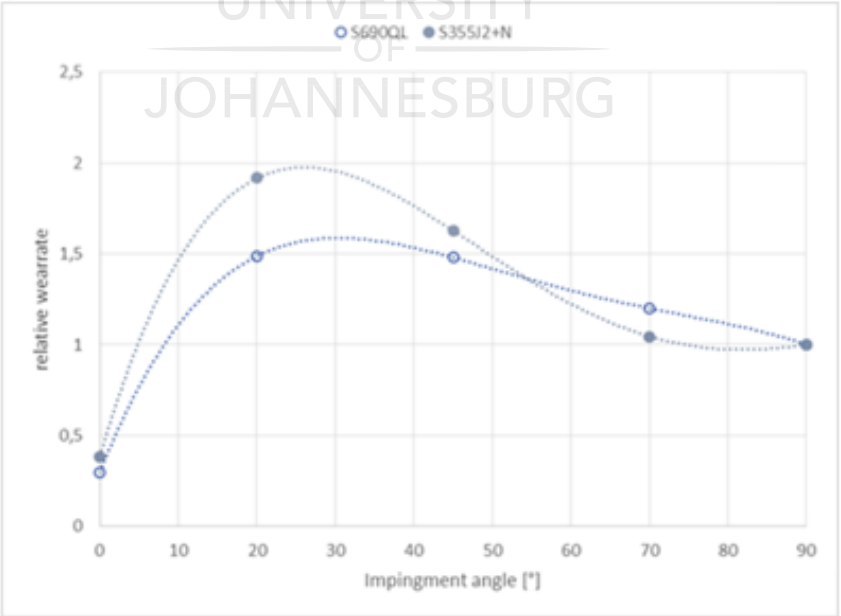

Fig. 5: Tested graph on wear rate vs. impingement angles [10].

A narration between results and pictures on observed wear damages taken at situ was necessary to be implemented to verify whether CFD results can reveal as predicted to what happen in situ during operation. Correlation of CFD results with picture indicated in Fig. 5 has validated that CFD results correlate with the tested theory in Fig 5. The relation was based on conclusion of studying CFD results and identified areas that relate to literature as highlighted under this study. By comparing angles of impingement at the blade leading edge, with blade pictures photographed at situ, as shown in Fig.6, rate of wear was higher on the blade leading edge next to the should on the picture and the rest of the blade was subjected to less uniform rate of wear. When relate the damages on the picture with CFD result in Fig. 3, it was observed that the rate of wear correlates with angles of impingement revealed by CFD results and where the blade was subjected to less uniform rate of wear, it was also observed that the angle of impingement from the CFD result ranges between 51° and 75° and according to Fig. 5 wear rate took place at a lower rate between velocity ranging from 55° to 90°. Therefore, CFD results has proven that theory established by other researcher against the CFD results and damages observed at situ can be applied in this study to implement a solution since all factors concerning impingement angles are verified. Blade was highly subjected to wear due to susceptible of ductile material at lower impact angles.

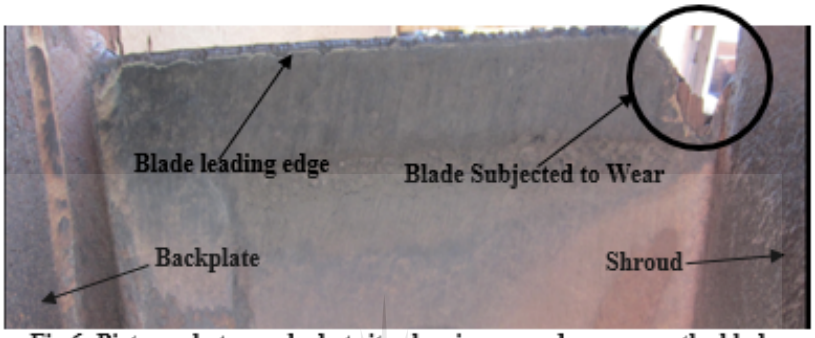

Fig.6: Picture photographed at situ showing wear damages on the blade.

Okonkwo [11] and Bagci [12], investigated the effect of velocity on the solid particle erosion rate of alloys and their results revealed that erosion rate is full dependent on velocity. Particle velocity is one of the major factor that contribute to wear acceleration rate formation [11, 12]. Therefore, an appropriate analysis on CFD results achieved after simulation must be conducted to understand the effect of velocity particles sliding over the impeller surfaces. This analysis of velocity particles has been inspired by the different velocities levels originate on the different parts of the impeller that has been revealed by the CFD results. Another correlation of results was based on particles velocity from CFD results against the blade picture photographed at situ indicated under Fig. 7. CFD results in Fig. 2 showing high velocity spot where velocity ranges between 44m/s to 78.5m/s maximum on the surface of the blade, whereby the study has analysed the relationship between velocity range and the picture in Fig. 6, a comparison of the damages observed on the picture against the CFD results was necessary to validate the simulation. On the same spot of the blade subjected to high velocity, it was discovered that wear on the attached picture in Fig. 6 has been formed on the similar spot of the blade at situ. The outcome of the analysis in terms of particle velocity effects can be concluded that the verification of the CFD results was a success due to positive correlation of wear pattern in relation to high spot velocity on the blade surface. Therefore, CFD simulation was able to reveal the effect of velocity particles.